A Study of The Omega Minus Hyperon

KAM-BIU LUK

February, 1983

Supported in part by:
National Science Foundation

Department of Physics and Astronomy

RUTGERS
THE STATE UNIVERSITY
OF NEW JERSEY

RU-83-8

A STUDY OF THE OMEGA MINUS HYPERON

By KAM-BIU LUK

A thesis submitted to

The Graduate School - New Brunswick

Rutgers, The State University of New Jersey,

in partial fulfillment of the requirements

for the degree of

Doctor of Philosophy

Graduate Program in Physics

Written under the direction of

Professor Thomas J. Devlin

and approved by

T. J. Devlin

Terence L Watts

David R. Harrington

Noémie Koller

New Brunswick, New Jersey

February 1983

ABSTRACT OF THE THESIS

A STUDY OF THE OMEGA MINUS HYPERON

by

KAM-BIU LUK

Thesis Director : Professor Thomas J. Devlin

A sample of 1,743 reconstructed $\Omega^- \to \Lambda K^-$ decays has been collected in the hyperon beam at Fermilab. The Ω^-'s were produced by 400 GeV/c protons incident on a solid beryllium target. The invariant production cross section for the Ω^-, with $0.35 \leq x \leq 0.73$ and $0.7 \leq p \leq 1.4$ GeV/c, was measured and parametrized with an expression which is proportional to $(1-x)^n$. The value of n for the best fit was found to be 5.86 ± 0.15. The lifetime of the Ω^- was determined to be $(0.815 \pm 0.030) \times 10^{-10}$ s. The Λ helicity measured as the product $\alpha_\Lambda \alpha_\Omega$ was -0.022 ± 0.051, giving a value of -0.03 ± 0.08 to the asymmetry parameter for the $\Omega^- \to \Lambda K^-$ decay. A new method of relating the polarization of the daughter Λ to the vector polarization of the Ω^- was derived. The average polarization of the Λ was 0.12 ± 0.08, implying that the vector polarization of the Ω^- should be positive if $\gamma_\Omega = 1$ or should be negative if $\gamma_\Omega = -1$. The magnetic dipole moment of the Ω^- was determined to be -2.1 ± 1.0 n.m..

ACKNOWLEDGEMENTS

I would like to thank Tom Devlin for introducing me to experimental high energy physics, and for his advice, tolerance and continuous support as my thesis adviser.

Many current and ex-members of the Rutgers-Michigan-Minnesota-Wisconsin Hyperon Collaboration contributed to this experiment. In particular, I would like to thank Bob Handler for writing the reconstruction program, Bryon Lundberg and Craig Dukes for their help with the data taking, and Gina Rameika for her suggestions in the early stage of the analysis. Thanks also go to Andy Beretvas, Ken Heller, Oliver Overseth, Marleigh Sheaff and Lee Pondrom for many helpful discussions.

Above all, I would like to thank my wife, Po-Ling, my parents, my brothers and sister for their understanding, support and encouragement that they have given me throughout my academic career.

天下萬物生於有
有生於無

Matter in the Universe is
originated from being,
Being from nothingness。

Laotse, Dao Dé Jing

TABLE OF CONTENTS

LIST OF TABLES

LIST OF FIGURES

CHAPTER 1

INTRODUCTION

The Fermilab Neutral Hyperon Beam Collaboration in 1976 discovered that the Λ hyperons produced by 300 GeV/c protons in the inclusive interaction p + Be -> Λ + X, where X stands for the unobserved particles, were polarized [1]. The polarization was of the order of 15 % at transverse momentum of 1 GeV/c and Feynman x of 0.5. This discovery was confirmed by several experiments performed with different kinds of target material at proton energies of 24, 28.5 and 400 GeV/c, and by p-p collisions at total center of mass energies of 53 and 62 GeV at the ISR [2]-[7].

Another series of experiments found that Ξ^0 hyperons inclusively produced by protons were polarized with magnitude and kinematic dependence similiar to the Λ's [8]-[9], but protons and $\bar{\Lambda}$'s were not polarized [6], [10]-[12]. By precessing the polarization vector in a uniform magnetic field, the magnetic moments of the Λ and the Ξ^0 were measured to high precision [8]-[9], [13].

Motivated by the neutral hyperon results, a charged hyperon beam was installed at Fermilab in November, 1979. Experiment E620 was then performed by the Hyperon Collaboration of Rutgers University, University of Michigan, University of Minnesota and University of Wisconsin. The goal of the experiment was to search for the inclusive polarization of the Σ^+, Σ^-, Ξ^- and Ω^- hyperons and to measure their magnetic moments if they were polarized.

Prior to E620 and the CERN-SPS charged hyperon experiments, the properties of the Ω^- were studied in bubble chamber experiments using low energy K^- beams. These investigations were hampered by low statistics, a consequence of limited energy available to produce Ω^-'s. However, the current value of the Ω^- mass, which is 1.67245 ± 0.00032 GeV/c [14], was determined by these bubble chamber experiments [15]-[22]. The two highest statistics experiments, each with 40 Ω^-'s, were able to measure the lifetime, the asymmetry parameter for the $\Omega^- \rightarrow \Lambda K^-$ decay and the spin of the Ω^- [21]-[22] with limited precision. The lifetime was found to be $(0.78\pm0.10)\times10^{-10}$ s, and the asymmetry parameter was measured to be 0.10 ± 0.3. For the spin determination, only the spin 1/2 assignment was ruled out. The quark model [23]-[24] predicts that the spin of the Ω^- should be 3/2.

With the advent of higher energy accelerators, it is now possible to construct secondary hyperon beams which provide a large number of Ω^-'s. In 1977, the CERN-SPS charged hyperon beam began operation [25]. With a 210 GeV/c proton beam striking a beryllium oxide target, an almost monochromatic secondary charged beam was produced. A sample of Ω^-'s produced at an angle of about 2 mrad was collected at momenta of 98 and 115 GeV/c. The lifetime, branching ratios of several decay modes and the asymmetry parameter were measured to the precision of a few percent. Based on 2,437 $\Omega^- \rightarrow \Lambda K^-$ decays, the lifetime was measured to be $(0.822\pm0.028)\times10^{-10}$ s [26]. With 1,400 $\Omega^- \rightarrow \Lambda K^-$ events, the asymmetry parameter reported in 1978 was 0.06 ± 0.14 [27]. For the first time, the branching ratios of the $\Omega^- \rightarrow \Lambda K^-$, $\Omega^- \rightarrow \Xi^0\pi^-$ and $\Omega^- \rightarrow \Xi^-\pi^0$ were determined to be 0.686 ± 0.013, 0.234 ± 0.013 and 0.080 ± 0.008 respectively [28]. This implied that the ratio of the branching ratios, $Br(\Xi^0\pi^-)/Br(\Xi^-\pi^0)$, was 2.93 ± 0.50. If the Ω^- decay obeyed the $\Delta I=1/2$ rule, a value of about 2 for the ratio would be expected. However, within the framework of QCD, the $\Delta I=1/2$ contribution to the Ω^- decay amplitude would be weaker than that to the other hyperons. Finjord [29] predicted that the ratio should be 3 which agreed with the experimental result. Furthermore, one $\Omega^- \rightarrow \Xi^0(1530)\pi^-$ and three $\Omega^- \rightarrow \Xi^0 e \bar{\nu}_e$ decays were also observed, giving branching ratios of the order of 2 x 10^{-3} and 1 x 10^{-2} respectively. In addition, the invariant cross section of the Ω^- produced by protons was measured to be (0.45 ± 0.08) μb/GeV^2/nucleon at x = 0.48 and (0.29 ± 0.08) μb/GeV^2/nucleon at x = 0.55 [25]. Since the Ω^-'s had very small transverse momentum, they would not have any vector polarization or higher odd rank tensor polarizations (these will be defined in section 6.1) even if they were polarized in the same manner as the other hyperons. As a result, there was no attempt to measure the magnetic moment of the Ω^- in this CERN experiment.

Recently, with 15,000 Ω^-'s, the CERN Hyperon Group remeasured the lifetime of the Ω^- to be $(0.803\pm0.012\pm0.013)\times10^{-10}$ s and the asymmetry parameters $\alpha_{\Lambda K}$ to be -0.017 ± 0.039 and $\alpha_{\Xi^0\pi^-}$ to be -0.013 ± 0.116 [30]. The results of the asymmetry parameters were consistent with the predictions that the $\Omega^- \rightarrow \Lambda K^-$ and $\Omega^- \rightarrow \Xi\pi$ decays be nearly parity conserving [29], [31]-[32].

In E620, a total of 1,743 recontructed $\Omega^- \rightarrow \Lambda K^-$ decays were collected which was the second biggest Ω^- sample in the world to date. This thesis presents the results of the study of this Ω^- sample. New measurements on the invariant differential production cross section of the Ω^- produced by proton, the lifetime of the Ω^- and the asymmetry parameter for the $\Omega^- \rightarrow \Lambda K^-$ decay are given. A new method of relating the polarization of the daughter Λ to the vector polarization of the Ω^- is described. The first measurements of the inclusive vector polarization of the Ω^- and its magnetic moment are also presented.

CHAPTER 2

APPARATUS

2.1 Introduction

In E620, Ω^- hyperons were produced by 400 GeV/c protons incident on a beryllium target. A secondary charged beam was formed and momentum selected by a magnetic channel. After the Ω^- passed through the channel, the charged particles of the decay sequence

$$\begin{array}{l} \Omega^- \rightarrow \Lambda K^- \\ \qquad\quad \hookrightarrow p\pi^- \end{array}$$

were detected by a multiwire proportional chamber spectrometer. The configuration of the apparatus in plan and elevation view are shown in Fig. 2.1. Primarily, it

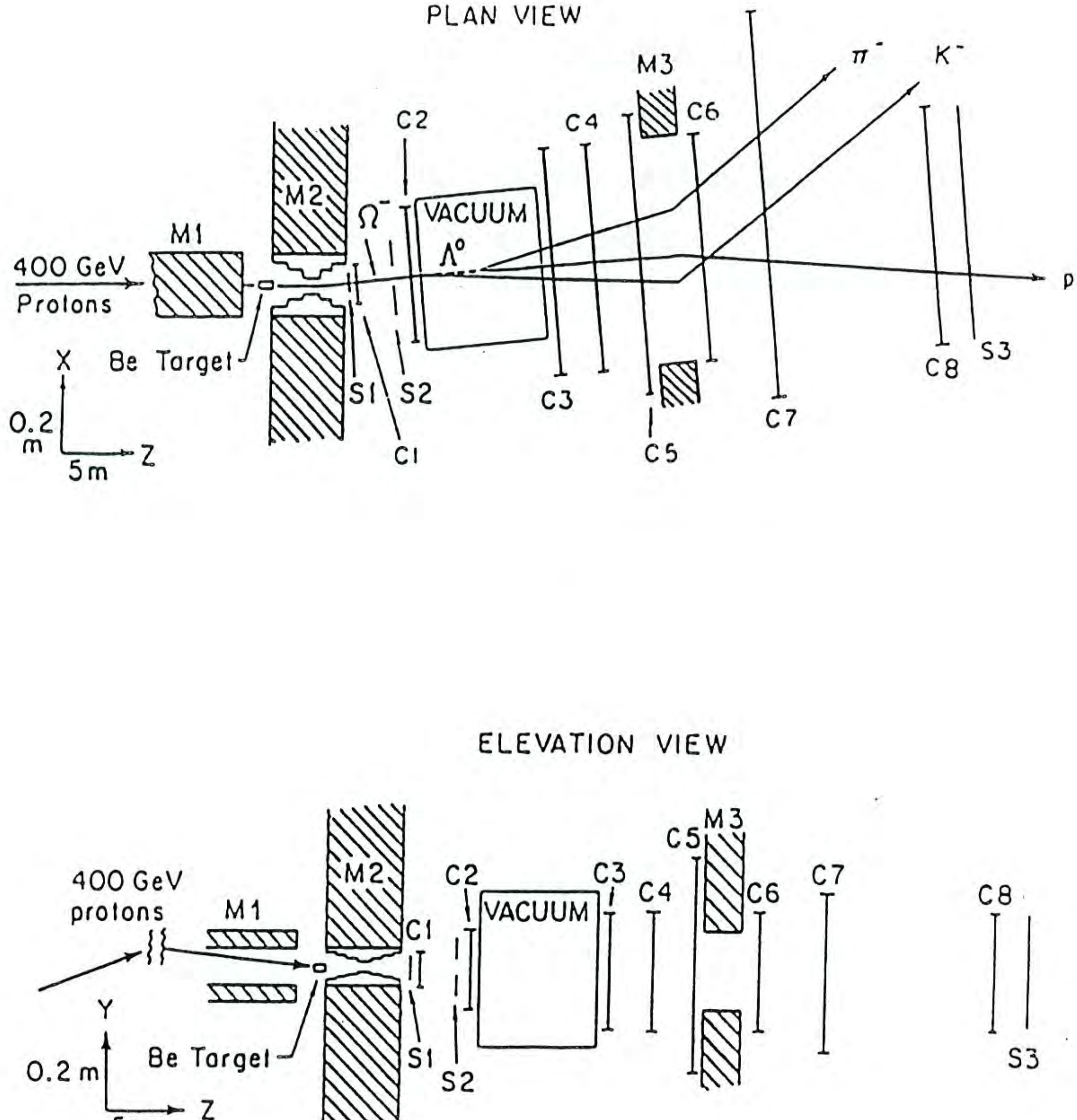

Figure 2.1 Plan and elevation views of the spectrometer with a typical event topology of the decay sequence $\Omega^- \rightarrow \Lambda K^-$, $\Lambda \rightarrow p\pi^-$ shown. M1-M3 are magnets, S1-S3 are scintillators and C1-C8 are multiwire proportional chambers.

was designed to maximize the detection efficiency of the $\Xi^- \to \Lambda\pi^-$, $\Lambda \to p\pi^-$ decay sequence, which has a similiar topological pattern as the decay of the Ω^-. The study of the Ξ^- hyperon is given in reference [33].

2.2 Proton Beam and Target Area

The Meson Laboratory M2 beam line at Fermilab was used for the experiment. The beryllium target was a cylindrical rod of 15.3 cm long and 0.635 cm in diameter. In this section, all distances will be measured either upstream (-) or downstream (+) from the center of the target. The 400 GeV/c diffracted proton beam was brought down the M2 line with a simple beam transport system as shown in Fig. 2.2. The proton beam was first brought to an intermediate horizontal and vertical focus at -250 m by a set of quadrupoles. Then a final focus was produced at the hyperon production target by another set of quadrupoles. The beam intensity was controlled by sets of horizontal and vertical collimators at -340 m and -250 m respectively, as well as by varying the incident angle of the primary proton beam at the meson target.

The incident angle of the secondary proton beam on the hyperon target was controlled by a set of dipole magnets which bent the beam in the vertical plane. After being deflected out of the horizontal median plane by a vernier magnet at -111.2 m, the beam was restored to that plane at the target by the M1 bending magnet which was at -7.54 m. In this way, it was possible to set the vertical production angle anywhere in the range from -10 mrad to +10 mrad.

The beam monitoring system, illustrated in Fig. 2.3, was made up of a segmented wire ion chamber (SWIC), an argon-filled ion chamber and a scintillator telescope. The centers of these instruments were aligned with the axis tangent to the central orbit at the entrance of the beam channel which will be described in the next section. The telescope, located at -1.55 m, consisted of three concentric scintillators, a 0.635 cm diameter counter, another one of 1.27 cm in diameter and a halo counter with a 0.635 cm circular hole in its center. At low intensities, typically less than 10^6 protons, the telescope served as a beam tuning monitor and was used to calibrate the ion chamber. During the experiment, the intensities, ranging from 2.5×10^7 to 2.5×10^8 protons per machine spill, were measured primarily by the ion chamber which was positioned at -1.11 m and the telescope was removed from the beam. The position and the sharpness of the proton beam spot were monitored by the SWIC at -0.91 m.

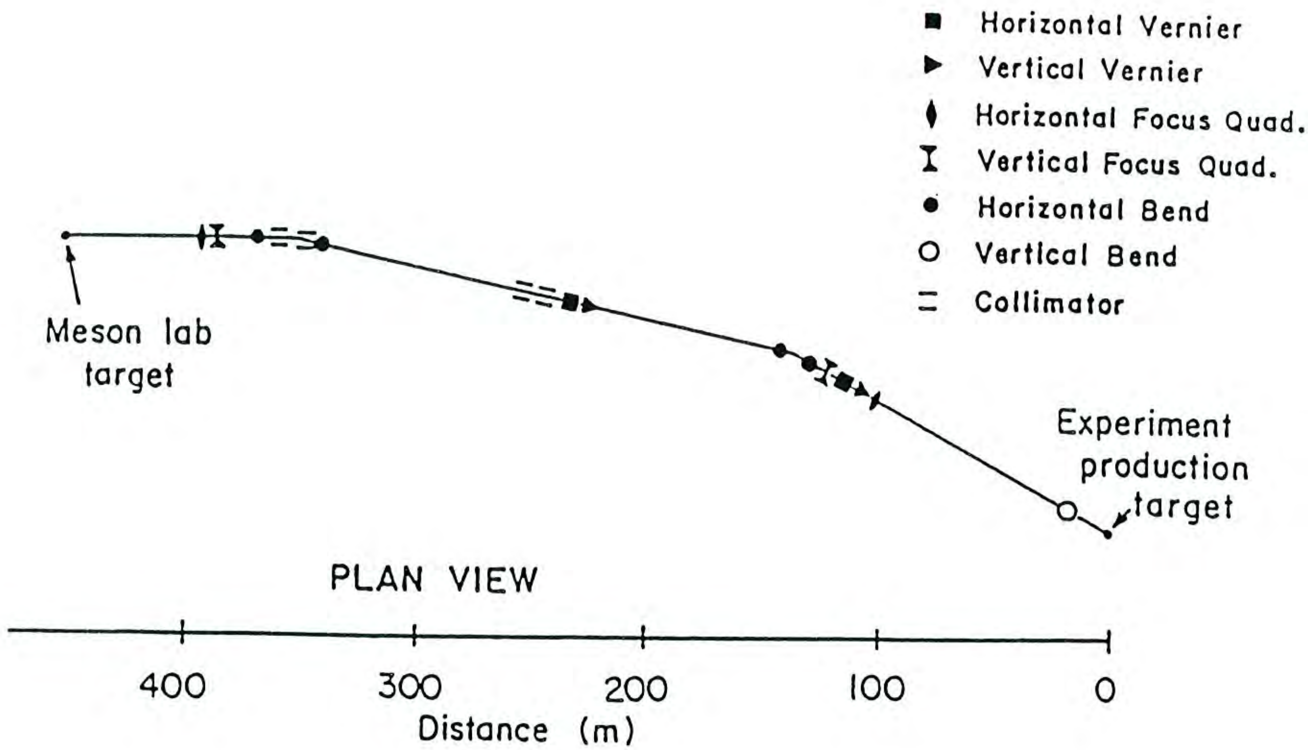

Figure 2.2 The M2 beam delivery system (not to scale).

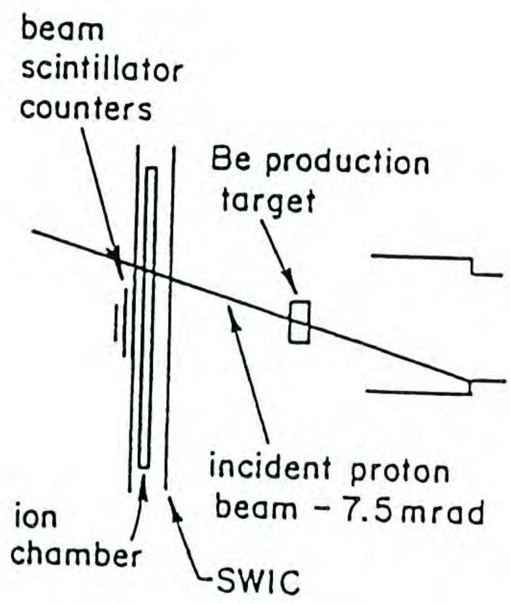

Figure 2.3 The hyperon production target and associated detectors. The horizontal scale has been greatly compressed for this drawing.

2.3 Secondary Charged Beam

The secondary charged beam was momentum selected by a collimation system embedded in a 5.28 m long dipole magnet M2 with a vertical uniform field. The design of the collimator is shown in Fig. 2.4. It consisted of nine brass blocks, each with a straight cylindrical hole approximately centered on the circular arc of the central orbit. The openings of these channels ranged from 1.27 cm to 2.54 cm in diameter. The fifth and the ninth blocks were reinforced by circular tungsten inserts of 0.4 cm and 1 cm diameter respectively. The entire channel provided a 10 mrad bend for the central ray. As a function of the momentum, the fractional acceptance of the channel with a 6.6 T-m field is shown in Fig. 2.5. At this field integral, the momentum of the central orbit was 200 GeV/c and the median momentum was about 190 GeV/c.

Apart from selecting a particular Ω^- momentum distribution and eliminating neutral and positively charged particles, the M2 magnet was also used to precess the spins of the Ω^-'s. The field in the vicinity of the channel was carefully mapped out in a previous experiment [34]. For each run, the field was measured by a proton magnetic resonance probe located at a fixed place in the eighth collimator block. The field integral was known to an

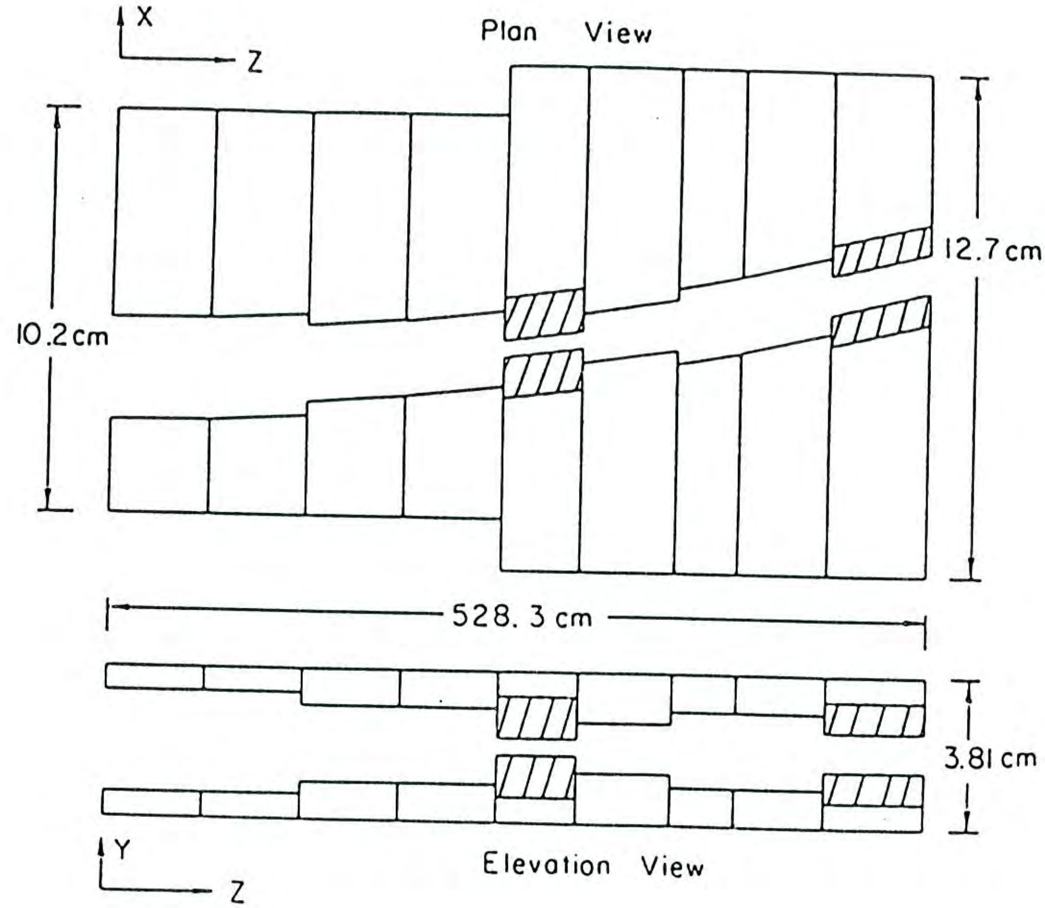

Figure 2.4 Plan and elevation views of the charged hyperon collimator. The cross-hatched regions represent tungsten inserts.

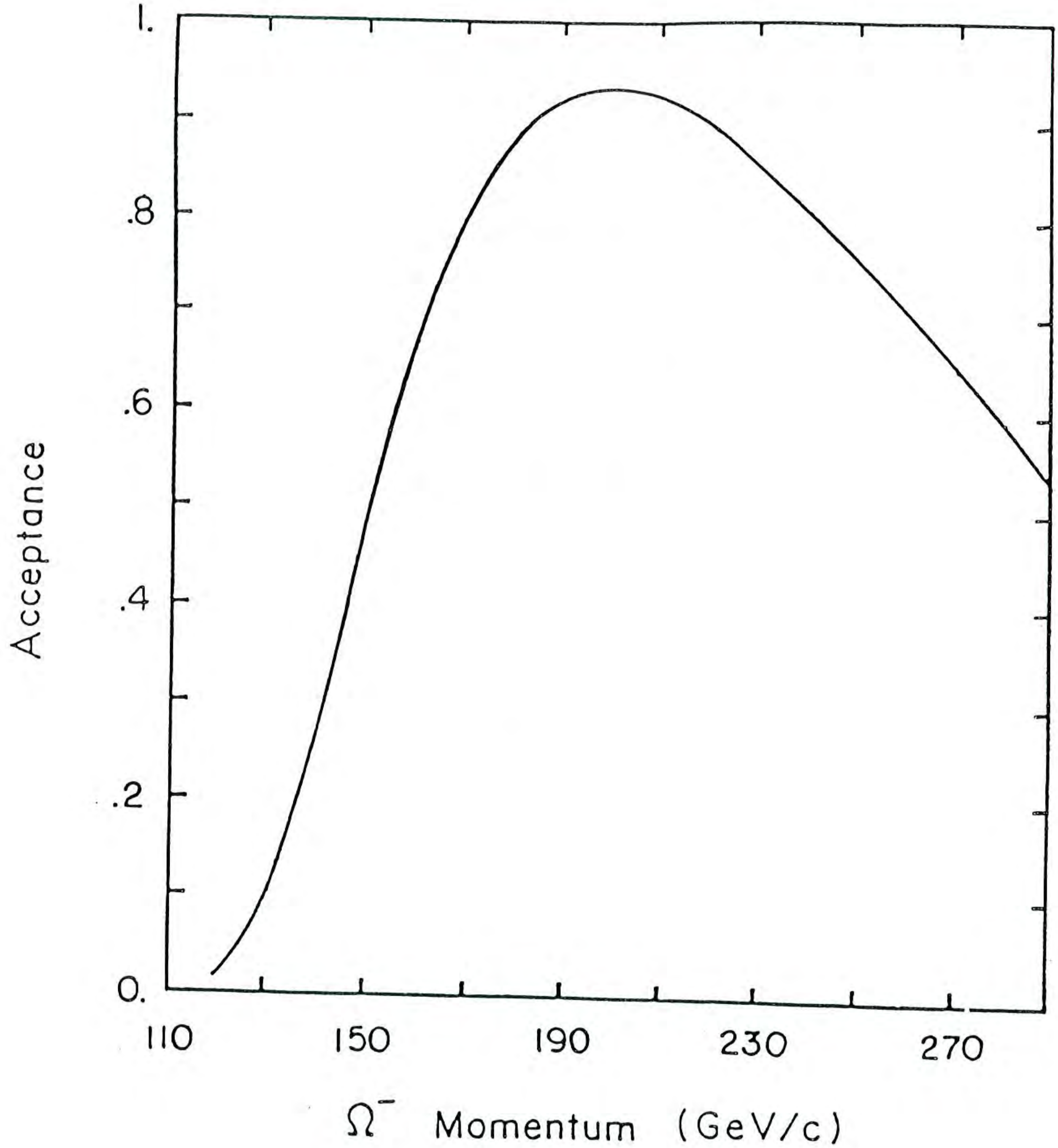

Figure 2.5 Fractional momentum acceptance for the charged hyperon beam channel with a 6.6 T-m field integral.

accuracy of about 0.1 %, and fluctuations in the field setting between successive runs were less than 0.1 %.

2.4 Coordinate Systems and Sign Conventions

The +z axis was defined everywhere as downstream and tangent to the central orbit of the curved channel. The +y axis pointed vertically upward and the +x axis was chosen to be $\hat{y} \times \hat{z}$. The origin of the spectrometer coordinate system was at the exit of the channel.

The sign of the production angle at the target was defined as positive when $\vec{p}_{in} \times \vec{p}_{out}$ was parallel to $\hat{x}$, where $\vec{p}_{in}$ is the momentum vector of the incident proton beam and $\vec{p}_{out}$ is the momentum vector of the produced particle.

The field in the M2 magnet was defined as positive when it was set along the $+\hat{y}$ so that negatively charged particles moving in the $+\hat{z}$ direction were bent toward $+\hat{x}$.

2.5 Spectrometer

As shown in Fig. 2.1, the spectrometer consisted of eight multiwire proportional chambers (MWPC), three scintillation counters and a superconducting momentum analyzing magnet, M3. The MWPC's were all installed with their wire planes perpendicular to the +z axis of the spectrometer coordinate system and were level to within 1 mrad.

The design of the proportional chambers and the associated readout electronics have been described in detail elsewhere [35]. Most chambers had a horizontal and a vertical signal plane with 2 mm wire spacing. In C4, the two orthogonal planes were rotated by 45 about the z axis, forming the U and V planes. There was an additional sense plane rotated by 45 degrees counterclockwise in C5 that had a wire spacing of $2\sqrt{2}$ mm. The rotated planes were used for associating the x and y views in the event reconstruction.

The chambers were filled with a gas mixture of 99.9 % argon and 0.1 % freon bubbled through methylal at 4 C°. The operating voltages of the chambers ranged from -3.1 to -3.5 kilovolts.

The analyzing magnet M3 was 2.50 m long and had an aperture of 20.3 cm by 61 cm. The magnet was operated at a current which gave a 1.8 tesla field in the +y direction. This corresponded to a field integral of 3.17 T-m or a transverse momentum transfer of 0.95 GeV/c. The field setting was constant in time to better than 0.5 % throughout the entire experiment.

The uniformity of the field was studied in an earlier experiment with a field map [34] and in the Σ^- phase of E620 with single charged particle tracks [36]. Field aberrations were determined up to the sextupole component and the two methods agreed. On the average, the strength of the non-uniformity was of order 1 % of the field setting.

Since the oppositely charged particles were separated after M3, C7 and C8 were divided into positive (R) and negative (L) segments. These two chambers were installed in such a way that the K^-s and π^-s from the $\Omega^- \rightarrow \Lambda K^-$ and $\Lambda \rightarrow p\pi^-$ decays would hit C7L whereas the protons would pass through C8R.

The presence of a charged particle was signaled by a 10 cm diameter scintillation counter S1 at the exit of the collimator. There was a halo veto counter S2 between C2 and C3. It had a 3.7 cm by 5.1 cm rectangular aperture in it. This limited the angular dispersion of the particles which would be detected by the spectrometer. S3 was a 20 cm by 60 cm counter placed behind C8. It covered most of the active region of C8. S3 served as the reference counter with a sharp timing pulse for the trigger logic.

To minimize the number of interactions and multiple scattering in the spectrometer, a 7.6 m long and 40.6 cm in diameter evacuated pipe was placed between C2 and C3. Furthermore, plastic bags filled with helium gas were installed between chambers, except the region between C2 and C3. About 90 % of the scattering occurred in the region upstream of C3. The estimated amount of material in this region was 3.6 % of a radiation length, or 1 % of a nuclear interaction length.

2.6 Trigger Logic and Data Acquisition

The prompt signals from the horizontal wires of each chamber were added together in an OR circuit to give an output pulse. Signals from the scintillation counters and some selected chambers were then combined to create the event trigger. Then the good event logic sent a pulse to each chamber to enable the storage of the wire hit information for the event. The information was kept until read out. Further triggers were inhibited by a 'busy' logic level or inhibit gate. A PDP 11/45 computer was employed to read information via a CAMAC interface. This process took about 0.5 msec to complete. Once the data transfer was over, the inhibit gate was turned off and all registers were reset for the next event. Information read in by the computer was temporarily stored in the core memory and subsequently transferred to disk.

At the end of the synchrotron cycle, the data on disk were copied onto a magnetic tape. Then the readings of 24 gated and ungated CAMAC scalers containing data from different logical combinations of various scintillators and chambers as well as the ion chamber were also recorded on tape. From the gated and ungated readings, the dead time of the experiment was found to range from 15 % to 30 %. This was mainly caused by the read-out process and the transfer of data from the buffers (core memory) to the disk.

Data were taken with two different versions of the trigger. The first one was

$$\Omega^- = S1.C7L.C7R.C8R.S3$$

Approximately 70,000 three-track events were reconstructed from this trigger. However, it was found that the yield of three-track events per raw data tape was low because the trigger was not restrictive enough to suppress background coming from the particle interactions in the spectrometer. Therefore, the trigger was modified to

$$\Omega^- = S1.\overline{S2}.C3.C7L.C8R.S3$$

which increased the yield from 6 % per tape to 9 % and provided approximately 300,000 reconstructed three-track events recorded on data summary tapes.

An auxilliary trigger

$$\pi^- = S1.\overline{S2}.S3$$

prescaled by a factor of 512 and 1,024 for the 5.13 T-m data and 6.6 T-m data respectively was mixed with the Ω^- trigger. This provided a sample of single tracks, mainly pions from the beryllium target, that was used for normalization and monitoring the chamber efficiencies.

Typically 100 to 300 triggers per machine cycle were recorded. It required about 2 hours to fill a magnetic tape with approximately 75,000 triggers. Data were taken at +5 and -5 mrad for the field integral of 6.6 T-m. At the 5.13 T-m field, data were taken at +7.5 and -7.5 mrad as well as +5 and -5 mrad. The number of raw data tapes taken for each running condition is summaried in Table 2.1.

2.7 Calibration

The relative alignment of the multiwire proportional chambers was checked from time to time. With the beryllium target removed and the M3 field switched off, the M2 magnetic field was tuned to such a value that a very low intensity 400 GeV/c proton beam was transmitted through the collimator channel. The trigger was simply $S1.\overline{S2}.S3$ without any prescale factor. The centroid of the proton beam in each chamber defined the center of the chamber to an accuracy of about 0.1 mm. In turn, the centers of the chambers established the z-axis of the spectrometer coordinate system.

Data set	Trigger	$\int B.dl$ (T-m)	Production angle (mrad) +5.0	-5.0	+7.5	-7.5
1	$S1 \cdot S3 \cdot C7L \cdot C7R \cdot C8R$	6.60	15	16		
2	$S1 \cdot \overline{S2} \cdot S3 \cdot C3 \cdot C7L \cdot C8R$	6.60	19	21		
3	$S1 \cdot \overline{S2} \cdot S3 \cdot C3 \cdot C7L \cdot C8R$	5.13	6	6		
4	$S1 \cdot \overline{S2} \cdot S3 \cdot C3 \cdot C7L \cdot C8R$	5.13			4	4

Table 2.1 Summary of Data tapes. About 75,000 triggers per tape.

CHAPTER 3

DATA ANALYSIS I: EVENT IDENTIFICATION

3.1 Event Reconstruction

The reconstruction program was designed to search for events that had the topological pattern of the $\Omega^- \rightarrow \Lambda K^-$, $\Lambda \rightarrow p\pi^-$ decay sequence, i.e. two negatively charged tracks, one positively charged track and two vertices. After being decoded and sorted, the wire hits were converted to x and y positions in the spectrometer coordinate system.

The first level filtering of events was based on the hit pattern in C3, C4, C5, C6 and C7. Triggers with too many or too few hits in these chambers were classified as class 2, 3, 4 or 5. The definition of the class codes is given in Table 3.1. Approximately 63 % of the triggers belonged to this group and were rejected. The next step was to look for three tracks in the y-z plane (y view). The track finding procedure was done by selecting hits that gave the best fit to straight lines. Triggers in classes 6 and 12 were thrown out at this stage. This threw away about 23 % of all triggers.

To reconstruct the tracks in the x-z plane (x view), hits in C4 and the U plane of C5 were employed to pick out the x hits associated with the y tracks. The x tracks were fitted separately upstream and downstream of the analyzing magnet. Then the upstream tracks were matched with the downstream tracks at the bend plane of M3. The matched tracks were arranged in such a way that the first one was the positive track whereas the second and the third were the low momentum and the high momentum negative tracks respectively. About 8 % of all triggers that did not have three matched x tracks were eliminated as classes 1, 7, 8 and 9.

For the remaining approximately 9 % of the triggers, the 'Λ' vertex was determined as the closest approach of the positive track to the low momentum negative track and the 'Ω^-' vertex as the closest approach of the

1	Three track event, only one hit in the x view after M3
2	Three of the four planes of C3 and C4 have less than two hits
3	Four of the six downstream y planes have 4 or more hits
4	Four of the six downstream y planes have less than two hits
5	Less than two of the y planes of C3, C5, C6 and C7 have two or three hits
6	Cannot find more than two points on one of the y view tracks
7	Three tracks in y view but cannot find them in x
8	Three tracks before M3, but only two tracks after
9	The stiff track bends the same way as one of the soft tracks
10	Bad chi-square in geometrical fit, chi-square set to 10,000
11	Geometrical chi-square greater than 100 and less than 10,000
12	Two track event in y view
0	Good three track topology

Table 3.1 Reconstruction Quality codes

reconstructed 'Λ' trajectory to the remaining negative track. If the 'Λ' vertex was upstream of the 'Ω^-' vertex, the negative tracks were interchanged and the vertices were recalculated. A geometric χ^2 based on the parameters of the tracks, chamber hits and the vertices was calculated. Nine percent of the three-track events having χ^2 greater than 100 for an average of 18 degrees of freedom were put in classes 10 and 11 which were removed from the sample. The geometric χ^2 distribution of the final good three-track events is shown in Fig. 3.1.

Using the reconstructed slopes of the tracks and the field strength of M3, the momentum components of the tracks were determined. The invariant mass of the vee formed by the first two tracks was calculated, assuming that the associated particles were a proton and a π^-. The distribution is shown in Fig. 3.2. The full width at half maximum of the distribution was approximately 4.0 MeV/c^2 and the mean was 1.1157 GeV/c^2, in good agreement with the known Λ mass. The vee was then kinematically fitted to a $\Lambda \rightarrow p\pi^-$ decay. The resulting kinematic χ^2 of the fit is shown in Fig. 3.3. Most of the events with the p-π^- invariant mass within $\pm$7.5 MeV/c^2 from the Λ mass were found to have a kinematic χ^2 less than 20.

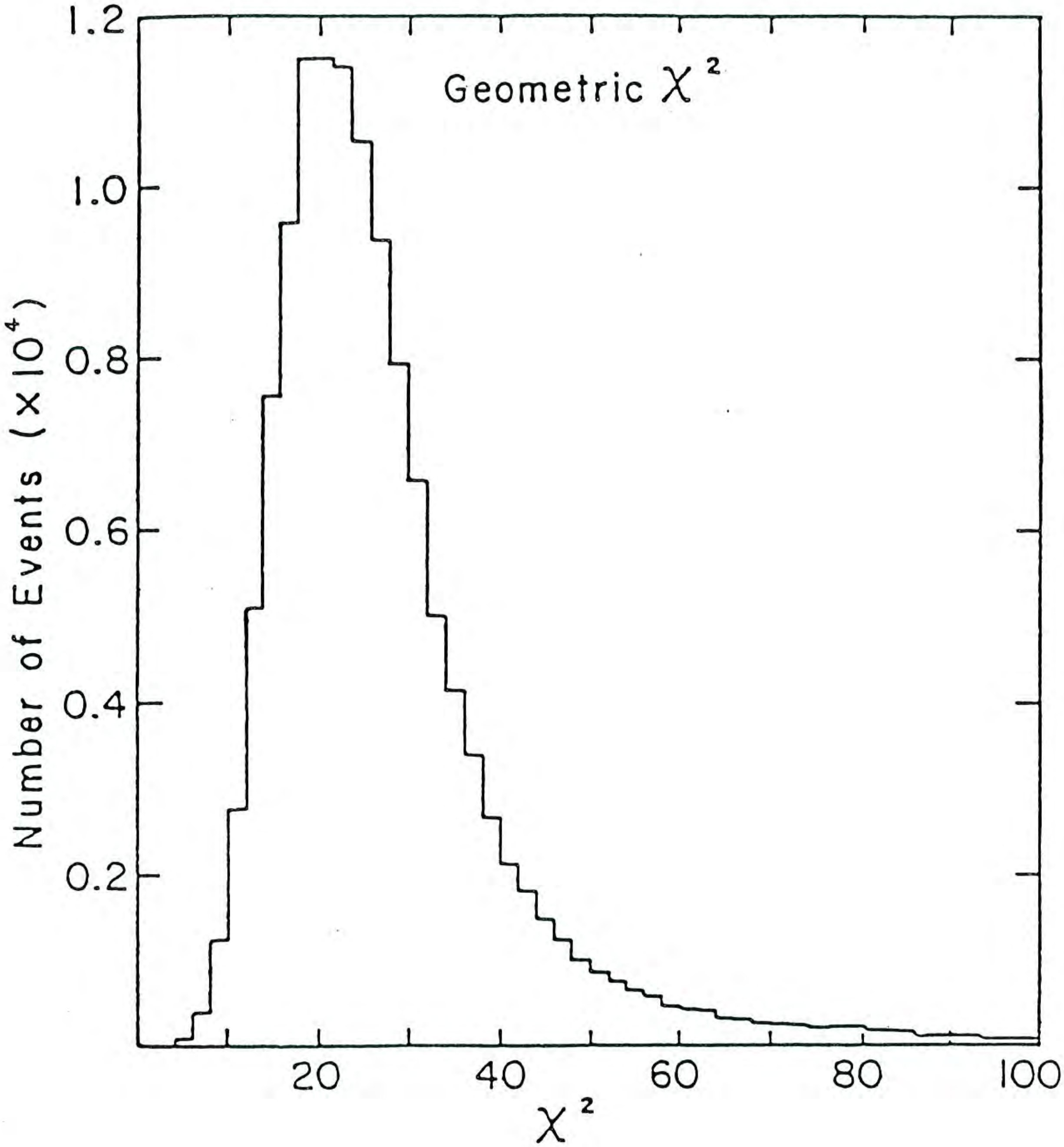

Figure 3.1 Geometric χ^2 distribution for three track events with vertex separation greater than zero. Typically there were ~~18~~ degrees of freedom for these events. 28

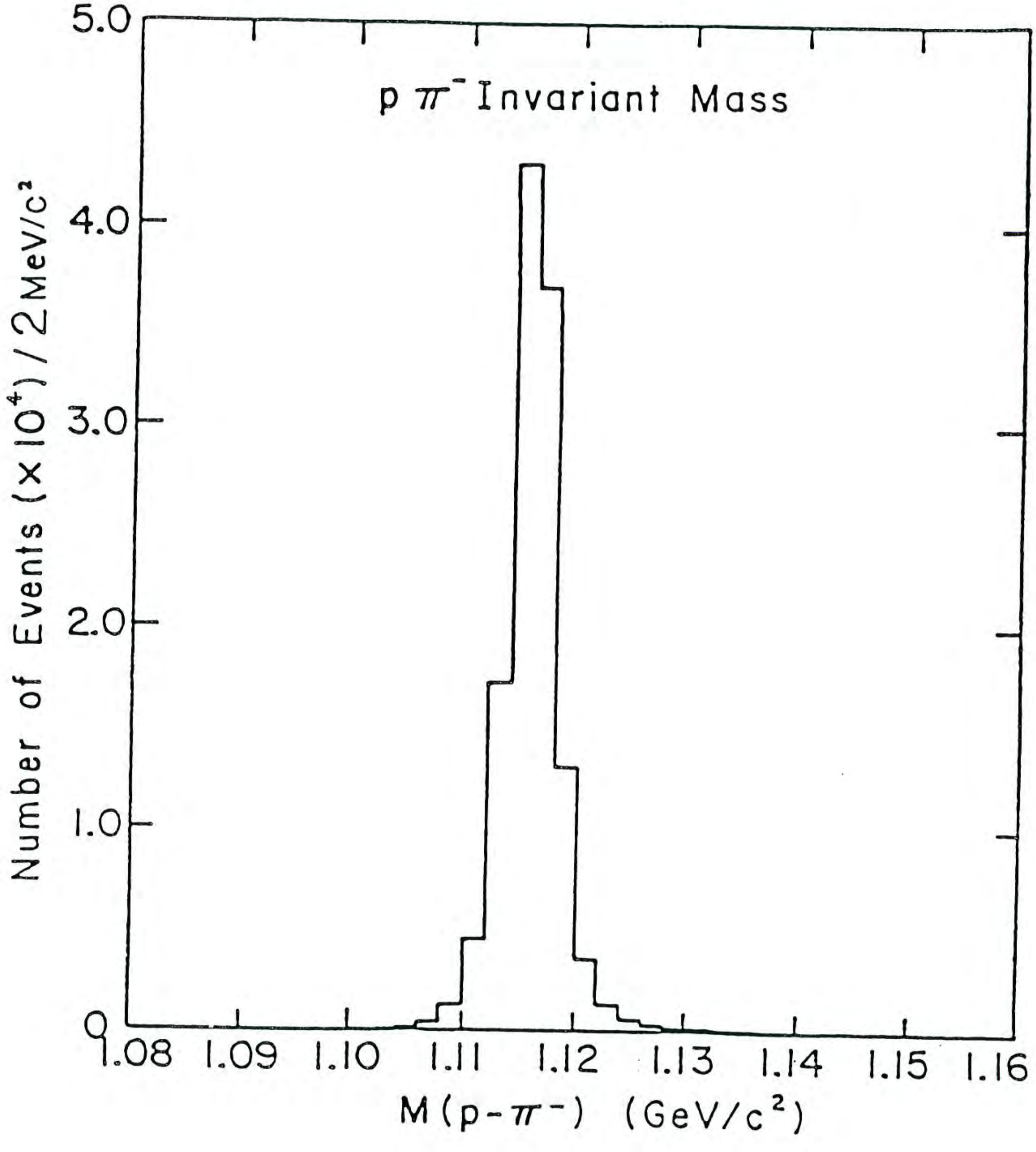

Figure 3.2 p-π^- invariant mass distribution for events with geometric χ^2 less than 100 and vertex separation greater than zero.

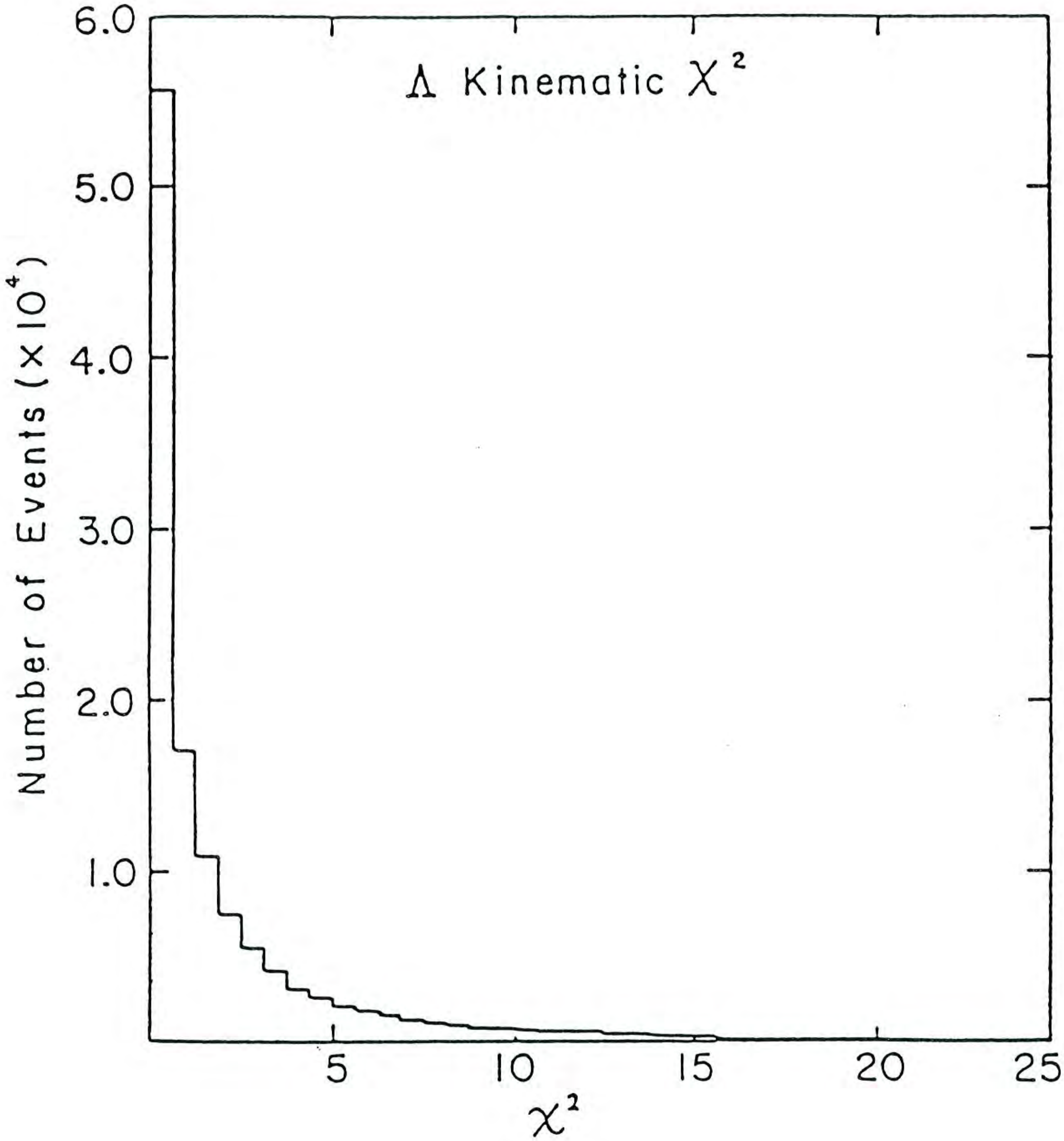

Figure 3.3 Kinematic χ^2 distribution for $p-\pi^-$ constrainted to fit the Λ mass. There was 1 degree of freedom.

The geometric χ^2, the vertices, the momentum components of the tracks, the kinematic χ^2 and the fitted Λ momentum vector as well as other relevent information of each event were written to a data summary tape. There were three data summary tapes containing approximately 380,000 good three-track events. From this point on, the analysis was performed with these data summary tapes.

3.2 Monte Carlo Simulation

The performance of the reconstruction program was studied with a Monte Carlo computer program which simulated the experiment as closely as possible.

A Monte Carlo event was generated as follow. In the target of 6 mm in diameter, a fictitious particle was produced at a point chosen from a gaussian distribution which simulated the beam spot. If the event was outside the physical size of the target, a new one was generated. The momentum of the particle was chosen from a spectrum which was designed in such a way that the momentum distribution of the accepted events would be the same as that of the experimental data. Another point at the upstream end of the defining collimator (the fifth collimator block) was generated at random in a disc of 4 mm in diameter. From these generated points and the momentum, the direction of the particle was determined. Then, the position of the particle at the downstream end of the defining collimator was calculated. If the particle passed through the defining collimator, it was allowed to decay according to the exponential decay law. The momentum vectors of the daughters could be generated correctly for a polarized or unpolarized parent particle in its rest frame. In the case that the generated decay position was inside the beam channel, the charged daughter particles were required to pass through the channel. Furthermore, any daughter particle with a lifetime less than 10^{-7} seconds was allowed to decay with the appropiate probability.

The particles were required to pass through all spectrometer apertures. The trajectories of the charged particles were modified with the appropiate amount of multiple Coulomb scattering, and their positions at the locations of the MWPC's were then calculated.

At intervals of 50 events, the mean field of M3 was allowed to fluctuate at random with a maximum variation of 0.5 %. In addition, the non-uniformity of the field described in section 2.5 was also implemented in the program.

If the event satisfied the trigger, then the calculated hit positions at the multiwire proportional chambers were digitized. On the average, for tracks within 6 % of the central region between two wires, both wires were hit. Chamber inefficiencies as well as random wire hits were also simulated. The inefficiency and the probability of getting two adjacent hits for each wire plane are tabulated in Table 3.2. These pieces of information as well as the number of random hits were estimated from the calibration runs and the single-track π^- triggers.

Wire hits were passed to the reconstruction program. The reconstruction efficiency was determined to be 77 %. Eight percent of the Monte Carlo events failed because of too many or insufficient wire hits. Another major cause of the failures was the small opening angle(s) between two or more tracks. This resulted in misindentification of tracks which occurred for 10 % of the events. The remaining 5 % of the events were three track events with a few wire hits assigned to the wrong track. As a result, these events had a geometric χ^2 greater than 100.

Approximately 8 % of the good three-track Monte Carlo events had a p-π^- invariant mass outside the interval of ± 7.5 MeV/c^2 from the Λ mass.

Chamber	Plane	Inefficiency (%)	Probability of 2-wire hits (%)
1	x	4.6	7.4
	y	3.5	5.3
2	x	3.4	2.5
	y	5.9	2.5
3	x	0.7	7.3
	y	0.8	5.4
4	v	2.3	6.1
	u	1.4	3.6
5	x	2.4	4.0
	y	3.2	7.2
	u	4.0	2.4
6	x	0.7	8.9
	y	3.7	4.5
7	x	0.6	8.9
	y	0.0	5.7
8	x	0.5	11.0
	y	1.1	13.0

Table 3.2 Inefficiencies and probabilities of getting 2 adjacent wire hits of the MWPC wire planes.

Both the generated and reconstructed information were written on disk in the same format as the data. These Monte Carlo events served as controls for the subsequent analyses.

In order to distinguish the events generated by the hybrid Monte Carlo program which will be discussed in the polarization analysis, the events produced according to the foregoing procedure are also known as the external Monte Carlo events.

3.3 Event Selection and Background Studies

In order to extract a clean $\Omega^- \to \Lambda K^-$ sample, several software constraints known as cuts were imposed on the data.

First of all, the p-π^- invariant mass of each event was required to be within ± 7.5 MeV/c^2 from the Λ mass. This ensured that there was indeed a Λ in the event. The number of real events remaining and the number of genuine $\Omega^- \to \Lambda K^-$ decays eliminated after each cut, estimated from the Monte Carlo simulation, are shown in Table 3.3.

Cut	Number of real events left	Accumulative loss of $\Omega^- \rightarrow \Lambda K^-$, (%)
0. No cuts	377,337	0.0
1. $M_{p\pi^-}$ between 1.108 and 1.123 GeV/c^2	340,153	7.8
2. $M_{\Lambda\pi^-} \geqslant$ 1.345 Gev/c^2	16,940	20.6
3. Vertex $Z_\Lambda \geqslant Z_\Omega \geqslant 0$ m	6,390	36.6
4. Cos $\theta_\Lambda \leqslant -0.4$ in Ξ^- rest frame	3,961	37.2
5. $R^2 \leqslant 1$ cm^2	2,812	38.4
6. Cos θ_K and φ_K cut in Ω^- r.f.	2,340	39.8
7. $M_{\Lambda K}$ between 1.662 and 1.682 GeV/c^2	1,743	44.4

Table 3.3 Number of real events remaining and accumulative loss of $\Omega^- \rightarrow \Lambda K^-$ decays estimated from Monte Carlo simulation with cuts applied to the samples.

The experimental data were then reconstructed as $\Omega^- \to \Lambda K^-$ decays. For each event, the remaining negative track was assumed to be a K^-. Using the fitted Λ momentum vector, the Λ-K^- invariant mass was determined. The distribution is shown in Fig. 3.4. The genuine Ω^- events were overwhelmed by background events. On the other hand, when the events were processed as $\Xi^- \to \Lambda \pi^-$ decays, a clear Ξ^- signal showed up in the Λ-π^- invariant mass distribution given in Fig. 3.5. Therefore, the Λ - π^- invariant mass of each event was required to be greater than 1.345 GeV/c^2. Monte Carlo studies showed that this should cut away at least 99 % of the $\Xi^- \to \Lambda\pi^-$ decays. The distributions of Λ-K^- invariant mass and the Λ-π^- invariant mass for the remaining events are shown in Figs. 3.6-3.7. Approximately 9,000 $\Xi^- \to \Lambda\pi^-$ decays were still left in the sample.

The Λ decay vertex was required to be downstream of the primary vertex. Furthermore, the z coordinate of the Ω^- vertex had to be positive. This cut guaranteed that the Ω^-'s passed through the entire length of the magnetic channel.

Apart from the $\Xi^- \to \Lambda \pi^-$ decay, the other potential sources of background could come from the $K^- \to \pi^+\pi^-\pi^-$, the $\Omega^- \to \Xi^0\pi^-$ and the $\Omega^- \to \Xi^-\pi^0$ decays. Applying the

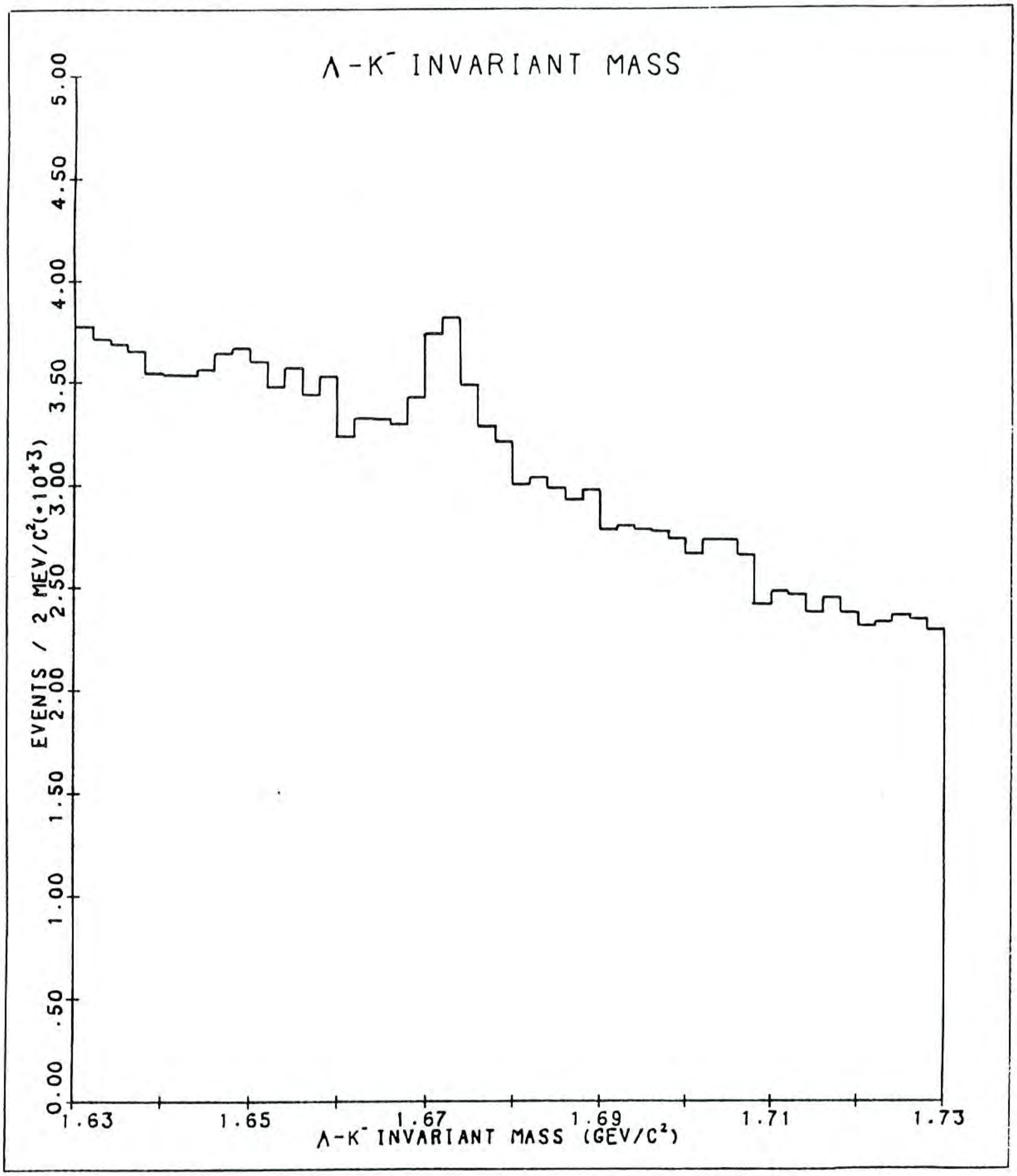

Figure 3.4 Λ-K^- invariant mass distribution for events with geometric χ^2 less than 100 and p-π^- invariant mass cut. The number of background events under the Ω^- peak is estimated to be about 3,200 per channel.

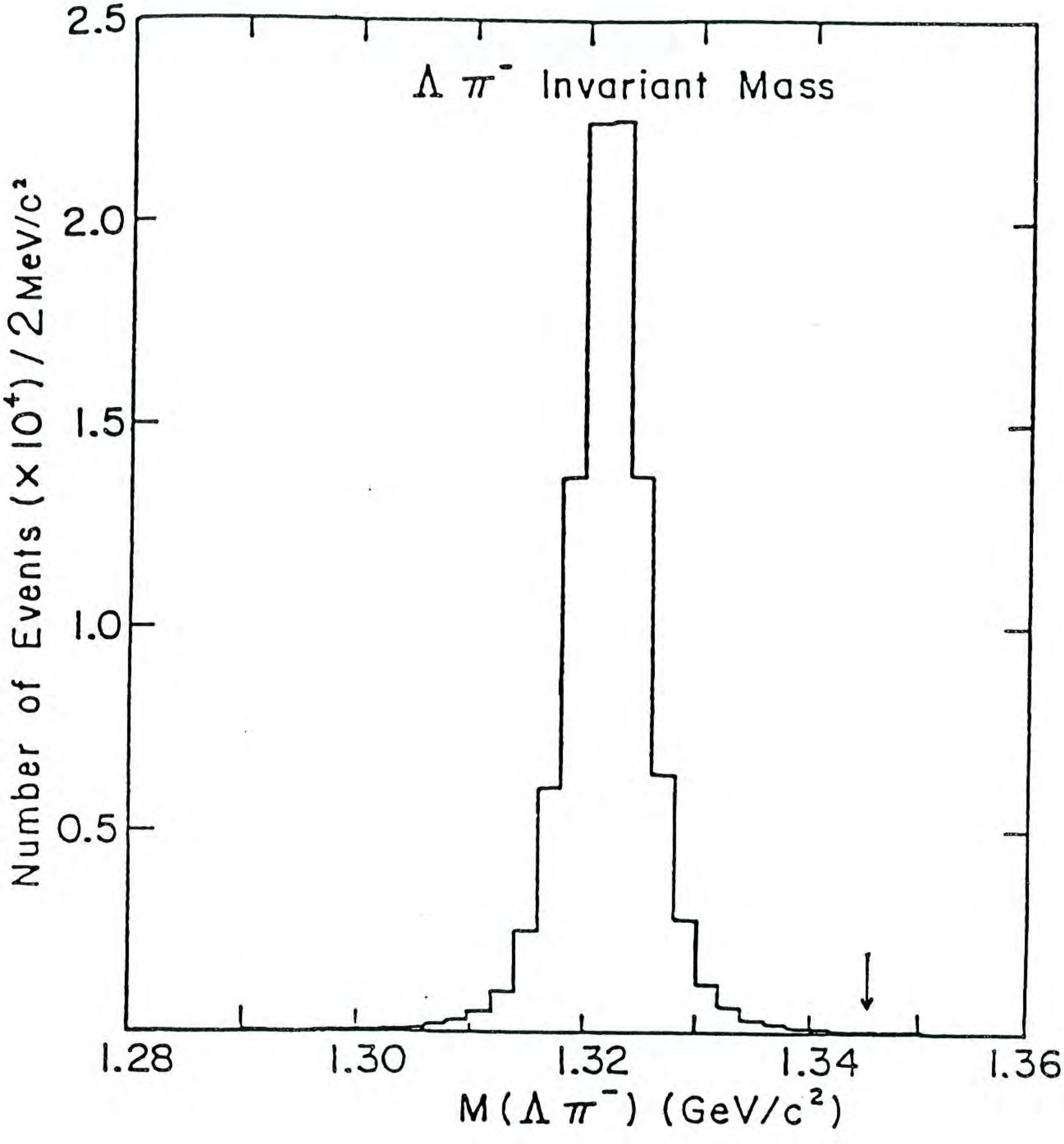

Figure 3.5 Λ - π^- invariant mass distribution for events with geometric χ^2 less than 100 and p-π invariant mass cut. The arrow shows where the cut was applied.

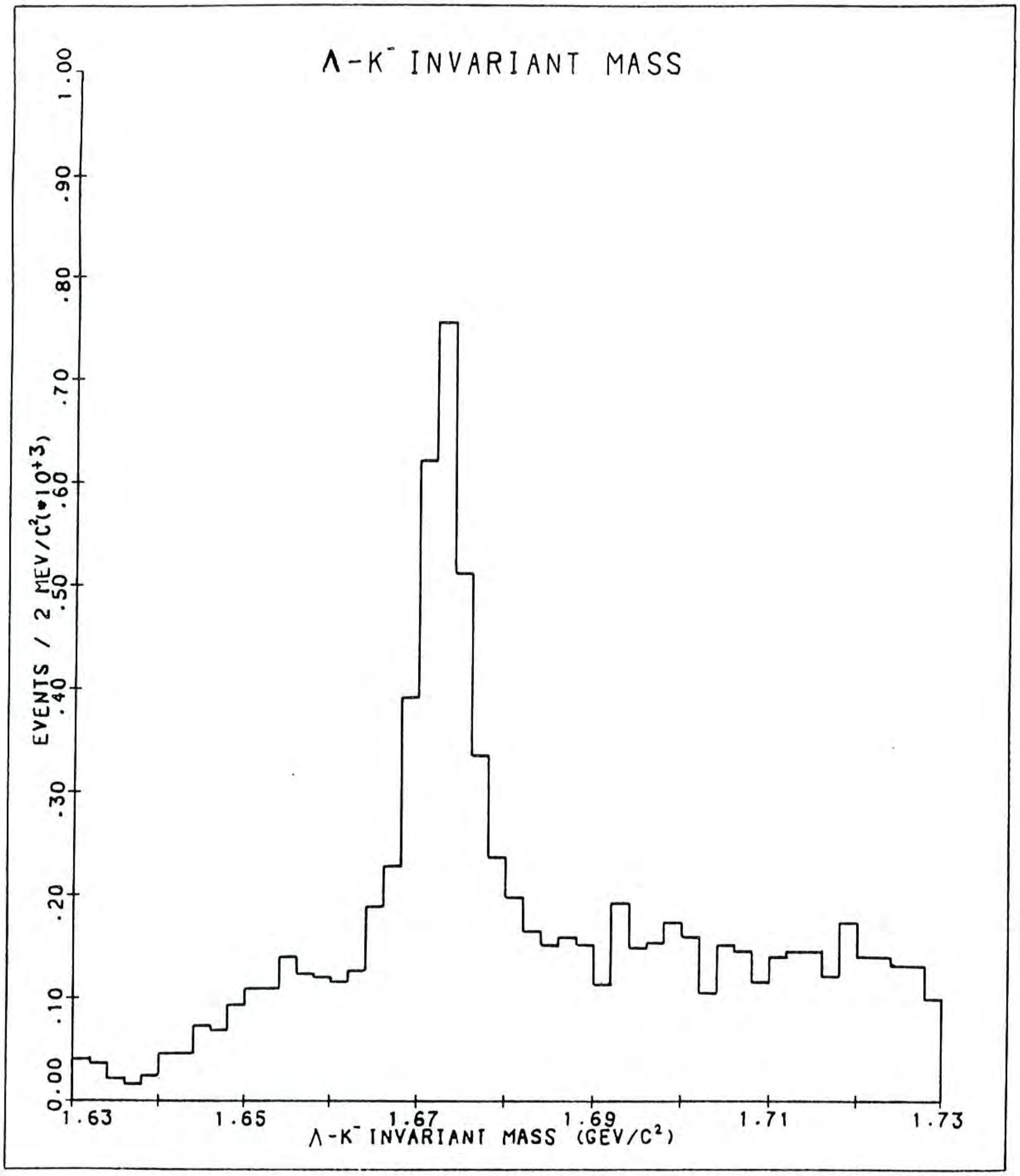

Figure 3.6 Distribution of the Λ-K^- invariant mass after the p-π^- and the Λ-π^- invariant mass cuts. The number of background events under the Ω^- peak is estimated to be about 150 per channel.

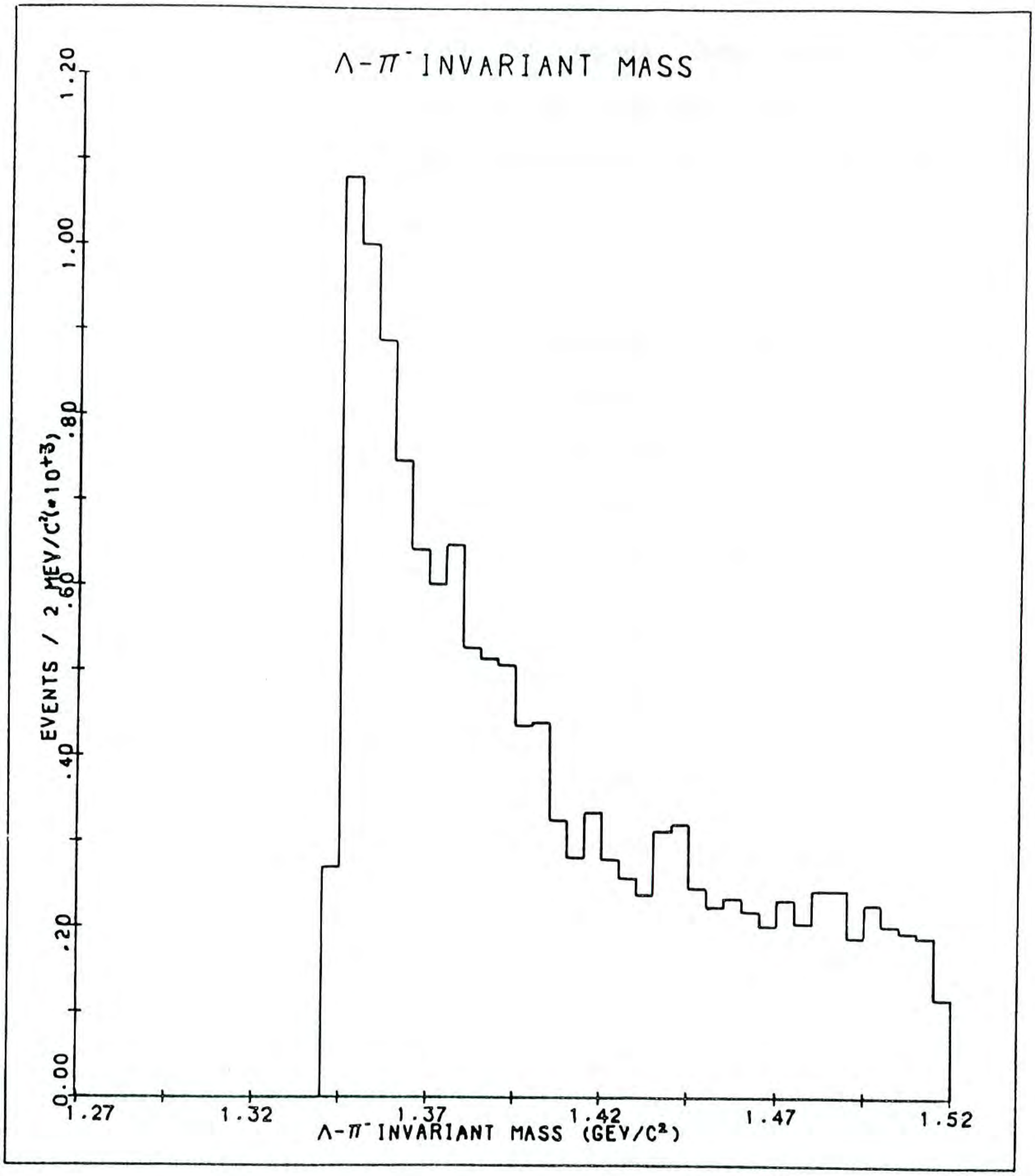

Figure 3.7 Distribution of the $\Lambda-\pi^-$ invariant mass for events that satisfied the p-π invariant mass and the $\Lambda-\pi$ invariant mass cuts.

cuts described above to the Monte Carlo samples, the $K^- \to \pi^+\pi^-\pi^-$ and the $\Omega^- \to \Xi^-\pi^0$ decays were reduced to a negligible level, but about 68 % of the $\Omega^- \to \Xi^0\pi^-$ decays still remained.

To further suppress the $\Omega^- \to \Xi^0\pi^-$ background, it was noticed in the Monte Carlo simulation that when the $\Omega^- \to \Xi^0\pi^-$ events were reconstructed under the $\Xi^- \to \Lambda\pi^-$ hypothesis, the $\cos\theta_\Lambda = \hat{\Lambda}.\hat{z}$ distribution in the rest frame of the Ξ^- was peaked at $\cos\theta_\Lambda = -1.$ and gradually dropped to zero at $\cos\theta_\Lambda = 1.$, where $\hat{z}$ is parallel to the z-axis of the spectrometer coordinate system and $\hat{\Lambda}$ is a unit vector along the direction of flight of the Λ in the Ξ^- rest frame. However, the $\cos\theta_\Lambda$ distribution of the $\Omega^- \to \Lambda K^-$ events in the Ξ^- rest frame extended only from $\cos\theta_\Lambda = -0.4$ to $\cos\theta_\Lambda = -1.$ This is shown in Fig. 3.8. Thus, requiring the $\cos\theta_\Lambda$ to be less than -0.4 for all events would remove approximately 45 % of the remaining $\Omega^- \to \Xi^0\pi^-$ events.

To eliminate some of the $\Omega^- \to \Xi^0\pi^-$ background and events coming from sources other than the target, the momentum of the Ω^- was traced back through the beam channel to the x-y plane containing the center of the target. The momentum was required to point to the center of the target within 1 cm. This cut away about 7 % of the

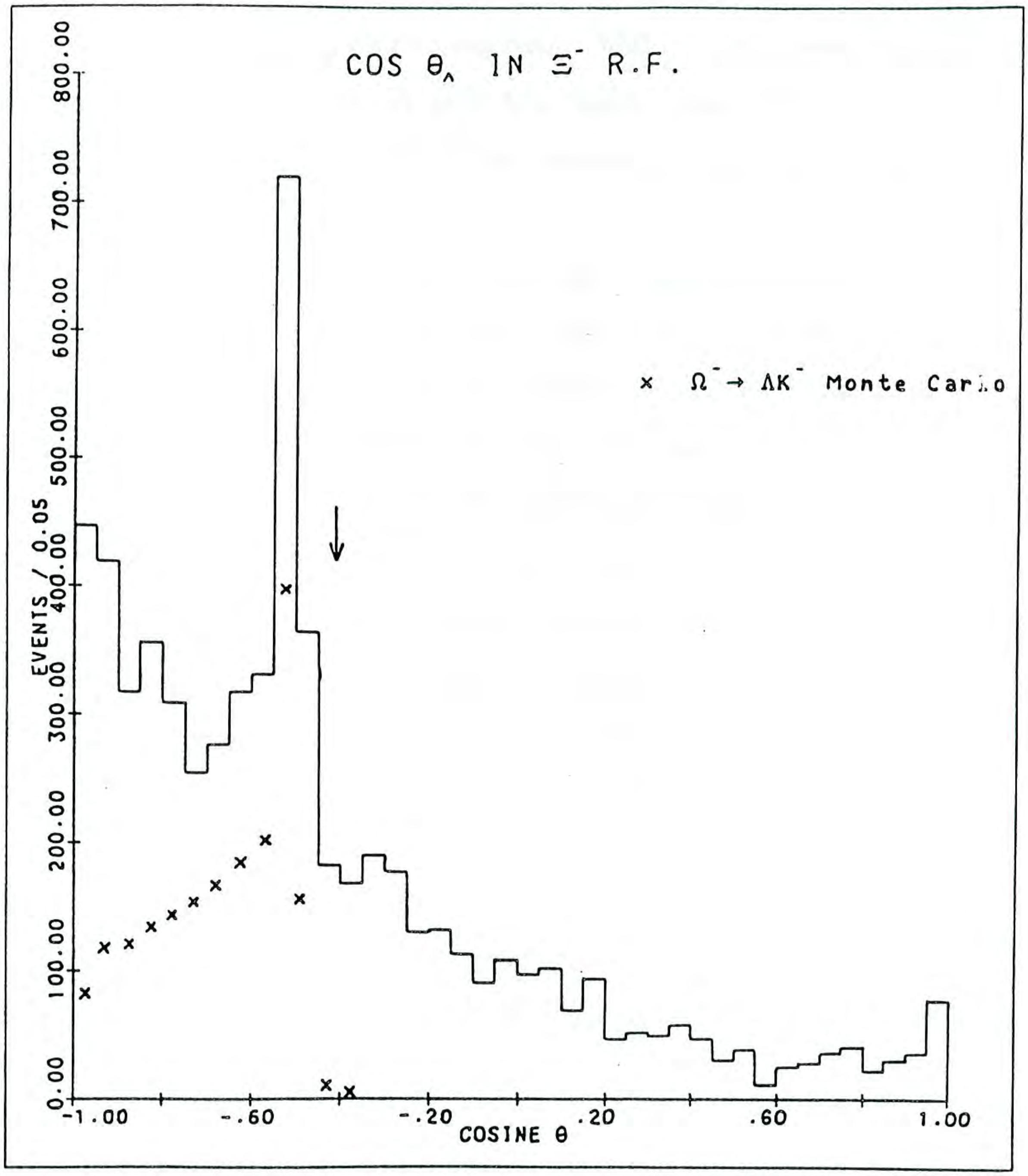

Figure 3.8 Distribution of the cos θ_Λ in the Ξ^- rest frame after p-π^- invariant mass, Λ-π^- invariant mass and decay vertex cuts. The distribution of the $\Omega^- \rightarrow \Lambda K^-$ events is also shown. The arrow shows where the cut was applied.

left over $\Omega^- \to \Xi^0\pi^-$ decays. The distributions of the Λ-K^- invariant mass and the Λ-π^- invariant mass for the remaining data are shown again in Figs. 3.9-3.10.

At this stage, the data was studied by examining the distribution of the K^- in the rest frame of the hypothetical Ω^- in terms of the parameters $\cos\theta_K = \hat{K}^-.\hat{z}$ and $\varphi_K = \tan^{-1}(\hat{K}^-.\hat{y}/\hat{K}^-.\hat{x})$, where $\hat{K}^-$ is an unit vector along the momentum vector of the K^- in the Ω^- rest frame, $\hat{x}$, $\hat{y}$ and $\hat{z}$ are parallel to the corresponding axes of the spectrometer coordinate system. The distribution is shown in Fig. 3.11. Events in the region $-1. \leqslant \cos\theta_K \leqslant -0.75$ were removed by the Λ-π^- invariant mass cut as the $\Xi^- \to \Lambda\pi^-$ background. Further investigation indicated that events clustered in the neighborhood of $\varphi_K = 0^\circ$ were $\Xi^- \to \Lambda\pi^-$ events in which the Ξ^- decayed in the collimator channel with the Λ and the π^- detected by the spectrometer. The Monte Carlo simulation was able to reproduce this effect. These events were eliminated from the sample by implementing a cut along the solid line shown in Fig. 3.11. This was the only way to keep the loss of the $\Omega^- \to \Lambda K^-$ events to a minimum.

The Λ-K^- invariant mass for events that passed all requirements is shown in Fig. 3.12. The full width at half maximum of the distribution was approximately 5.8 MeV/c^2.

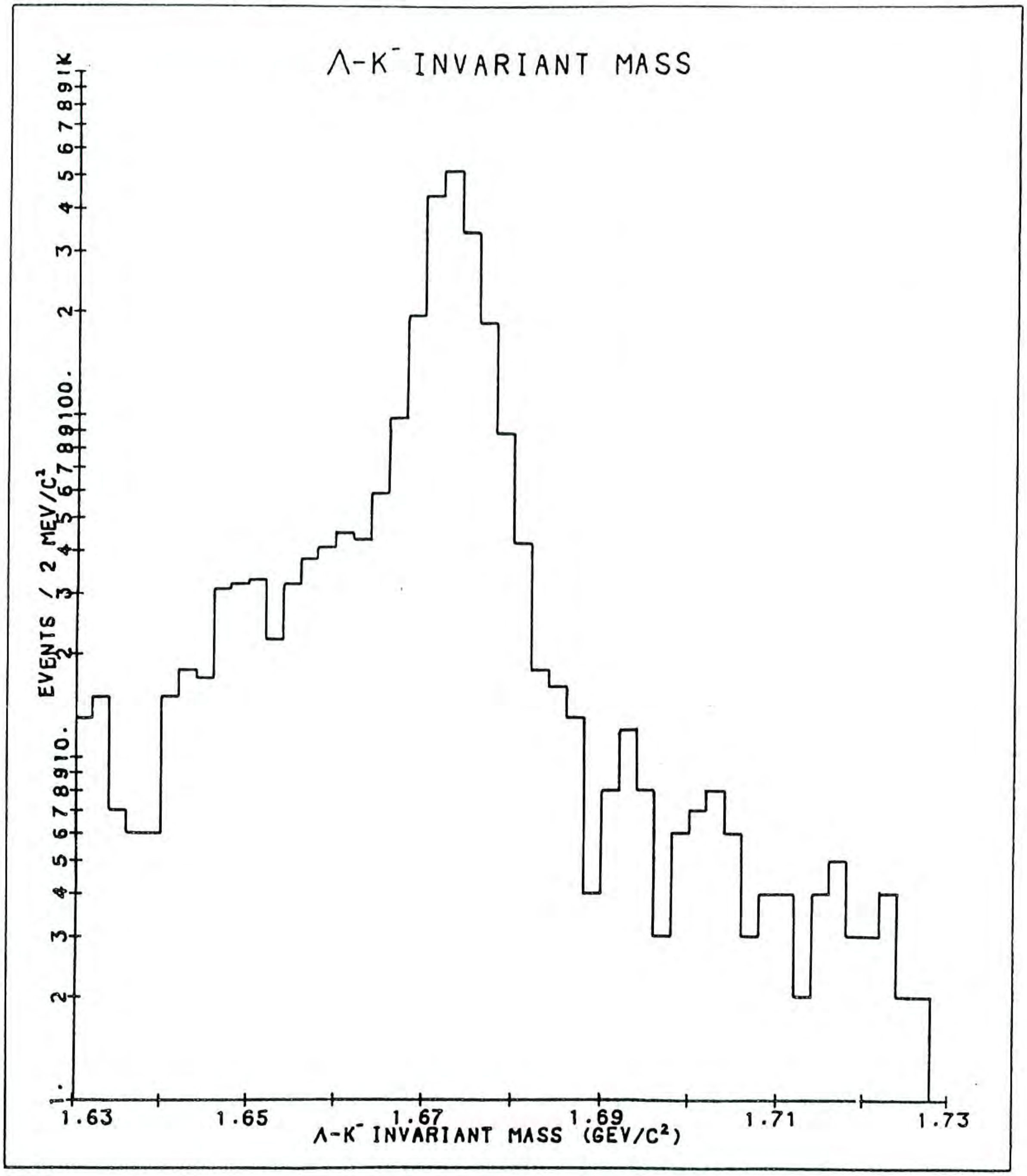

Figure 3.9 The distribution of the Λ-K^- invariant mass that satisfied cuts up to the target pointing cut. Background events under the Ω peak are estimated to be about 25 per bin. Note that this is a logarithm scale when comparing with Figs. 3.4 and 3.6.

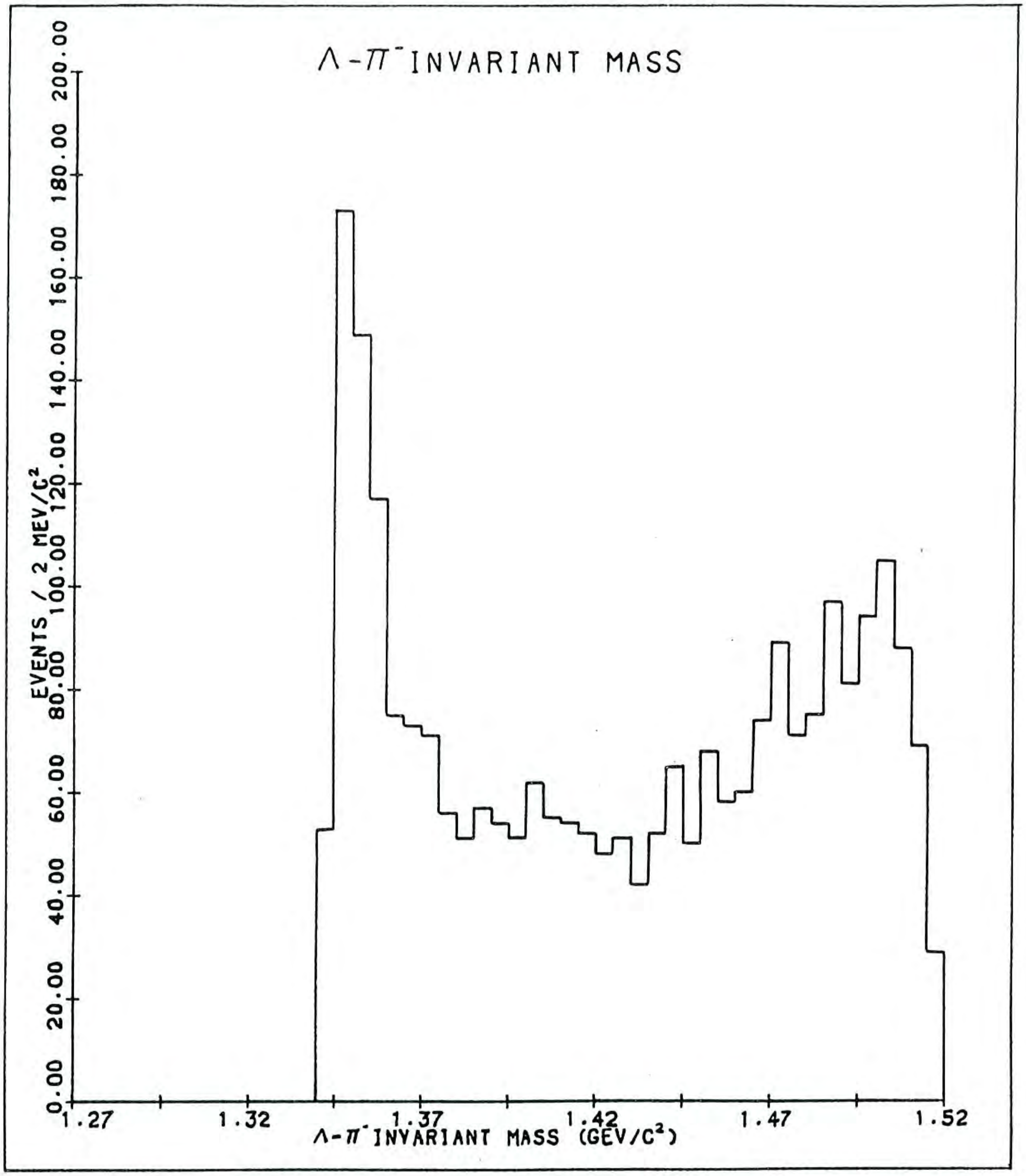

Figure 3.10 The distribution of the Λ-π^- invariant mass for events that satisfied all cuts up to the target pointing cut.

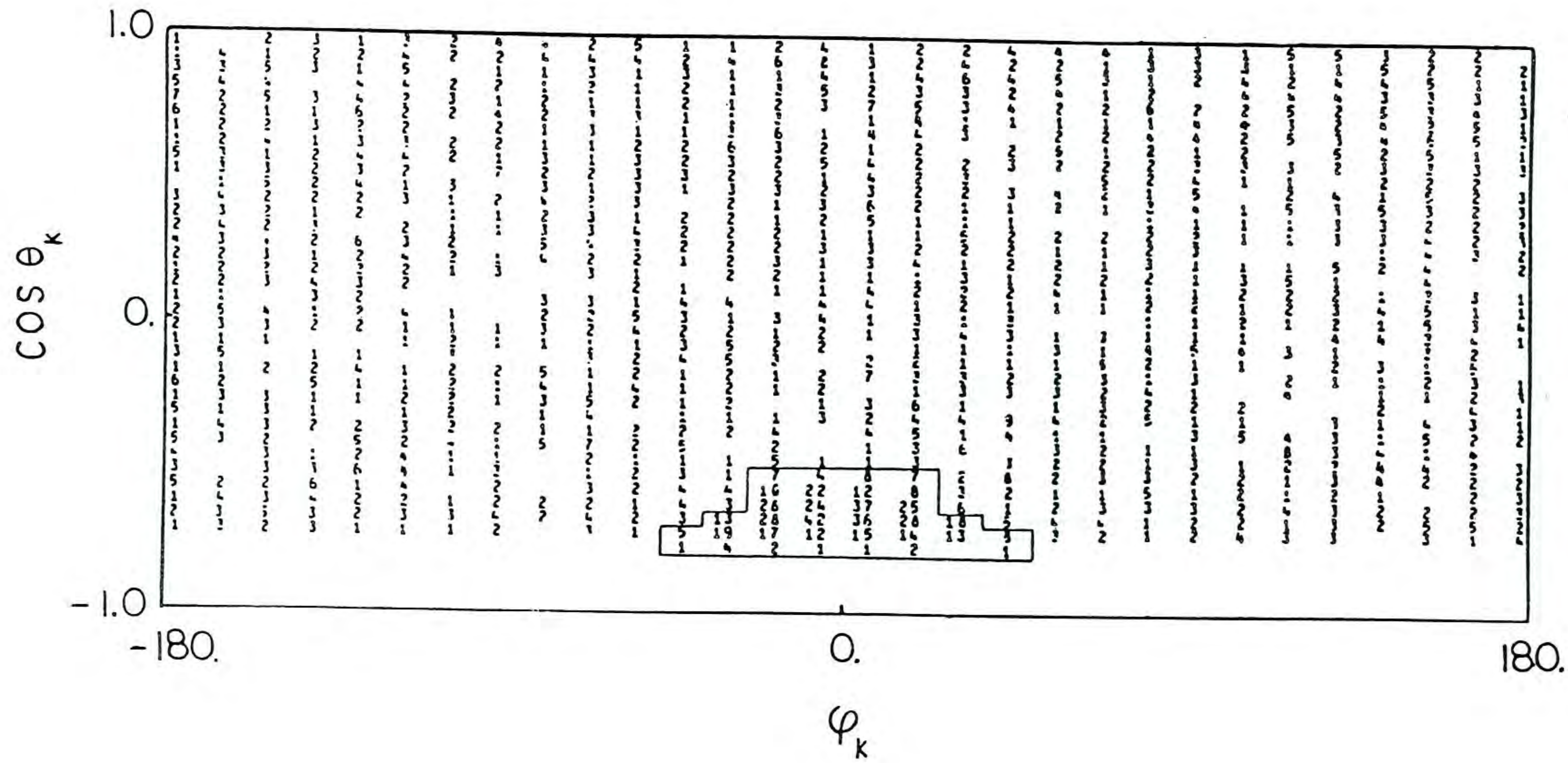

Figure 3.11 The angular distribution of the K^- in the Ω^- rest frame for events that satisfied cuts up to the target pointing cut. Events inside the enclosed region were eliminated. See text for discussion.

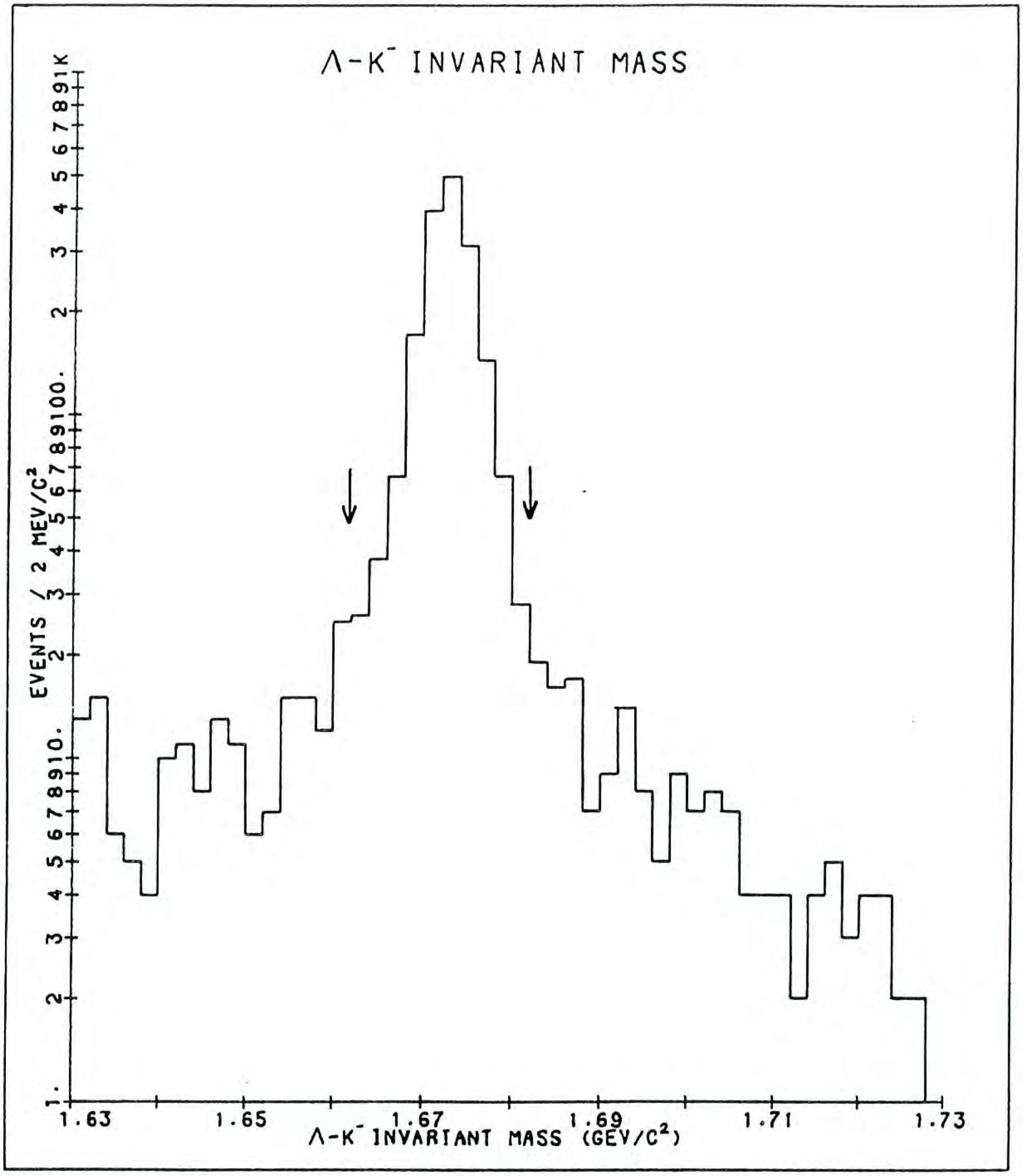

Figure 3.12 The distribution of the Λ-K^- invariant mass for events that satisfied all cuts but without the Λ-K^- invariant mass cut. Events outside the arrows were eliminated. Background events under the Ω^- peak are estimated to be about 10/bin. Note that this is a logarithm scale.

There were 1,743 events in the interval of ±10 MeV/c^2 from the Ω^- mass (1.6725 GeV/c^2, [14]). The number of background remaining in the interval was estimated as follow. An analytic curve consisting of a linear part, a Gaussian and a Lorentzian with the same width was fitted to the experimental distribution from 1.63 GeV/c^2 to 1.73 GeV/c^2. The background lying within the interval was then estimated from the linear part of the fit. This lead to approximately 58 ± 8 events, equivalent to 3.3 % of the sample, left as background. Based on Monte Carlo studies, $\Omega^- \to \Xi^0\pi^-$ decays could contribute half of the 3.3 %. The other 50 % came from poorly reconstructed $\Xi^- \to \Lambda\pi^-$ events. The Monte Carlo simulation indicated that approximately 40 % of the good three-track $\Omega^- \to \Lambda K^-$ decays were removed by the seven cuts described in this section.

The geometric χ^2, kinematic χ^2, momentum and the Λ-K^- invariant mass distributions for the 1,743 events that are within ±10 MeV/c^2 from the Ω^- mass are shown in Figs. 3.13 - 3.20. The distributions are compared with those of the Monte Carlo events. The breakdown of the 1,743 events by the production angle and the field integral is tabulated in Table 3.4.

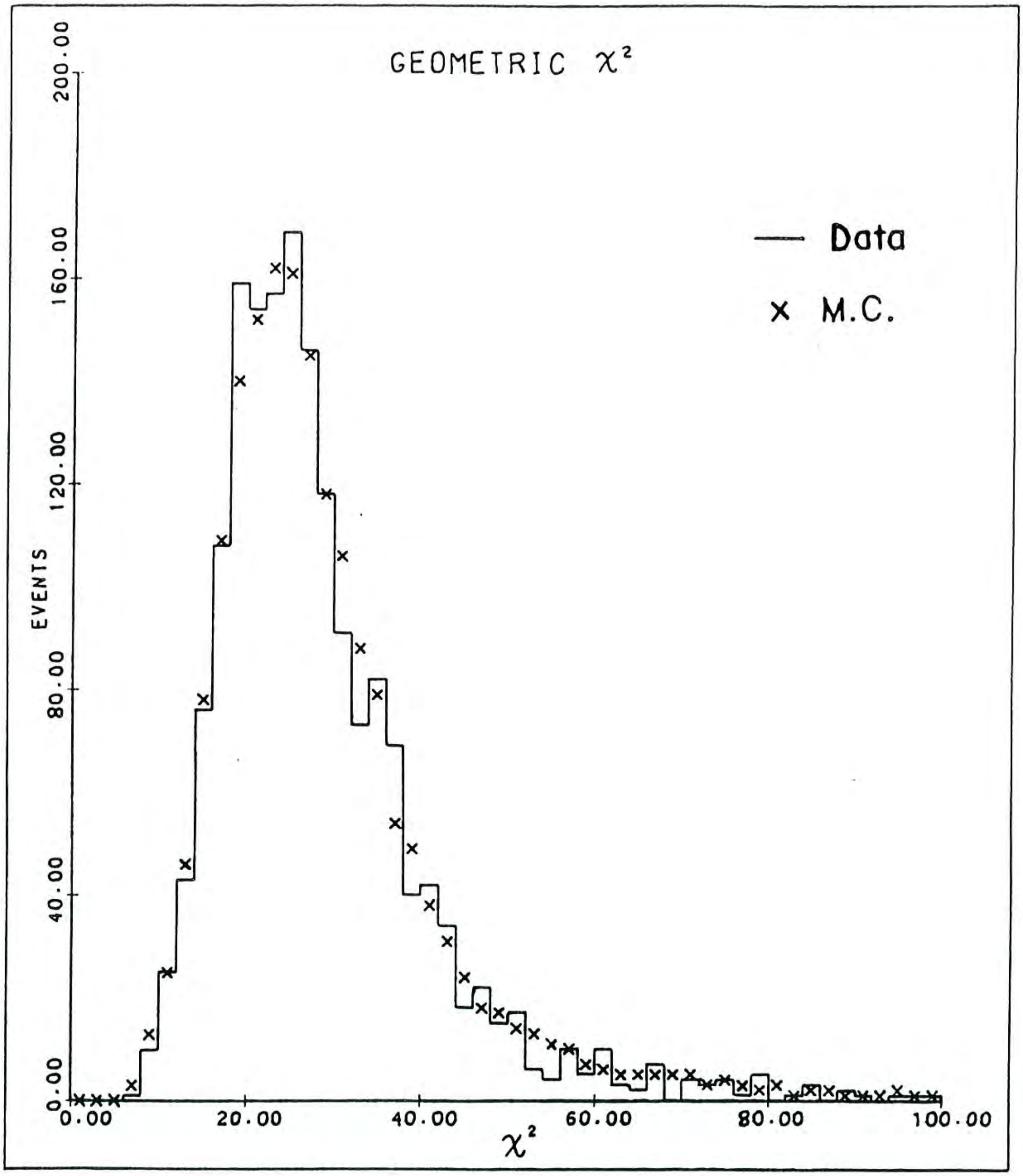

Figure 3.13 The distribution of the geometric χ^2 for events that passed all cuts.

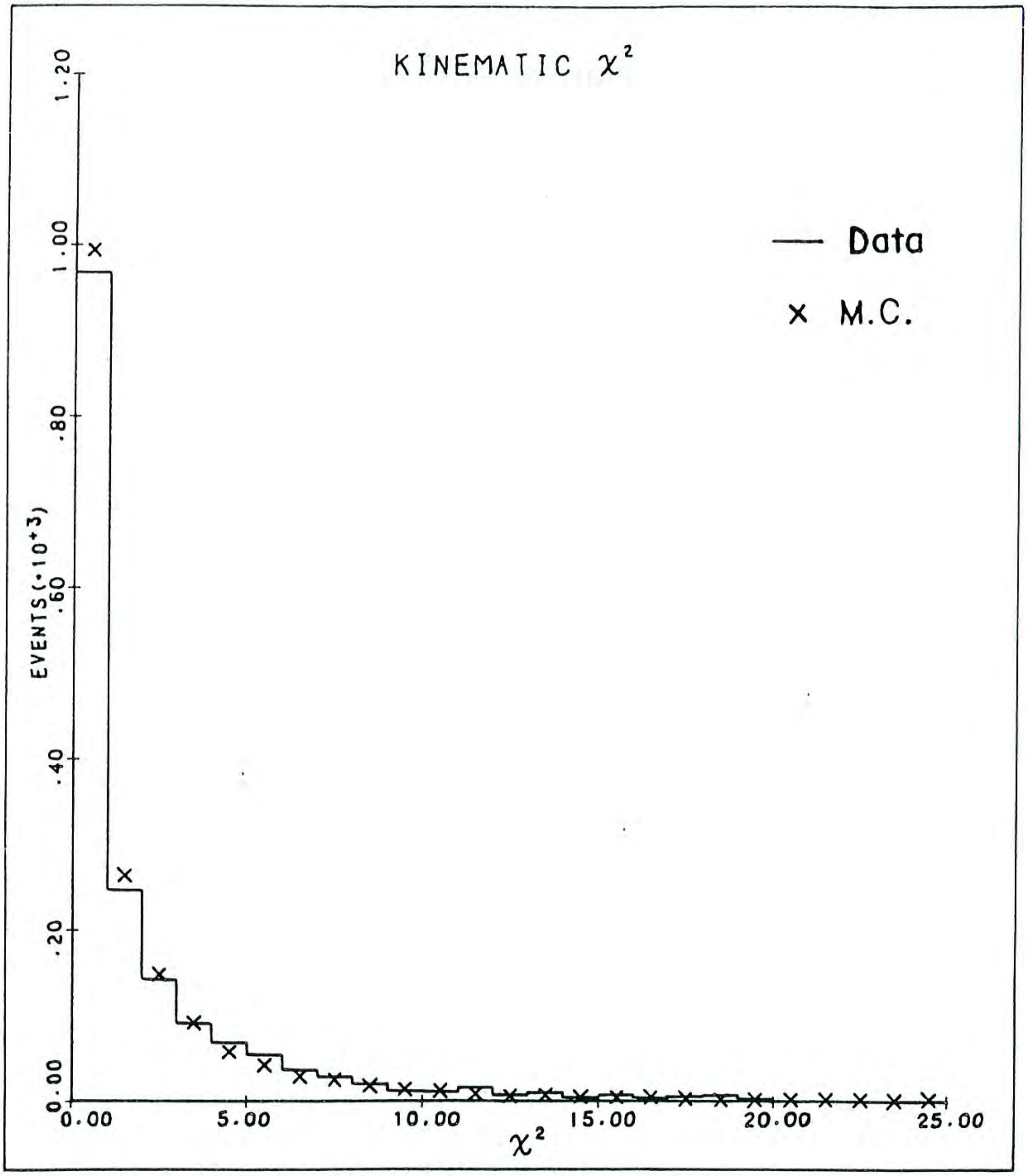

Figure 3.14 The distribution of the kinematic χ^2 for events that passed all cuts.

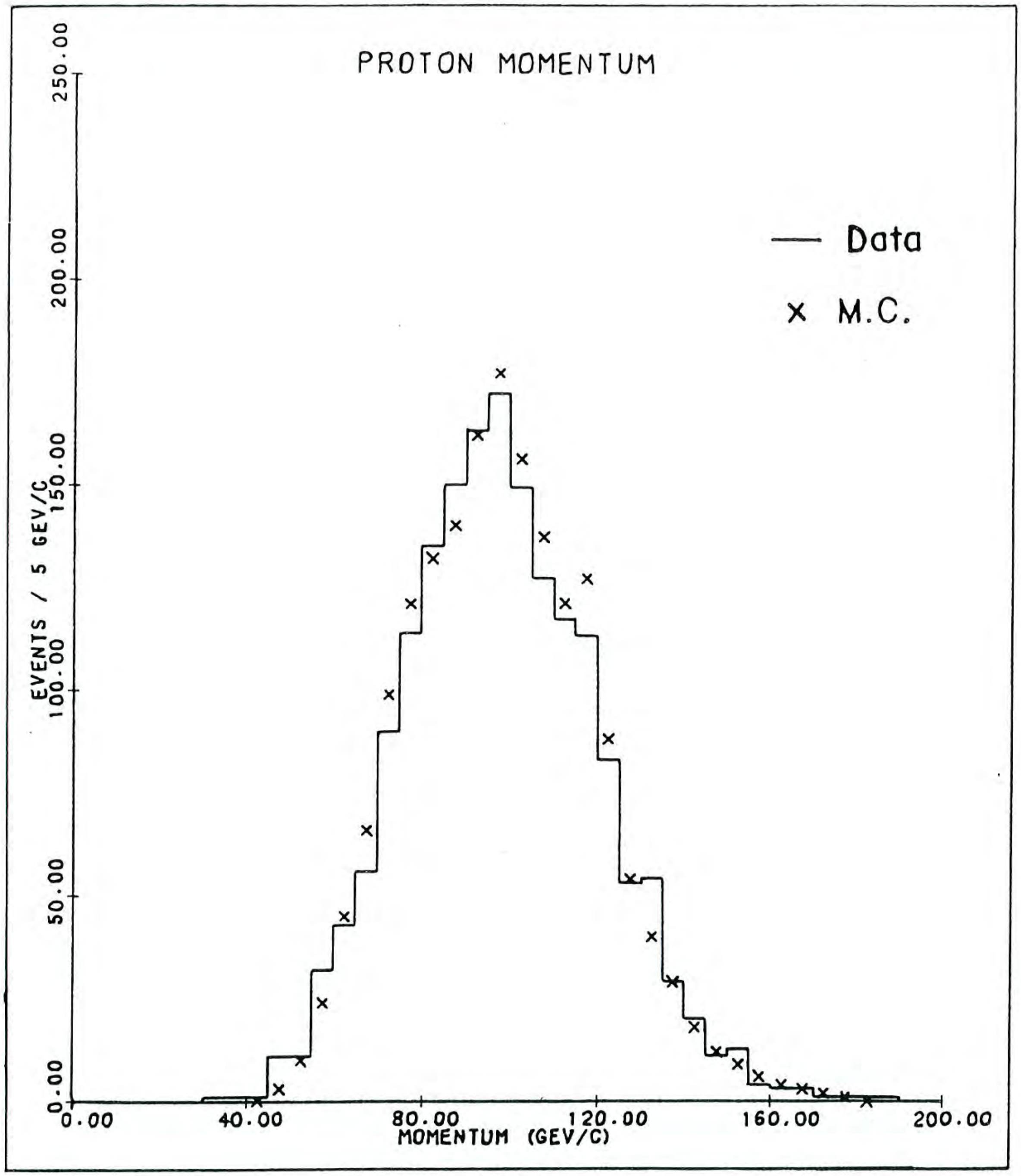

Figure 3.15 The distribution of the proton momentum for events that passed all cuts.

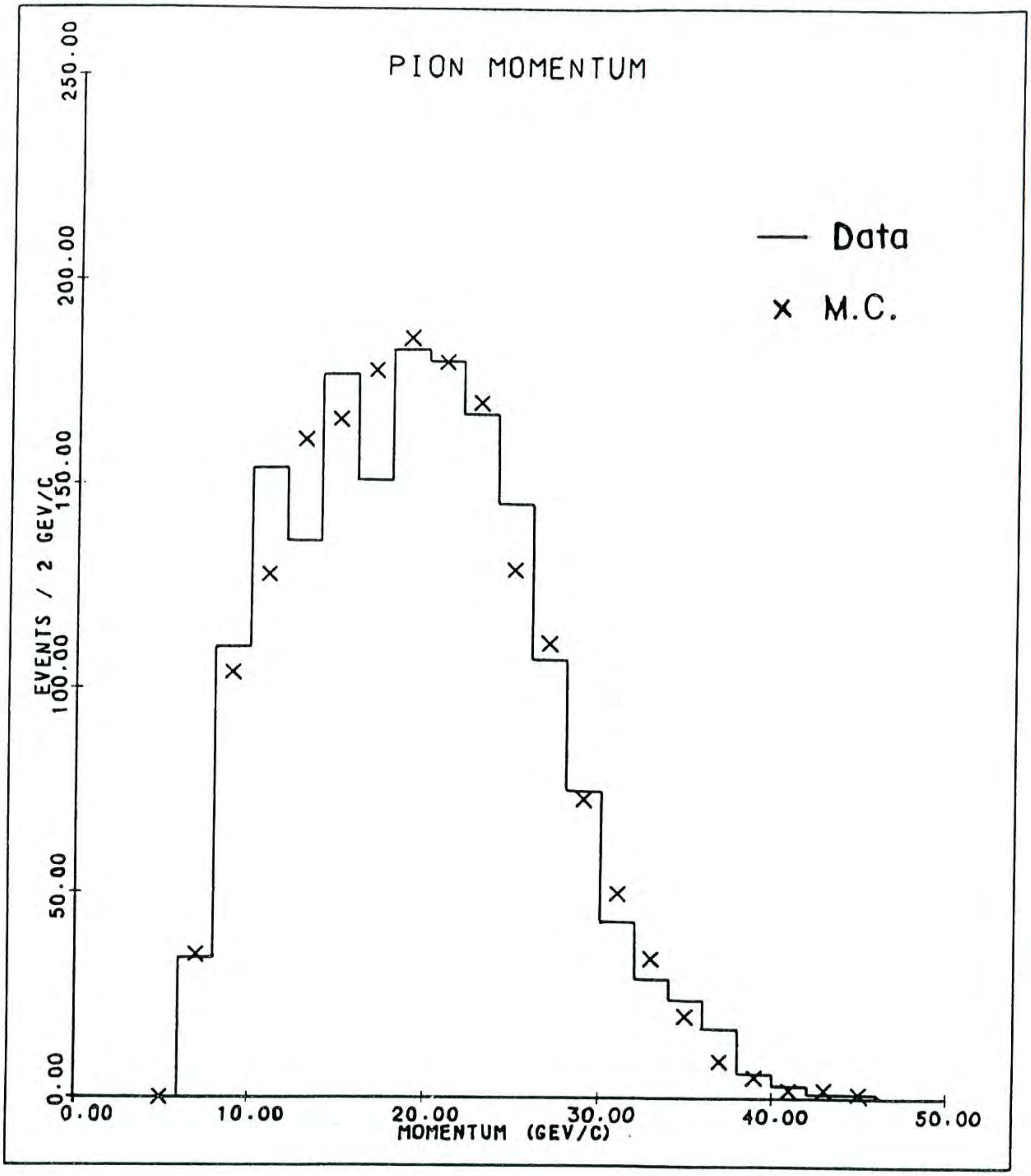

Figure 3.16 The distribution of the π^- momentum for events that passed all cuts.

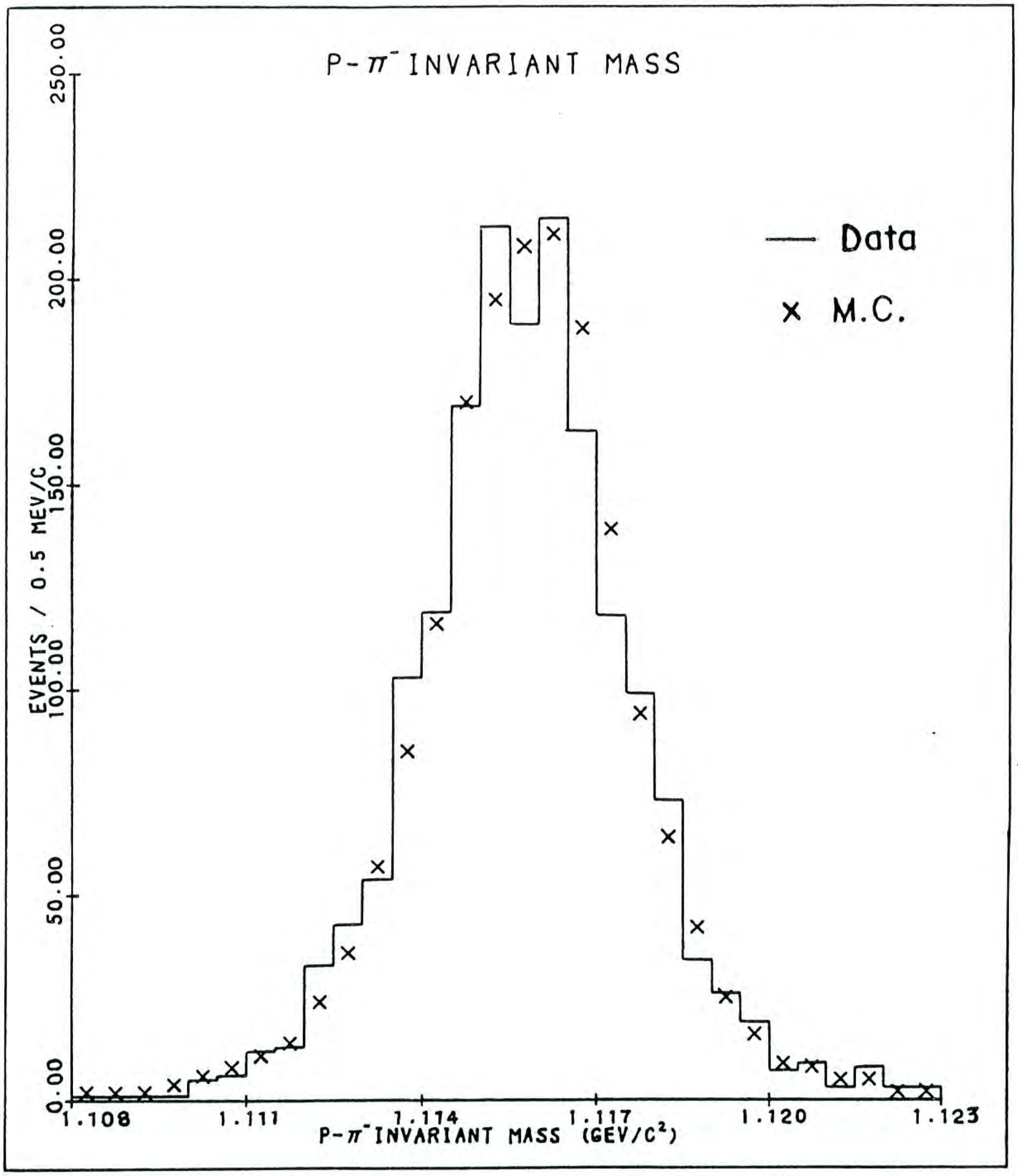

Figure 3.17 The distribution of the p-π^- invariant mass for events that passed all cuts.

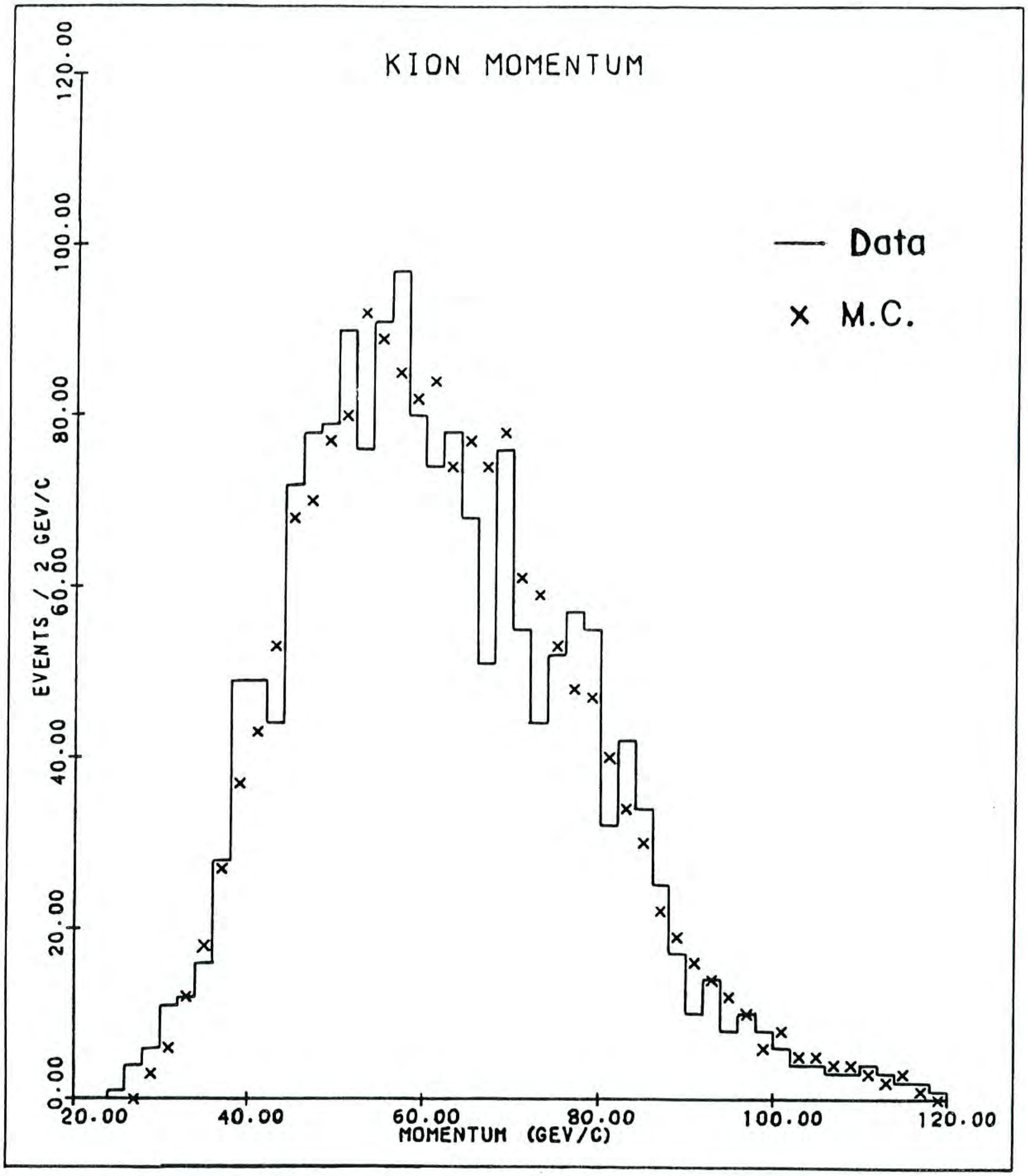

Figure 3.18 The distribution of the K^- momentum for events that passed all cuts.

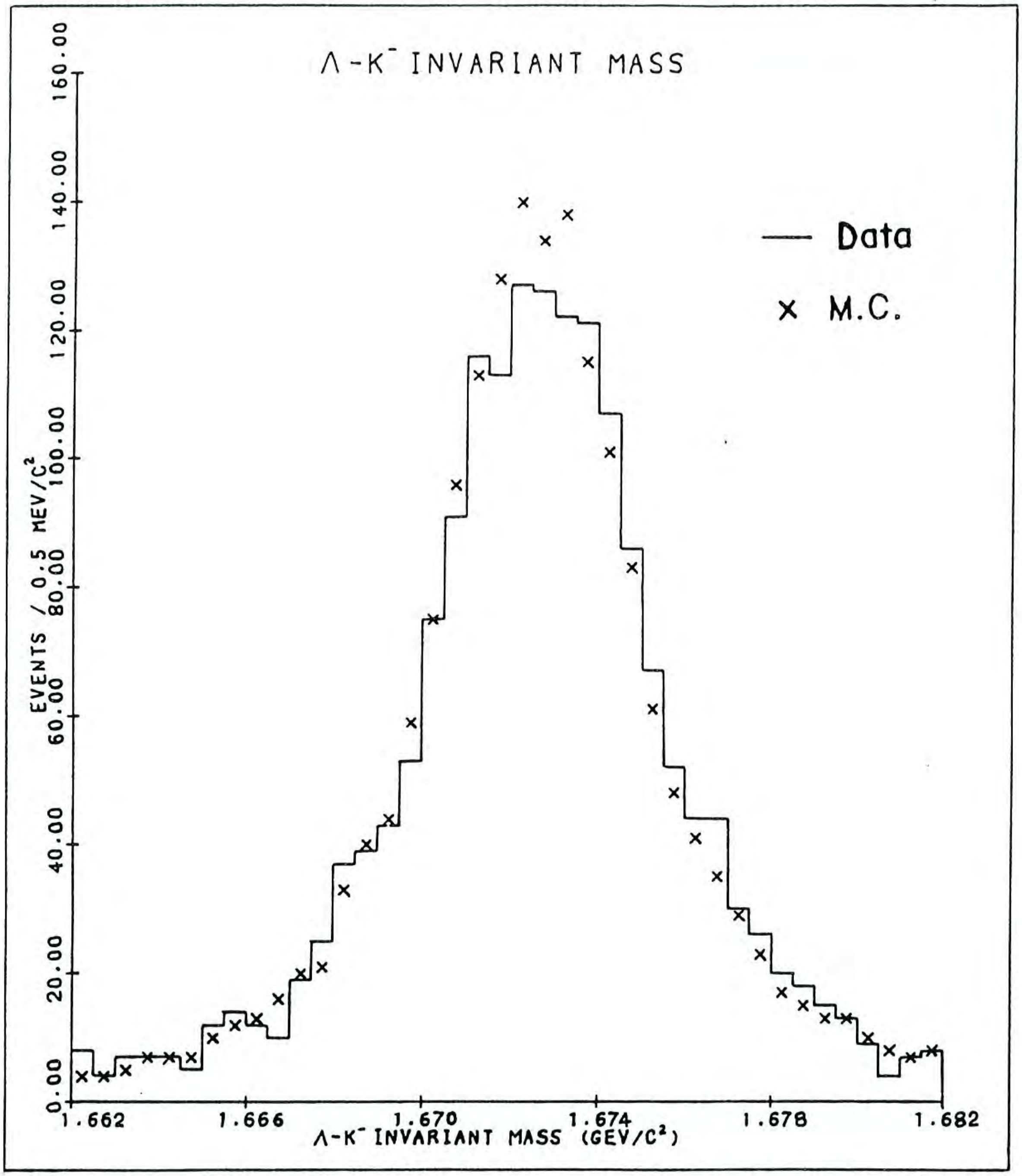

Figure 3.19 The distribution of the Λ-K^- invariant mass for events that passed all cuts.

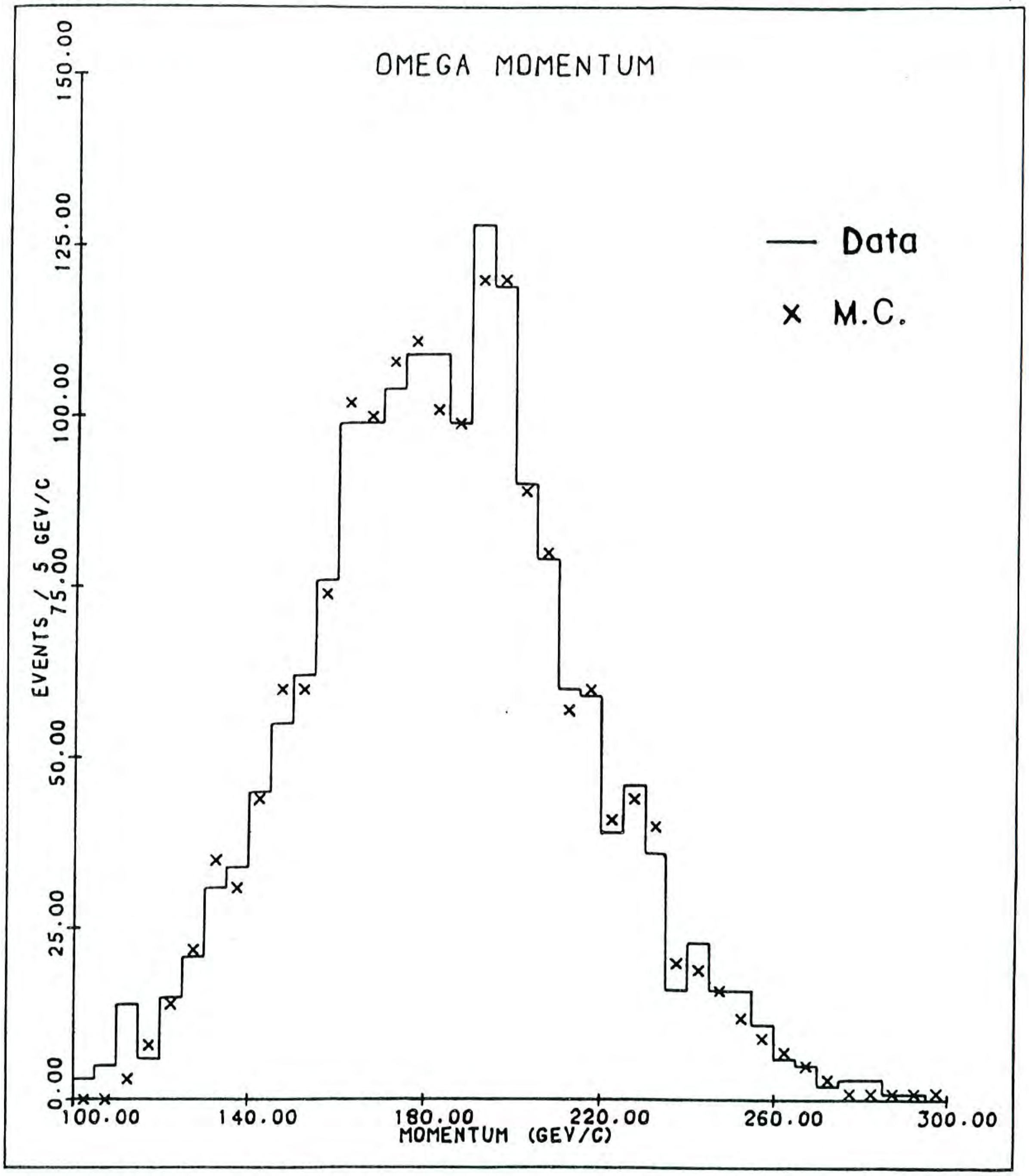

Figure 3.20 The distribution of the Ω^- momentum for events that passed all cuts.

$\int B.dl$ (T-m)	Production angle (mrad)			
	5.0	-5.0	7.5	-7.5
6.60	667	651		
5.13	122	128	81	94

Table 3.4 Distribution of number of events in the final $\Omega^- \rightarrow \Lambda K^-$ sample.

CHAPTER 4

DATA ANALYSIS II : CROSS SECTION

4.1 Introduction

The invariant differential cross section for the Ω^- produced in the inclusive reaction $p + Be \rightarrow \Omega^- + X$, where X stands for the unobserved particles, is defined to be

$$E\,\frac{d^3\sigma}{dp^3} = \frac{E_{lab}}{p^2_{lab}} \cdot \frac{N(p)}{B_\Omega B_\Lambda} \cdot \frac{A}{N_A \rho L} \cdot \frac{1}{\Delta p\, \Delta\Omega} \cdot \frac{C}{N_b\, \epsilon(p)} \qquad (4.1)$$

where E_{lab} and p_{lab} are the average energy and momentum, measured in the laboratory, of the events in a particular momentum bin, N(p) is the number of events observed in the bin, B_Ω and B_Λ are the branching ratios of the $\Omega^- \rightarrow \Lambda K^-$

decay and the $\Lambda \to p\pi^-$ decay respectively, N_A is ~~the~~ Avogadro's number, A, ρ and L are the atomic weight, the density and the length of the beryllium target respectively, Δp is the width of the momentum bin, $\Delta\Omega$ is the solid angle acceptance of the collimator, C is the target absorption correction factor, N_b is the number of protons striking the beryllium target and $\epsilon(p)$ is the total acceptance including the lifetime correction, the spectrometer acceptance and the fractional acceptance of the beam channel.

4.2 Normalization

In the early stage of E620, the ion chamber (IC) was calibrated against the 0.635 cm diameter scintillation counter (P) and the halo counter (H) with a beam intensity less than 10^6 protons per spill. Essentially, the scintillator and the halo counter measured the number of protons hitting and missing the target respectively. The calibration constant for the ion chamber expressed as (P+H)/IC was determined to be $(1.76 \pm 0.08) \times 10^4$ protons per IC count.

The targeting efficiency was determined in two ways. It was first given by the ratio P/(P+H). Then, it was estimated by studying the beam profile in the SWIC pictures taken during the experiment. Both methods gave an efficiency of 0.8 ± 0.1.

The number of protons hitting the target, N_b, was calculated as the product of the gated IC reading, the calibration constant and the targeting efficiency.

4.3 Monte Carlo Acceptance

The total acceptance as a function of the laboratory momentum of the Ω^-, $\epsilon(p)$, was determined with the Monte Carlo program. For each momentum value, fictitious events were generated according to the description given in section 3.2 but without decays inside the channel. The resulting channel acceptance at 6.6 T-m, the geometric acceptance of the spectrometer including trigger requirement but no channel acceptance, and the total acceptance which also included the efficiencies of the reconstruction process and the software cuts are shown in Fig. 4.1. The channel acceptance and the total acceptance at 5.13 T-m are different and are shown in Fig. 4.2.

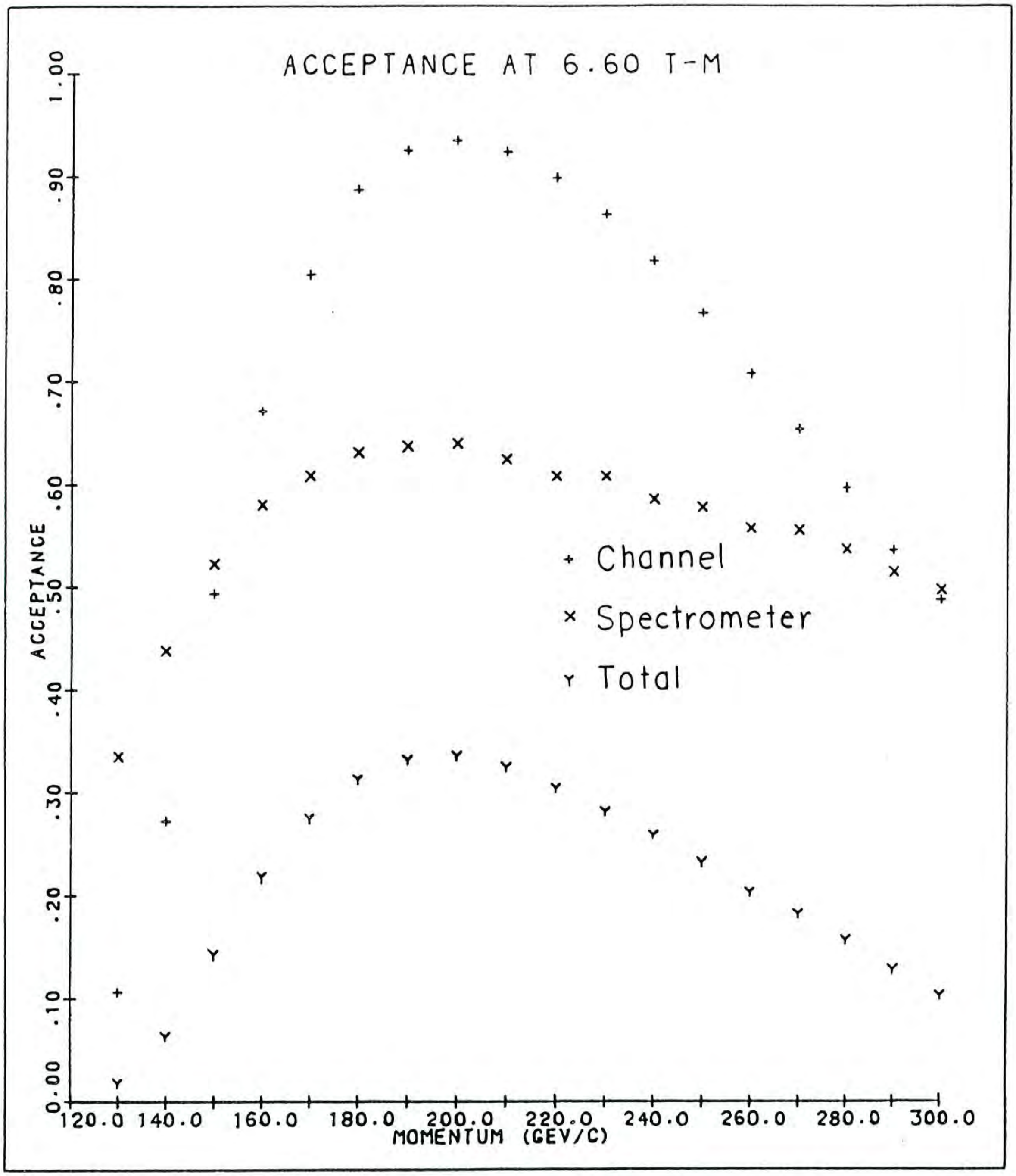

Figure 4.1 Beam channel acceptance with a field integral of 6.6 T-m, spectrometer acceptance and the total acceptance.

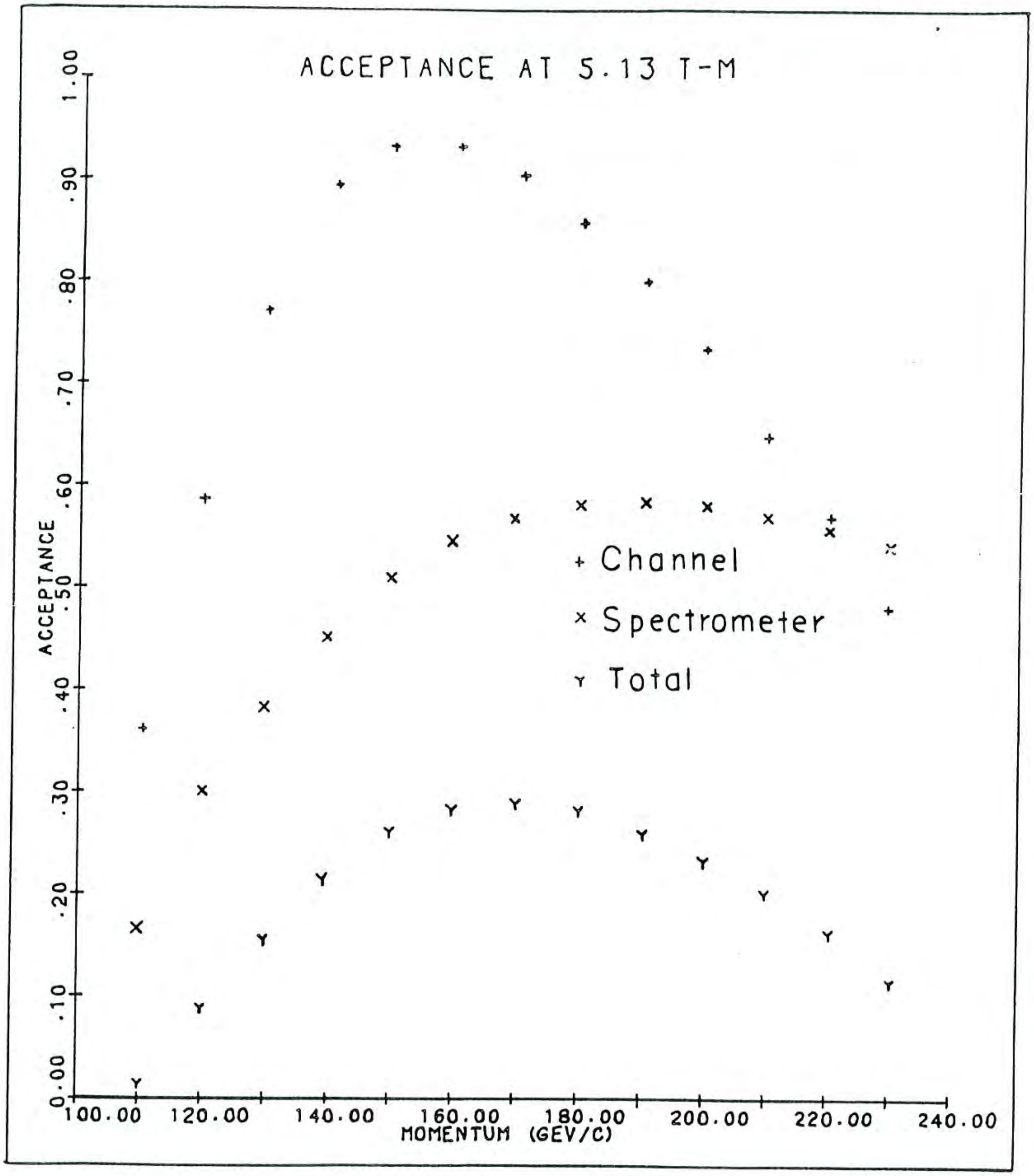

Figure 4.2 Beam channel acceptance with a field integral of 5.13 T-m, spectrometer acceptance and the total acceptance.

4.4 Cross Section Measurement and Results

The observed momentum spectra at 5 mrad and field integral of 6.6 T-m, and at 7.5 mrad and 5.13 T-m are shown in Figs. 4.3-4.4 respectively. In the calculation of the invariant cross section, the experimental data were grouped into momentum bins which were 10 GeV/c wide for the 5 mrad events taken at 6.6 T-m and 30 GeV/c for the 7.5 mrad data. For the 5 mrad sample at 6.6 T-m, events with momentum less than 135 GeV/c were not included in the cross section measurement because the total acceptance was poorly known.

The values used for the branching ratios of the $\Omega^- \to \Lambda K^-$ and the $\Lambda \to p\pi^-$ were 0.686 and 0.642 respectively [14]. The absorption correction factor for the beryllium target was determined in a previous experiment [35] and was taken to be 1.26 ± 0.07. Since the downstream end of the defining collimator was 3.21 m away from the center of the target, the solid angle was estimated to be

$$\Delta\Omega = \pi \frac{(0.002)^2}{(3.12)^2} = 1.2 \text{ microsteradians} \quad .$$

Due to the uncertainty in the position of the target and the penetration of particles through the edge of the defining collimator, the uncertainty in the solid angle acceptance was approximately 10 %.

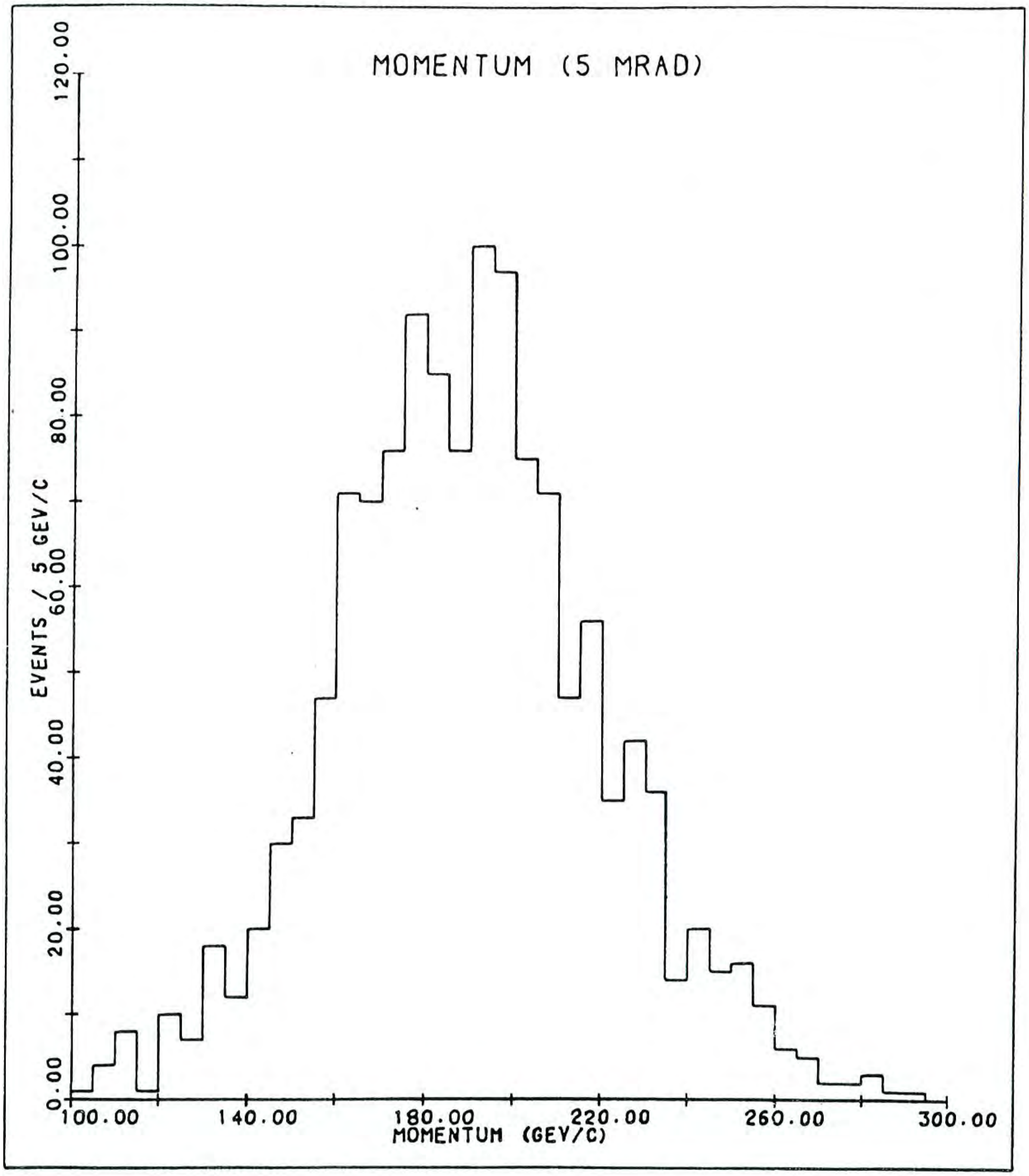

Figure 4.3 The distribution of the Ω^- momentum for the 5 mrad sample taken at 6.6 T-m.

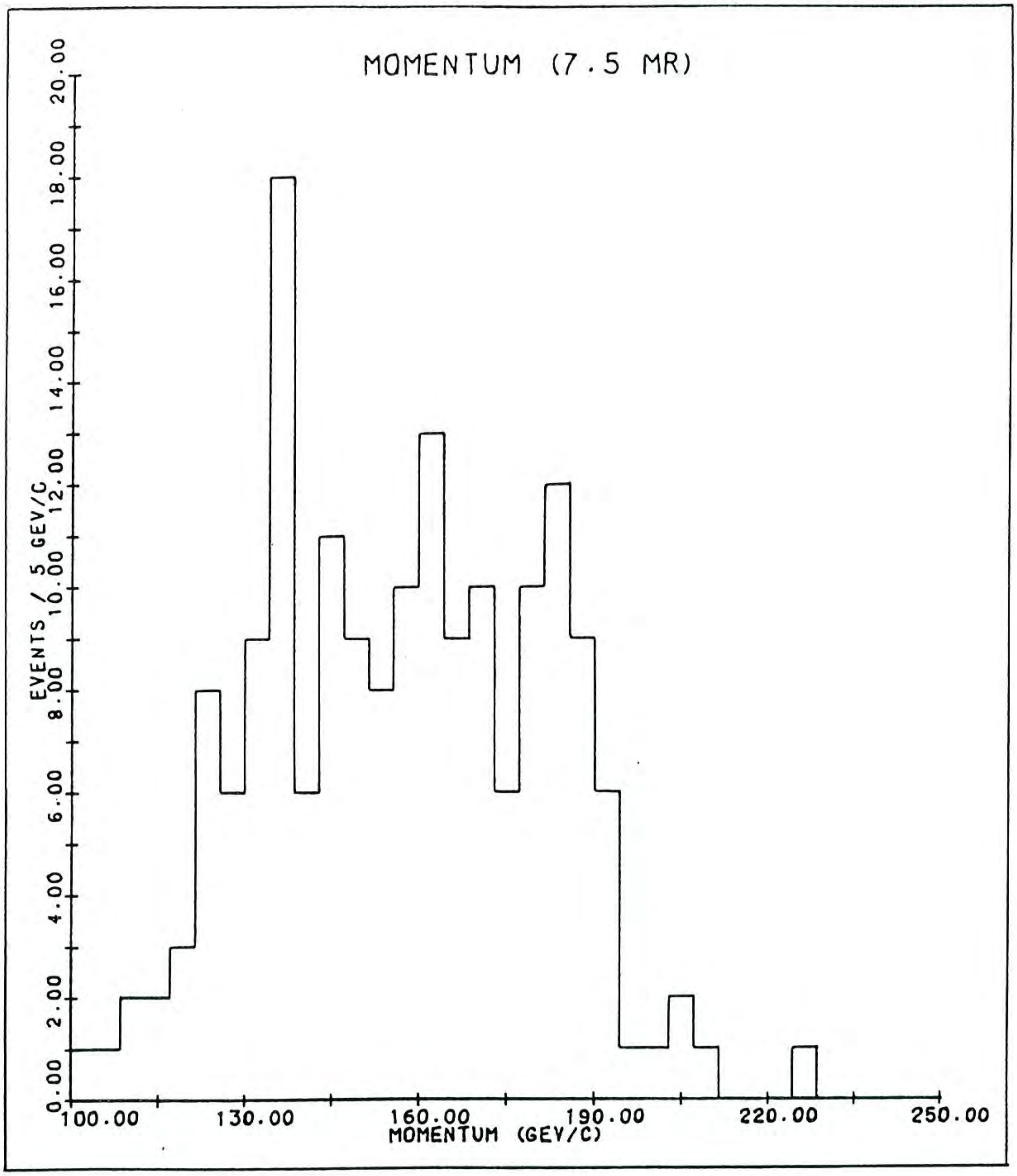

Figure 4.4 The distribution of the Ω^- momentum for the 7.5 mrad data taken at 5.13 T-m.

Furthermore, the uncertainty in the production angle was of the order of 0.1 mrad.

The invariant differential production cross section of the Ω^- as a function of the Ω^- momentum in the laboratory was calculated from expression 4.1. The results are shown in Fig. 4.5 and are also tabulated in Tables 4.1 and 4.2 for the 5 mrad and the 7.5 mrad sample respectively. The uncertainties are purely statistical.

The major sources of systematic error came from the calibration constant of the ion chamber with uncertainty of 5 %, the targeting efficiency with uncertainty of 12 %, the target absorption correction factor with 5 % variation, the channel acceptance with uncertainty of 10 % as well as the uncertainty in the solid angle acceptance. Adding these up in quadrature, the systematic error in the differential cross section measurment was estimated to be approximately 20 %.

The invariant cross sections at 5 and 7.5 mrad were fitted to the expression

$$E\frac{d^3\sigma}{dp^3} = a(1-x)^n \tag{4.2}$$

where x is the Feynman x approximated by the ratio of the laboratory momentum of the Ω^- to the momentum of the

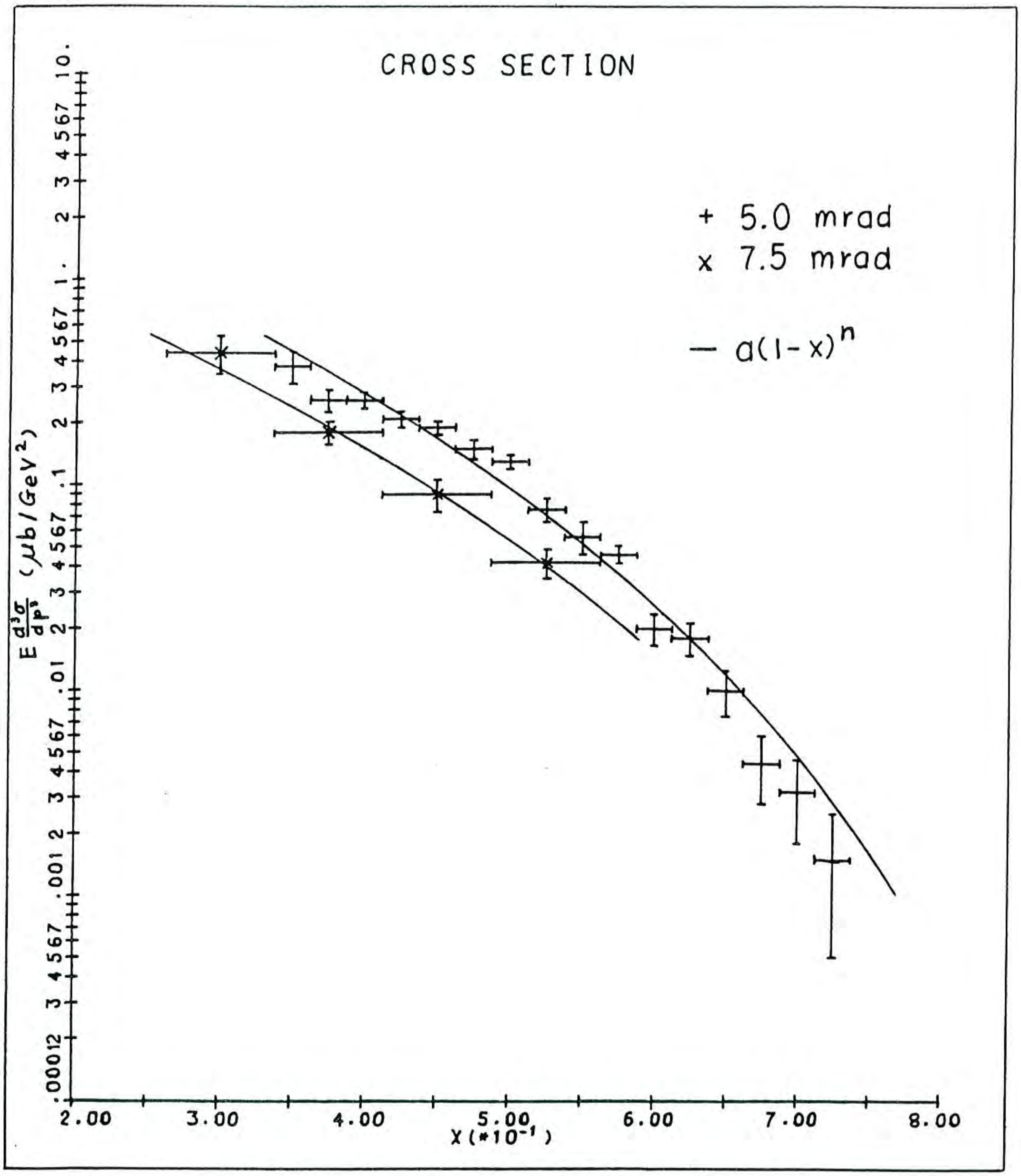

Figure 4.5 The invariant cross section for the Ω^- produced at 5 mrad and 7.5 mrad.

Momentum (GeV/c)	$E\frac{d^3\sigma}{dp^3}$ ($\mu b/GeV^2$)
135 - 145	0.38 ± 0.07
145 - 155	0.26 ± 0.03
155 - 165	0.26 ± 0.02
165 - 175	0.21 ± 0.02
175 - 185	0.19 ± 0.01
185 - 195	0.15 ± 0.02
195 - 205	0.13 ± 0.01
205 - 215	0.076 ± 0.010
215 - 225	0.056 ± 0.010
225 - 235	0.046 ± 0.005
235 - 245	0.020 ± 0.004
245 - 255	0.018 ± 0.003
255 - 265	0.010 ± 0.003
265 - 275	0.0044 ± 0.0016
275 - 285	0.0032 ± 0.0014
285 - 295	0.0015 ± 0.0010

Table 4.1 Invariant cross section of Ω^- produced in p + Be -> Ω^- + X at 5.0 mrad as a function of the Ω^- momentum. An overall normalization uncertainty of ± 20 % is not included.

Momentum (GeV/c)	$E\frac{d^3\sigma}{dp^3}$ ($\mu b/GeV^2$)
105 - 135	0.44 $\pm$ 0.09
135 - 165	0.18 $\pm$ 0.02
165 - 195	0.090 $\pm$ 0.016
195 - 225	0.042 $\pm$ 0.007

Table 4.2 Invariant cross section of Ω^- produced in p + Be -> Ω^- + X at 7.5 mrad as a function of the Ω^- momentum. An overall normalization uncertainty of $\pm$ 20 % is not included.

incident proton, a and n are parameters in the fit. Alternatively, another expression of the form

$$E \frac{d^3\sigma}{dp^3} = a(1-x)^n \exp(-bp_T^2) \qquad ,$$

where p_T is the transverse momentum of the Ω^- and b is an additional parameter, was used. The parameter b can be related to the mean transverse momentum, $\langle p_T \rangle$, through the equation

$$1/b = 2\langle p_T \rangle^2 \quad .$$

Without taking the systematic error into account, the results of the fit are tabulated in Table 4.3. Since the mean transverse momenta of the two data samples were approximately 1 GeV/c, the expected values for b would be closed to 0.5 $(\mathrm{GeV/c})^{-2}$, in good agreement with the results of the fits. The best fits of equation (4.2) to the data are shown in Fig. 4.5.

Production angle (mrad)	$E\frac{d^3\sigma}{dp^3} = a(1-x)^n\ e^{-bp_T^2}$			χ^2/DOF
	a (μb/GeV^2)	n	b (GeV^{-2})	
5.0	5.60±0.58	5.87±0.15	0. (fixed)	3.0
	4.74±0.47	4.90±0.40	0.51±0.20	3.0
7.5	2.75±0.99	5.68±0.66	0. (fixed)	1.1
	1.74±0.33	3.27±1.84	0.54±0.53	1.3

Table 4.3 Parameters obtained in fits of the data to a function of x and p_T^2 .

CHAPTER 5

DATA ANALYSIS III : LIFETIME

5.1 Introduction

Consider a system of particles with lifetime τ, mass m and momentum p in the laboratory. If $N(0)$ is the number of particles at an arbitrary chosen reference point, then the number of particles at a distance z, $N(z)$, away from the reference point is related to $N(0)$ through the well known exponential expression

$$N(z) = N(0)\, e^{-\frac{zm}{pc\tau}} \tag{5.1}$$

where c is the speed of light. Therefore, in principle, the lifetime of the particle can be measured from the decay vertex distribution by using equation (5.1).

In practice, the particles have a spread in momentum, the acceptance is not perfect and the reconstruction process can distort the vertex distribution. Thus, the number of particles observed at z is not given by equation (5.1) but is modified to

$$N(z) = \int \epsilon(p,z)\ N(p,0)\ e^{-\frac{zm}{pc\tau}}\ dp \qquad (5.2)$$

where $\epsilon(p,z)$ is the acceptance function with the momentum and decay position dependence explicitly shown, and N(p,0) is the number of particles with momentum p at the reference origin. In other words, it is neccessary to unfold the acceptance of the apparatus and the momentum spectrum of the data in order to determine the lifetime of the particle from the decay vertex distribution. This can be achieved by the Monte Carlo method.

5.2 Monte Carlo Method

In this method, sets of external Monte Carlo events with different input values for the lifetime of the Ω^- are generated and reconstructed according to the procedures described in section 3.2. As indicated in equation (5.2), the decay vertex distribution is a function of the momentum and the lifetime. The momentum spectrum of the Ω^- of each Monte Carlo sample has to be simulated as closely as possible to that of the experimental data. Once the momentum distribution is reproduced correctly, any discrepancy between the Monte Carlo events and the real data in the decay vertex distribution of the Ω^- should be due to the lifetime dependence.

There is an efficient way to generate the Monte Carlo samples. First of all, a grand Monte Carlo sample with a lifetime τ_0, which is greater than the value of the expected lifetime, is generated. Then a Monte Carlo sample with a lifetime τ_i less than τ_0 is created in the following way. For each event in the grand sample, a random number is generated. If the random number is less than the relative survival probability given by

$$\mathrm{Prob}(p, Z, \tau_i) = \frac{e^{-\frac{Zm}{pc\tau_i}}}{e^{-\frac{Zm}{pc\tau_0}}} ,$$

the event is accepted as an event of the sample with a lifetime τ_i. Due to the acceptance of the spectrometer, the momentum distribution of the Monte Carlo sample may not be the same as that of the real events. In order to reproduce the momentum spectrum of the data, the number of Monte Carlo events accepted in a momentum bin, $N_j^{MC}(p)$, is limited to

$$N_j^{MC}(p) = k\ N_j^{R}(p)$$

where $N_j^{R}(p)$ is the number of real events in the same momentum bin and k is the normalization constant.

The χ^2 of comparison between the decay vertex distribution of the i-th Monte Carlo set, with input lifetime τ_i, and that of the data is calculated from the expression

$$\chi_i^2 = \sum_{j=1}^{n} \frac{(N_j^R - k_i^{-1} N_{ij}^{MC})^2}{N_j^R + k_i^{-2} N_{ij}^{MC}}$$

where n is the number of bins that the vertex distribution is divided into, N_j^R and N_{ij}^{MC} are the number of experimental and Monte Carlo events in bin j respectively. The most probable value for the lifetime is obtained as the $c\tau$ related to the minimum of the χ^2 distribution. The uncertainty associated with the $c\tau$ at the minimum χ^2 is calculated from the range of $c\tau$ when the χ^2 is allowed to change from its minimum value by one. Since there are n vertex bins and one parameter in the fit, the number of degrees of freedom is simply n-1.

5.3 Lifetime Measurement and Result

Before this experiment, the world average of the lifetime of the Ω^- was $c\tau_\Omega$ = 2.45 cm or τ_Ω = $(0.82 \pm 0.03) \times 10^{-10}$ s [14]. The input value for the lifetime of the Ω^- to the computer program in terms of $c\tau$ was chosen to be 3.5 cm whereas the world average value of the Λ lifetime ($c\tau_{\Lambda}$ = 7.89 cm) was used. Sets of Monte Carlo events with the Ω^- lifetime ranged from $c\tau_{\Omega}$ = 3.0 cm to $c\tau_{\Omega}$ = 2.0 cm were created according to the method described in the foregoing section. The χ^2 distribution, with the vertex in the decay region between 0.5 m and 8.5 m, as a fuction of $c\tau_{\Omega}$ is shown in Fig. 5.1. The Ω^- decay vertex and the Λ decay vertex distributions of the Monte Carlo events at $c\tau_{\Omega}$ of 2.5 cm are compared to those of the real data in Figs. 5.2-5.3.

The lifetime of the Ω^- was measured for each of three momentum bins in two decay regions. The results are given in Table 5.1. The value of the lifetime for events with the vertex in the interval between 0.5 m and 8.5 m was determined to be 2.45$\pm$0.09 cm or $(0.815\pm0.030)\times10^{-10}$ s, with a χ^2 of 25.2 per 16 degrees of freedom. The effect of background on the measurement was also studied by including events with the Λ-K^- invariant mass in the interval between 1.63 GeV/c^2 and 1.73 GeV/c^2 with the vertex in the decay region between 0.5 m and 8.5 m, the lifetime of the Ω^- was unchanged within the quoted uncertainty.

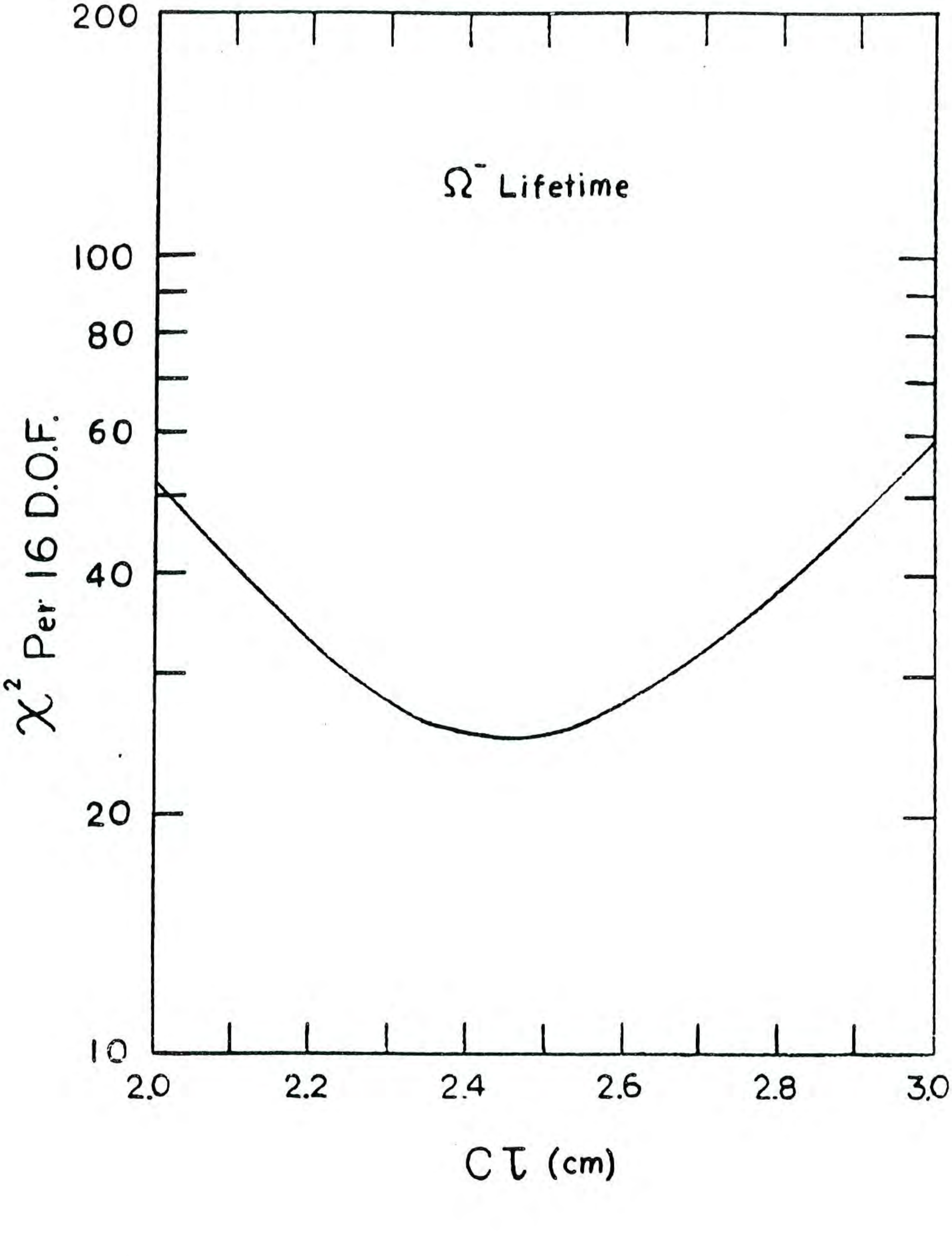

Figure 5.1 The χ^2 distribution as a function of the lifetime of the Ω^- expressed as $c\tau_\Omega$.

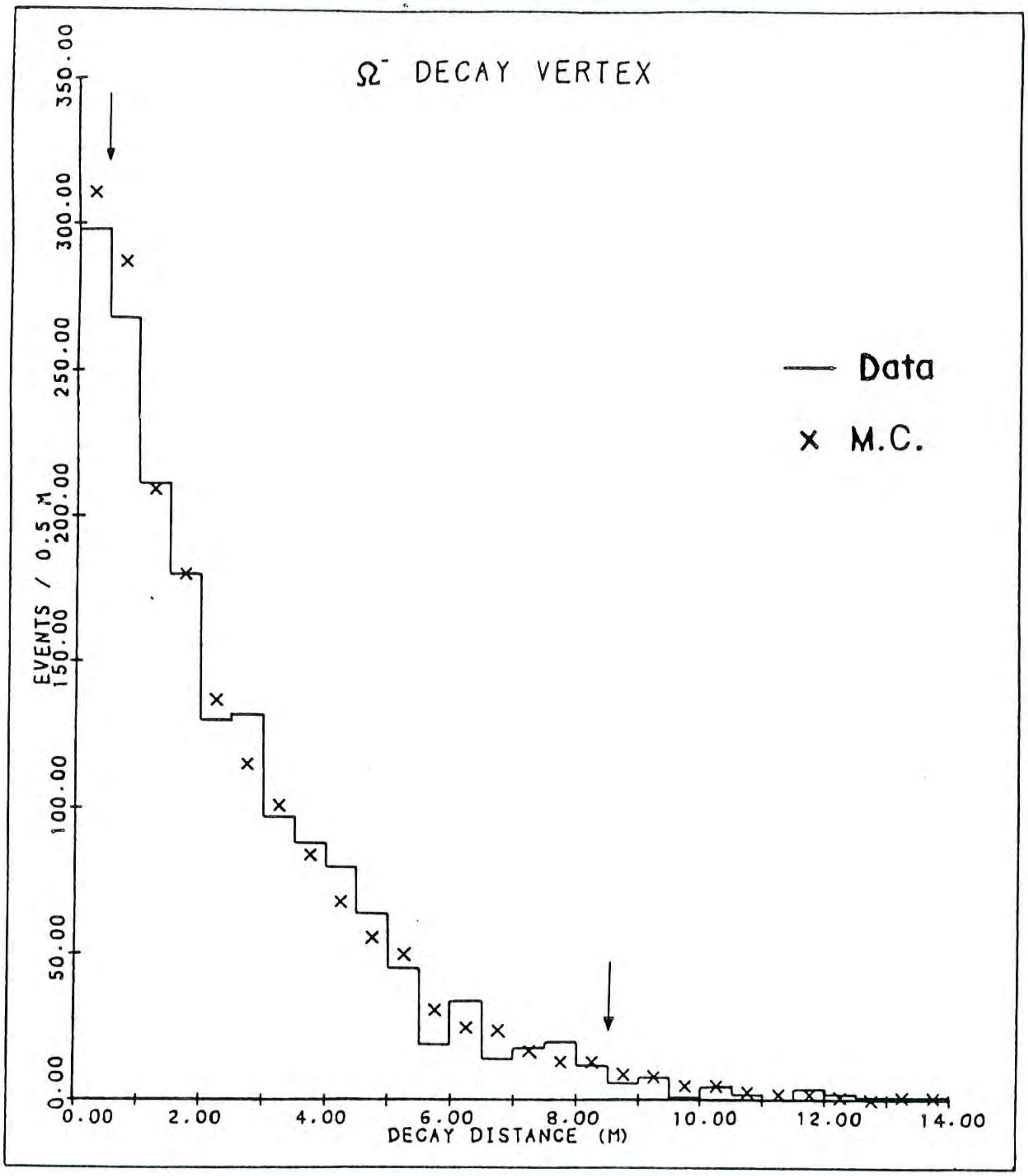

Figure 5.2 The decay vertex distribution of the Ω^- with an input lifetime of $c\tau_\Omega$ = 2.5 cm. The arrows show where the cut was applied.

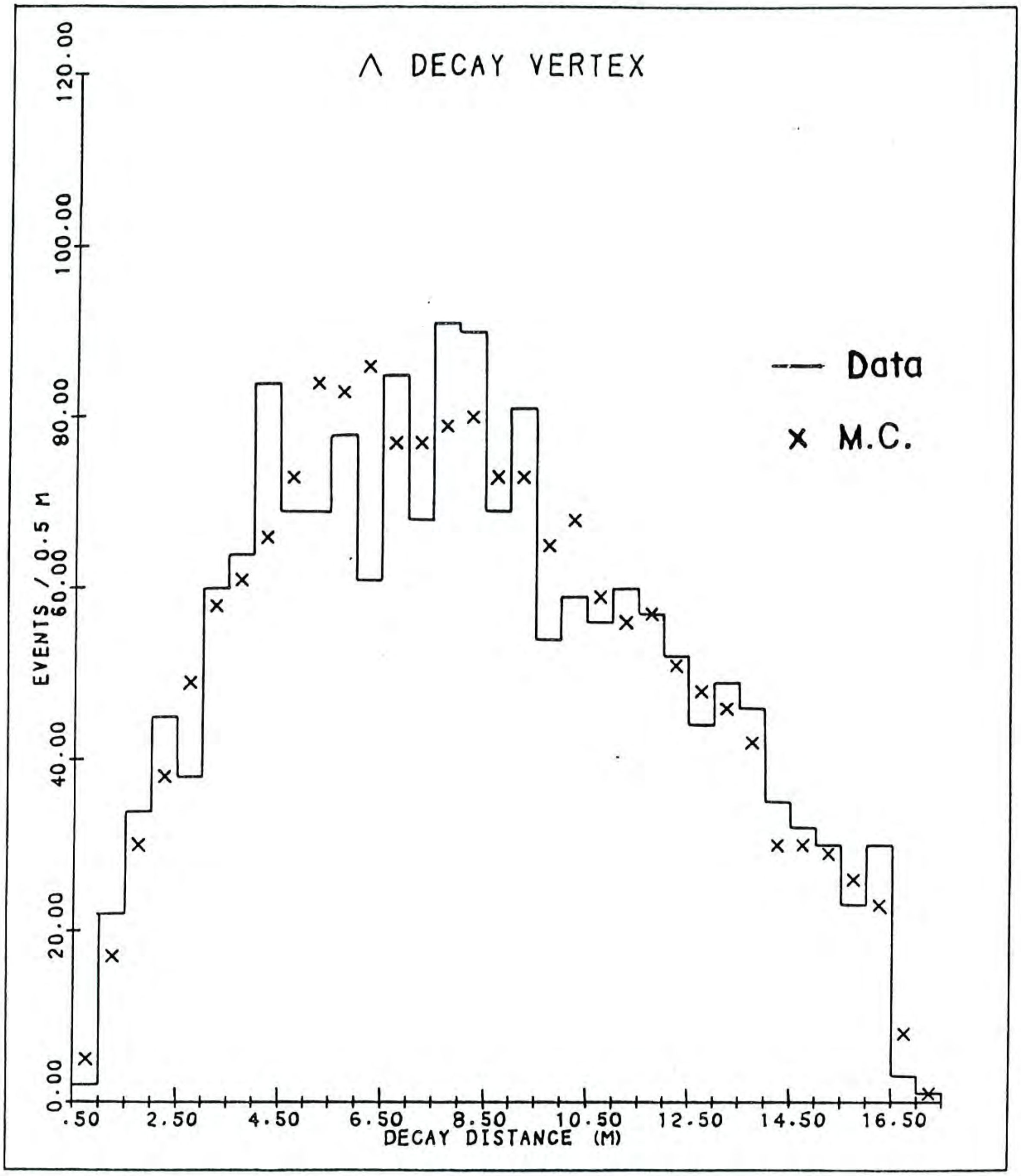

Figure 5.3 The distribution of the Λ decay vertex at $c\tau_{\Omega}$ = 2.5 cm.

Mean momentum (Gev/c)	Decay region (m)	$c\tau_\Lambda$ (cm)	χ^2	
152	$0.5 \leqslant z \leqslant 8.5$	~~2.48±0.10~~ 2.67 ±0.11	15.8/16	weighted average.
185	$0.5 \leqslant z \leqslant 8.5$	~~2.15±0.10~~ 2.14 ± 0.10	16.7/16	2.43±0.0
219	$0.5 \leqslant z \leqslant 8.5$	~~2.54±0.12~~ 2.60 ±0.13	10.9/16	
155	$1.5 \leqslant z \leqslant 6.5$	2.40±0.19	10.1/10	
188	$1.5 \leqslant z \leqslant 6.5$	2.25±0.19	11.5/10	2.37 ±0.11
221	$1.5 \leqslant z \leqslant 6.5$	2.47±0.21	10.2/10	

Table 5.1 The measured lifetime expressed in $c\tau_\Lambda$ for different momentum bins in two decay regions.

CHAPTER 6

DATA ANALYSIS IV : POLARIZATION

6.1 General Aspects of the Ω^- Decay

Since the Ω^- is a baryon, its spin must be a half integer ($J = 1/2, 3/2, 5/2$, and so on). Several experiments have attempted to determine its spin, but failed to achieve a conclusive result. So far, only the spin 1/2 assignment is ruled out. In all other respects it fits perfectly into the s-wave SU(3) decuplet. For this reason it is usually assumed to have spin 3/2. However, in the following discussion, this assumption will not be used.

For the weak decay $\Omega^- \rightarrow \Lambda K^-$, the nonconservation of parity implies that the orbital angular momentum of the final state can be $J \pm 1/2$, with amplitude $A_{j\pm\frac{1}{2}}$. In terms of the decay amplitudes, three asymmetry parameters for the decay are defined

$$\alpha = 2\,\frac{Re(A^{*}_{j-1/2}\ A_{j+1/2})}{|A_{j-1/2}|^2 + |A_{j+1/2}|^2}$$

$$\beta = 2\,\frac{Im(A^{*}_{j-1/2}\ A_{j+\frac{1}{2}})}{|A_{j-1/2}|^2 + |A_{j+1/2}|^2}$$

$$\gamma = \frac{|A_{j-1/2}|^2 - |A_{j+\frac{1}{2}}|^2}{|A_{j-1/2}|^2 + |A_{j+\frac{1}{2}}|^2}$$

such that

$$\alpha^2 + \beta^2 + \gamma^2 = 1.$$

In order to discuss the measurement of the decay parameter and the vector polarization of the Ω^- in the following sections, it is necessary to know the distribution and the polarization of the Λ in the decay of the Ω^-. First of all, two coordinate systems, $S = (\hat{x},\hat{y},\hat{z})$ and $S' = (\hat{X},\hat{Y},\hat{\Lambda})$, are defined in the Ω^- rest frame, where $\hat{z}$ is the axis of quantization, $\hat{\Lambda}$ is a unit vector along the Λ flight path and

$$\hat{X} = \frac{\hat{\Lambda} \times (\hat{\Lambda} \times \hat{Z})}{|\hat{\Lambda} \times (\hat{\Lambda} \times \hat{Z})|}$$

$$\hat{Y} = \frac{\hat{Z} \times \hat{\Lambda}}{|\hat{Z} \times \hat{\Lambda}|} .$$

The angular distribution and the polarization components of the Λ along $\hat{X}$, $\hat{Y}$ and $\hat{\Lambda}$ are determined to be [37]-[38]

$$I(\theta,\varphi) = A(\theta,\varphi) + \alpha\, B(\theta,\varphi) \tag{6.1}$$

$$I\vec{P}_\Lambda \cdot \hat{\Lambda} = \alpha\, A(\theta,\varphi) + B(\theta,\varphi) \tag{6.2}$$

$$I\vec{P}_\Lambda \cdot (\hat{X}+i\hat{Y}) = (i\beta-\gamma)(2J+1) \sum_{\substack{L=1\\ odd}}^{2J} \sum_{M=-L}^{L} \left(\frac{2J+1}{4\pi}\right)^{1/2} n^J_{L0}\, t_{LM} \left[L(L+1)\right]^{-1/2} \times D^L_{M1}(\varphi,\theta,0) \tag{6.3}$$

with

$$A(\theta,\varphi) = \sum_{\substack{L=0\\ even}}^{2J} \sum_{M=-L}^{L} n^J_{L0}\, t_{LM}\, Y^*_{LM}(\theta,\varphi)$$

and

$$B(\theta,\varphi) = \sum_{\substack{L=1\\ odd}}^{2J} \sum_{M=-L}^{L} n^J_{L0}\, t_{LM}\, Y^*_{LM}(\theta,\varphi)$$

where θ,φ are the polar angles of the Λ in the Ω^- rest frame, $Y_{LM}(\theta,\varphi)$ are the spherical harmonics, $D^L_{M1}(\varphi,\theta,0)$ are the Wigner rotation matrices, the quantities n^J_{L0} are proportional to the Clebsch-Gordan coefficients $\langle JJ\tfrac{1}{2}\text{-}\tfrac{1}{2}|L0\rangle$,

$$n^J_{L0} = (-1)^{J-1/2}\sqrt{\frac{2J+1}{4\pi}}\langle JJ\tfrac{1}{2}\text{-}\tfrac{1}{2}|L0\rangle$$

and t_{LM} are known as the multipole moments that are related to the expectation values of the spin components of the Ω^-. In particular, the components of the vector polarization of the Ω^- defined by

$$\vec{P} = \langle\vec{J}\rangle/J$$

are expressed in terms of the t_{1M}, where $M = 0,\pm 1$, as

$$P_x = \sqrt{\frac{J+1}{J}}\,\frac{(t_{1-1} - t_{11})}{\sqrt{2}}$$

$$P_y = i\sqrt{\frac{J+1}{J}}\,\frac{(t_{1-1} + t_{11})}{\sqrt{2}}$$

$$P_z = \sqrt{\frac{J+1}{J}}\,t_{10} \qquad .$$

In addition, t_{00} is normalized to 1 and $t_{L-M} = (-1)^M\ t^*_{LM}$. Sometimes, the multipole moments t_{LM} are also called the tensor polarization of rank L. Therefore, in general, a particle with spin greater than 1/2 can have vector polarization (L=1) as well as tensor polarizations (L > 1).

It is clear from equations (6.2) and (6.3) that the polarization information of the Ω^- is passed onto the daughter Λ which will decay via weak interactions. Therefore, the determination of the decay parameter and the vector polarization of the Ω^- is reduced to the problem of measuring the Λ polarization by studying the proton distribution in the $\Lambda \rightarrow p\pi^-$ decay.

6.2 Λ Polarization Measurement

For the $\Lambda \rightarrow p\,\pi^-$ decay, the distribution of the proton is given by

$$dn/d\Omega_p = \frac{1}{4\pi}(\ 1 + \alpha_\Lambda \vec{P}_\Lambda . \hat{p}\ ) \tag{6.4}$$

where Ω_p and $\hat{p}$ are the solid angle and the momentum unit vector of the proton in the Λ rest frame respectively, and α_Λ is the asymmetry parameter of the $\Lambda \to p\pi^-$ decay. Since equation (6.4) is independent of the azimuthal angle, it can be rewritten as

$$dn/d(\cos\theta) = 1/2(1+\alpha_\Lambda \vec{P}_\Lambda . \hat{n} \cos\theta) \tag{6.5}$$

where $\hat{n}$ is an arbitrarily chosen unit vector and $\cos\theta = \hat{n}.\hat{p}$. If α_Λ and $\vec{P}_\Lambda$ are nonzero, then the distribution of the proton will be anisotropic in space with respect to $\hat{n}$. Since expression (6.5) is linear in $\hat{n}.\hat{p}$, the component of the Λ polarization along $\hat{n}$ can be measured as $\alpha_\Lambda \vec{P}_\Lambda . \hat{n}$ from the slope of the equation. In practice, the distribution is modified by the acceptance of the apparatus which has been discussed in the invariant cross section and lifetime measurement.

A version of the Monte Carlo technique known as the Hybrid Monte Carlo method can be employed to take care of the geometric acceptance problem as well as determining the polarization in an efficient way [39]. In this method, a Monte Carlo event is generated with all parameters the same as the real event except the cos θ value which is randomly chosen between +1 and -1. The Monte Carlo event is accepted if its proton and pion satisfy the same software trigger and apertures as the real event. For each real event, Monte Carlo events are generated until 10 accepted events are found. If less than 10 events are accepted in 200 trials, the real as well as the accepted Monte Carlo events are excluded from the analysis.

Apart from the geometric acceptance distortion, the cos θ distribution of the accepted Monte Carlo events is further biased by the polarization of the real events. This bias must be removed before the polarization determination can be performed. This can be done by assigning to j-th Monte Carlo event of the i-th real event a weight

$$W_{ij} = (1+\alpha_\Lambda \vec{P}_\Lambda . \hat{n} \cos \theta_{ij})/(1+\alpha_\Lambda \vec{P}_\Lambda . \hat{n} \cos \theta_i)$$

where $\alpha_\Lambda \vec{P}_\Lambda . \hat{n}$ is treated as an unknown quantity.

The Monte Carlo data can now be compared with the real data by forming a χ^2 expression

$$\chi^2 = \sum_{k=1}^{20} (N_k^R - N_k^{MC}/N_0)^2 / N_k^2$$

where N_k^R is the number of real events with cos θ belonging to bin k, N_k^{MC} is the number of Monte Carlo events with cos θ falling in bin k and $N_0 = 10$ is a normalization constant. Each N_k^{MC} is given by

$$N_k^{MC} = \sum_{i,j} W_{ij}\,(k)$$

where the sum is over each event i and each Monte Carlo event j such that $\cos\theta_{ij}$ lies in bin k. The best value for the polarization is obtained as the $\alpha_\Lambda \vec{P}_\Lambda . \hat{n}$ value that gives the minimum χ^2. Further details about the Hybrid Monte Carlo method can be found in reference [39]. These techniques will be applied to determine the Ω^- decay parameter and the vector polarization.

6.3 Decay Parameter Analysis

The joint distribution of the proton (in the lambda rest frame) and the lambda (in the Ω^- rest frame) for the decay sequence $\Omega^- \rightarrow \Lambda K^-$ and $\Lambda \rightarrow p\pi^-$ is

$$\begin{aligned}(dN_p/d\Omega_p)(dN_\Lambda/d\Omega_\Lambda) &= I(\theta_\Lambda,\varphi_\Lambda)\,.\,\frac{1}{4\pi}(1+\alpha_\Lambda\vec{P}_\Lambda . \hat{p}) \\ &= \frac{1}{4\pi}(I_\Lambda + \alpha_\Lambda I_\Lambda \vec{P}_\Lambda . \hat{\Lambda}\;\; \hat{\Lambda} . \hat{p} \\ &\quad + \alpha_\Lambda I_\Lambda \vec{P}_\Lambda . \hat{X}\;\; \hat{X} . \hat{p} + \alpha_\Lambda I_\Lambda \vec{P}_\Lambda . \hat{Y}\;\; \hat{Y} . \hat{p}) \qquad (6.6)\end{aligned}$$

where I_Λ, $I_\Lambda \vec{P}_\Lambda . \hat{\Lambda}$, $I_\Lambda \vec{P}_\Lambda . \hat{X}$ and $I_\Lambda \vec{P}_\Lambda . \hat{Y}$ are given in equations (6.1), (6.2) and (6.3). After integrating equation (6.6) over the solid angle of the Λ and the azimuthal angle of the proton with respect to the coordinate system S', the final proton distribution in the Λ rest frame is given by

$$dN_p/d(\cos\theta_p) = (1/2)(1+\alpha_\Lambda\alpha_\Omega \cos\theta_p)$$

which is independent of the spin of the Ω^- and it implies that

$$\vec{P}_\Lambda = \alpha_\Omega \hat{\Lambda} \ .$$

Since the polarization is along the Λ momentum, it is helicity which is invariant under rotation. Hence, the various measured momentum-4-vectors can be Lorentz transformed directly from the laboratory frame to the Λ rest frame. Fig. 6.1 shows the relationship between the various momenta in the Λ rest frame. Thus, using the Hybrid Monte Carlo method, a measurement of the proton angular distribution with respect to $\hat{n} = -\hat{\Omega}^-$ yields the product $\alpha_\Lambda \alpha_\Omega$. Since α_Λ is known, α_Ω can be determined in this manner.

6.4 Ω^- Vector Polarization Analysis

Another expression for the average distribution of the proton can be calculated from equation (6.4) by integrating over the solid angle of the Λ with respect to a coordinate system parallel to S. The result is (see appendix for details)

$$(dN_p/d\Omega_p) = \frac{1}{4\pi}\left\{1+\frac{\alpha_\Lambda}{2(J+1)}\left[1+(2J+1)\gamma_\Omega\right]\vec{P}_\Omega\cdot\hat{p}\right\} \quad . \qquad (6.7)$$

Comparing with equation (6.4), the average lambda polarization is found to be

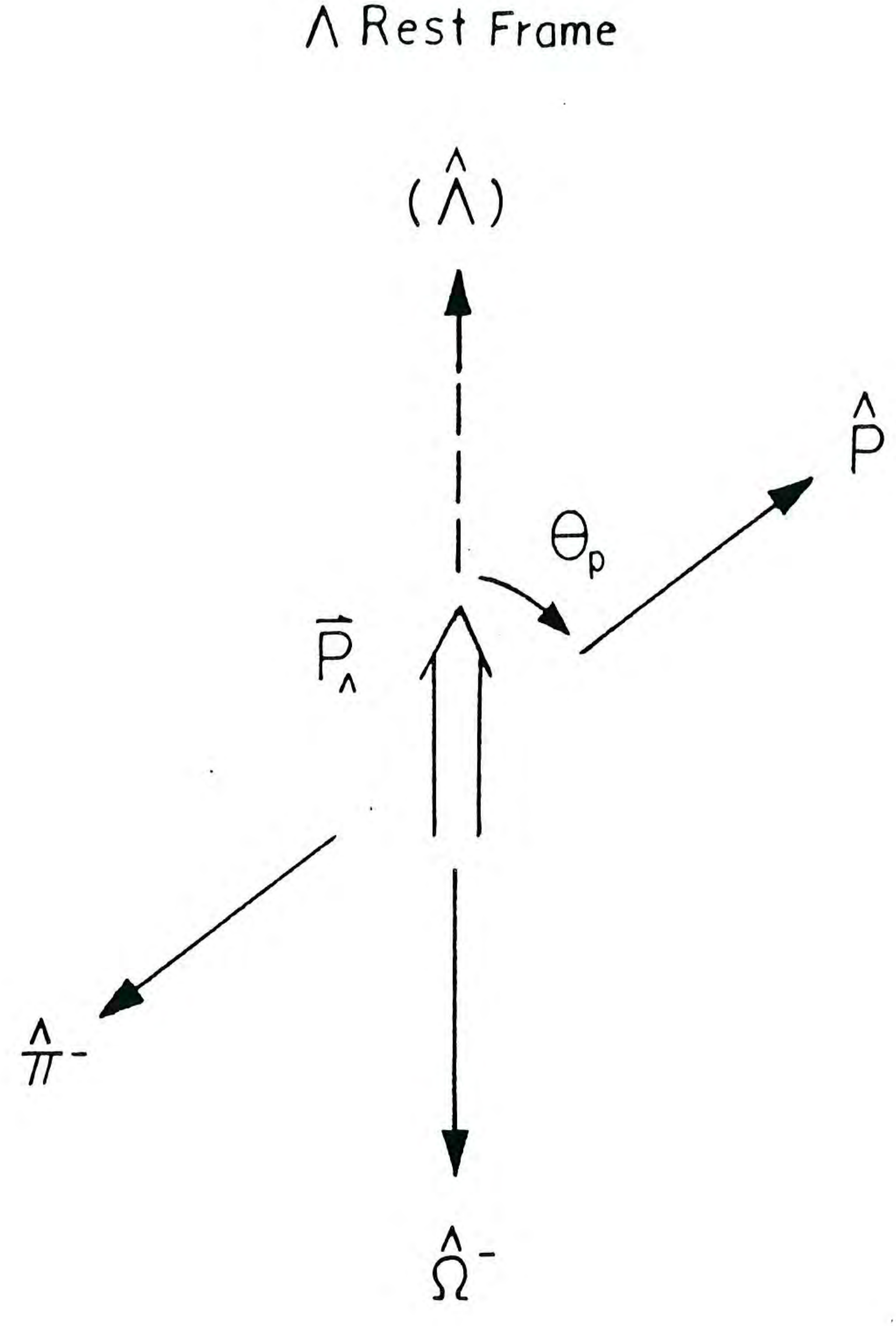

Figure 6.1 Definition of the unit vectors in the Λ rest frame in the α_Ω analysis.

$$\vec{P}_\Lambda = \frac{1}{2(J+1)}\left[1+(2J+1)\gamma_\Omega\right]\vec{P}_\Omega \tag{6.8}$$

which is not related to any multipole moments except the vector polarization of the Ω^-. Equation (6.8), derived here for the first time, is the generalization of the expression employed to measure the polarization of the Ξ^0 which is a spin 1/2 particle [8].

Before this experiment, the decay parameter α_Ω for the $\Omega^- \to \Lambda K^-$ decay was determined to be -0.018 ± 0.038 [30]. This implies that $\gamma_\Omega = \pm1$. If γ_Ω is 1, then equation (6.8) is reduced to

$$\vec{P}_\Lambda = \vec{P}_\Omega$$

which is independent of the spin of the Ω^-; whereas for $\gamma_\Omega = -1$, the relation is

$$\vec{P}_\Lambda = -\frac{J}{J+1}\vec{P}_\Omega \quad .$$

Using the general procedure described in section 6.2, the lambda polarization can be measured by determining its components along the spectrometer axes. That is, $\hat{n}$ is consecutively chosen to be $\hat{x}$, $\hat{y}$ and $\hat{z}$. In the Hybrid Monte Carlo program, the proton and the π^- are transformed directly from the laboratory frame to the Λ rest frame without going into the Ω^- rest frame. Furthermore, the parameters of the K^- from the real event are kept the same for the Monte Carlo events.

6.5 Vector Polarization and Biases

Besides the geometric acceptance, any inefficiency in the reconstruction process or any hidden instrumental deficiencies can give rise to asymmetry in the distribution of interest. These spurious signals are called biases. In other words, the measured asymmetry actually is the sum of the vector polarization and the biases,

$$\alpha_\Lambda \vec{P}_\Lambda . \hat{n}(\theta) = \alpha_\Lambda \vec{P}_\Lambda . \hat{n} + B \quad .$$

The vector polarization is an odd function of the production angle whereas the biases are independent of the production angle. For the negative angle data, the measured signal is given by

$$\alpha_\Lambda \vec{P}_\Lambda . \hat{n}(-\theta) = - \alpha_\Lambda \vec{P}_\Lambda . \hat{n} + B \quad .$$

This implies that the vector polarization is

$$\alpha_\Lambda \vec{P}_\Lambda . \hat{n} = (1/2)(\alpha_\Lambda \vec{P}_\Lambda . \hat{n}(\theta) - \alpha_\Lambda \vec{P}_\Lambda . \hat{n}(-\theta)) \qquad (6.9)$$

and the biases are determined to be

$$B = (1/2)(\alpha_\Lambda \vec{P}_\Lambda . \hat{n}(\theta) + \alpha_\Lambda \vec{P}_\Lambda . \hat{n}(-\theta)) \qquad (6.10)$$

This reflects the importance of taking data at production angles of $+\theta$ and $-\theta$.

The vector polarization, the biases, as well as the $(g/2 - 1)$ factor, can also be determined by the χ^2 method. The conservation of parity in strong interactions involving unpolarized beam and target demands that the spin of the Ω^- produced at non-zero production angle be normal to the production plane defined by $\vec{p}_{in} \times \vec{p}_{out}$. In the presence of the magnetic field of M2, the precession angle of the vector polarization, measured in radians, is given by [40]

$$\begin{aligned} \varphi &= (q/m_\Omega c^2\beta)(g/2 - 1)\int \vec{B}.\vec{dl} \\ &= -0.179(g/2 - 1)\int \vec{B}.\vec{dl} \qquad (6.11) \end{aligned}$$

where q is the charge of the Ω^-, $\int \vec{B}.\vec{dl}$ is the field integral measured in T-m, $\beta = 1$ is the Lorentz factor and the quantity g/2 is related to the magnetic dipole moment of the Ω^-, μ_Ω, through the equation

$$\mu_\Omega = (g/2)(q/m_\Omega c)J_m . \qquad (6.12)$$

where J_m is the spin component along the axis of quantization. With the measured asymmetries, $\alpha_\Lambda \vec{P}_\Lambda.\hat{n}$, a χ^2 expression can be written down as

$$\chi^2 = \sum_{j,k} \left\{ \frac{[(\alpha_\Lambda P_{\Lambda x})_{jk} - B_x \pm \alpha_\Lambda P_{\Lambda K} \cos \varphi_{jk}]^2}{\sigma_{x\,jk}^2} + \frac{[(\alpha_\Lambda P_{\Lambda z})_{jk} - B_z \pm \alpha_\Lambda P_{\Lambda K} \sin \varphi_{jk}]^2}{\sigma_{z\,jk}^2} \right\} \quad (6.13)$$

where j runs over two field integrals and k over production angles $+\theta$ and $-\theta$. The biases B_x and B_z are assumed to be constants. The LOWER sign of the $\pm$ symbol in the expression refers to the POSITIVE production angle. The polarization, P_0, the biases and the (g/2 - 1) factor will be determined as those values that minimize the χ^2.

6.6 Result of the α_Ω Measurement

Data taken at $\pm$5 mrad and $\pm$7.5 mrad were combined. With the selected 1,743 events, $\alpha_\Lambda \alpha_\Omega$ was measured for each of three Ω^- momentum bins. The results are listed in Table 6.1. The overall value of $\alpha_\Lambda \alpha_\Omega$ was determined to be -0.022 ± 0.051. This is not the weighted average of the results given in Table 6.1. Since α_Λ was known to be 0.642 ± 0.013 [14], the value obtained for α_Ω, the decay parameter of the $\Omega^- \to \Lambda K^-$ decay mode, was -0.034 ± 0.079.

Monte Carlo studies indicated that the biases introduced by the reconstruction process and the software cuts were less than 0.01. The effect of the background on the α_Ω measurement was examined by including events with

Mean momentum (GeV/c)	$\alpha_\Lambda \alpha_\Omega$
152	-0.047 ± 0.091
185	0.063 ± 0.087
218	-0.068 ± 0.081

weighted average $= -0.02 \pm 0.05$

Table 6.1 $\alpha_\Lambda \alpha_\Omega$ measured for three different momentum bins.

the Λ-K invariant mass in the interval between 1.63 GeV/c^2 and 1.73 GeV/c^2, $\alpha_\Lambda \alpha_\Omega$ was found unchanged within the statistical uncertainty.

6.7 Results of the Vector Polarization Measurement

The 1,743 events were divided into four data sets. Two of them were taken at $\pm$5 mrad and 6.6 T-m. For the sake of the magnetic moment measurement which is independent of the production angle but depends on the field integral, the 5 mrad (-5 mrad) and the 7.5 mrad (-7.5 mrad) data with the same field integral of 5.13 T-m were combined into two sets.

The measured asymmetries, $\alpha_\Lambda \vec{P}_\Lambda . \hat{n}$ where $\hat{n} = \hat{x}$, $\hat{y}$ and $\hat{z}$, for the sets are listed in Table 6.2. The momentum-averaged signals and biases for the two different field integral values are listed in Table 6.3. The magnitudes of $\vec{P}_\Lambda$ for the 6.6 T-m and 5.13 T-m data were 0.12 ± 0.09 and 0.13 ± 0.17 respectively.

Since the vector polarization at the target was along the x-axis of the target coordinate system, and the precession was in the x-z plane, there should be no y-component which was confirmed by the measurement.

Angle (mrad)	$\int B.dl$ (T-m)	Asymmetry
+5.0	6.60	x −0.008 ± 0.077
		y 0.088 ± 0.071
		z −0.126 ± 0.081
−5.0	6.60	x −0.162 ± 0.077
		y 0.092 ± 0.071
		z −0.094 ± 0.081
+5.0 & +7.5	5.13	x 0.065 ± 0.148
		y 0.079 ± 0.145
		z 0.078 ± 0.172
−5.0 & −7.5	5.13	x −0.065 ± 0.148
		y 0.071 ± 0.145
		z 0.186 ± 0.172

Table 6.2 The measured asymmetries along the laboratory axes x, y and z.

Angle (mr)	$\int B.dl$ (T-m)	Polarization ($\alpha_\Lambda P_\Lambda$)	Bias (B)
5.0	6.60	x 0.077 ± 0.055 y −0.002 ± 0.050 z −0.016 ± 0.057	x −0.085 ± 0.055 y 0.090 ± 0.050 z −0.110 ± 0.057
5.0 and 7.5	5.13	x 0.065 ± 0.105 y 0.004 ± 0.102 z −0.054 ± 0.121	x 0.000 ± 0.105 y 0.075 ± 0.102 z 0.132 ± 0.121

Table 6.3 The polarization components and biases of the data at two field integrals.

6.8 Magnetic Dipole Moment

In the following discussion, the measured vector polarizations for the Ω^- are assumed to be significant.

A priori, the initial direction of the vector polarization is known to be parallel or antiparallel to the x-axis and the sense of precession as well as the number of revolutions in the magnetic field are unknown. Thus, there are an infinite number of solutions for the magnetic moment. However, the precession angle is proportional to the field integral and if the factor $(g/2 - 1)$ in equation (6.11) is non-zero, then by varying the magnetic field, the ambiguity in the magnetic moment can be resolved.

In the case of the Ω^-, since the sign of the γ_Ω was not measured, the initial direction of the polarization could not be determined. The four lowest order precession conditions are illustrated in Fig. 6.2. The values of the factor g/2 calculated from the polarizations at 6.60 T-m and 5.13 T-m are shown in Table 6.4. According to equation (6.12), the magnetic moment, μ_Ω, measured in nuclear magnetons (n.m.) is related to g/2 by the expression

$$\begin{aligned} \mu_\Omega &= 3(g/2)(q/e)(m_p/m_\Omega) \text{ n.m.} \\ &= -1.683(g/2) \text{ n.m.} \end{aligned} \tag{6.14}$$

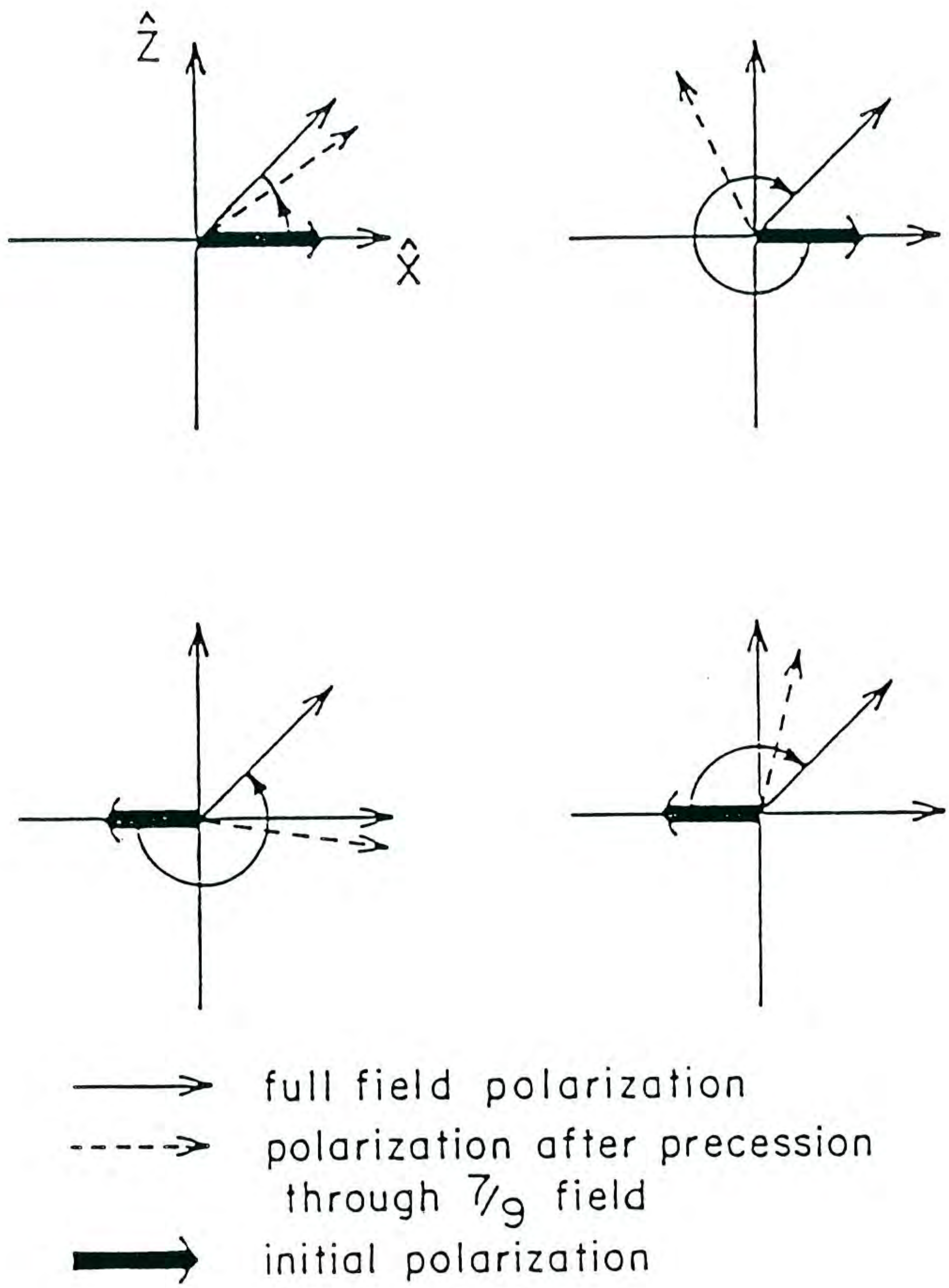

Figure 6.2 The four lowest order precession ambiguities shown for a polarization which has precessed through the full field and the four possible directions after precession through a 7/9 field.

P_0	Sense of rotation	Precession angle at		$g/2 - 1$	Magnetic moment (n.m.)
		5.13 T-m	6.60 T-m		
$-x$ $+x$	clockwise	$-220^\circ \pm \infty$	$-192^\circ \pm 42^\circ$	$+2.84 \pm 0.62$	-6.5 ± 1.0
$-x$ $+x$	counter-clockwise	$+140^\circ \pm \infty$	$+168^\circ \pm 42^\circ$	-2.48 ± 0.62	2.5 ± 1.0
$+x$ $-x$	---	$-40^\circ \pm \infty$	$-12^\circ \pm 42^\circ$	$+0.18 \pm 0.62$	-2.0 ± 1.0
$+x$ $-x$	counter-clockwise	$+320^\circ \pm \infty$	$+348^\circ \pm 42^\circ$	-5.14 ± 0.62	7.0 ± 1.0

Table 6.4 The four lowest order precessions, the associated $(g/2 - 1)$ factors and the magnetic moments. P_0 shows the direction of the polarization vector at target, the top one stands for the case $\vec{P}_\Lambda = \vec{P}_\Omega$ and the bottom is for the case $\vec{P}_\Lambda = -J/(J+1)\ \vec{P}_\Omega$. The magnetic moments are calculated assuming the spin projection is $3\hbar/2$.

where e and m_p are the charge and the mass of the proton respectively and the spin projection of the Ω^- along the quantization axis is assumed to be $3\hbar/2$. Using equation (6.14), magnetic moments corresponding to each g/2 value were worked out and are listed in Table 6.4. The most reasonable solution obtained was -2.0 ± 1.0 n.m.. Therefore, if γ_Ω is 1, then $\vec{P}_\Omega$ should point in the +x direction at the target and its magnitude should be 0.12 ± 0.09 and 0.13 ± 0.17 for the 6.6 T-m and 5.13 T-m data respectively. In the case that γ_Ω is -1, then the magnitudes of $\vec{P}_\Omega$ should be multiplied by a factor of (J+1)/J and $\vec{P}_\Omega$ should point in the -x direction.

The master χ^2 fit also gave a consistent result. The magnitudes of $\vec{P}_\Lambda$ were 0.12 ± 0.08 and 0.12 ± 0.16 for the 6.6 T-m and 5.13 T-m data respectively. The biases along the x and z axes were -0.07 ± 0.05 and -0.06 ± 0.05 respectively. The value obtained for g/2 was 1.26 ± 0.59, corresponding to a value of -2.1 ± 1.0 n.m. for the magnetic moment, and the χ^2 per degree of freedom was 1.3.

CHAPTER 7

CONCLUSIONS

The invariant differential production cross section of the Ω^- produced from 400 GeV/c protons on beryllium at production angles of 5 mrad and 7.5 mrad has been measured. If the invariant cross section was parametrized with an expression proportional to $(1-x)^n$, then n was found to be 5.87 ± 0.15 for the 5 mrad data and 5.68 ± 0.66 for the 7.5 mrad sample. In the fragmentation model proposed by Gunion [41], the valence quarks of the incident proton emit three gluons which, in turn, create three strange-antistrange quark pairs. Subsequently, the strange quarks combine to form the Ω^-. According to this picture, the exponent n is predicted to be 5 which is in fair agreement with the result of this experiment. In other words, the Ω^- is centrally produced in the p-Be reaction.

The lifetime of the Ω^- was determined to be
0.815±0.06
(~~0.83±0.06~~) $\times 10^{-10}$ s in this experiment. This is consistent with the other experimental results and the comparison is shown in Fig. 7.1.

The asymmetry parameter for the $\Omega^- \rightarrow \Lambda K^-$ decay mode, α_Ω, was determined to be -0.03 ± 0.08 which can be compared to the latest value of -0.018 ± 0.039 reported by the CERN charged hyperon group. The comparison of the results from various experiments is shown in Fig. 7.2. Furthermore, the measurement is consistent with the theoretical prediction that the $\Omega^- \rightarrow \Lambda K^-$ decay be almost parity conserving [29], [31]-[32].

The search for the inclusive vector polarization of the Ω^-'s produced by protons in this experiment was not conclusive due to the limited statistics. The magnitude of the polarization of the daughter Λ was measured to be 0.12 ± 0.08 for the 5 mrad data at 6.6 T-m. Since the sign of the decay parameter γ_Ω and the spin of the Ω^- were unknown, the direction of the polarization of the Ω^- remained undetermined. However, if the 1.5 signal was assumed significant, then the possible interpretations are: if $\gamma_\Omega = +1$, then $\vec{P}_\Omega$ was along +x and, if $\gamma_\Omega = -1$, then $\vec{P}_\Omega$ was along -x.

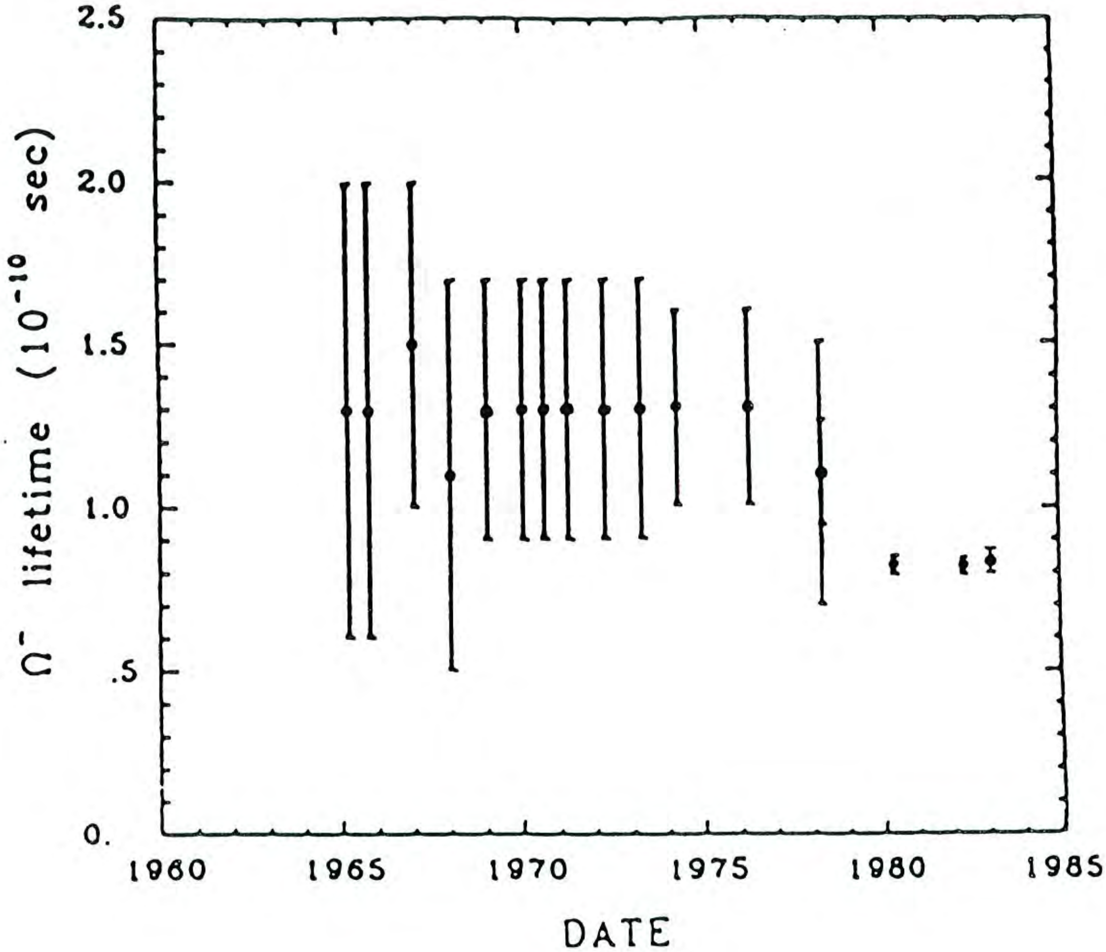

Figure 7.1 Measurements of the Ω^- lifetime (taken from Reference 14). The last point is the result of this experiment.

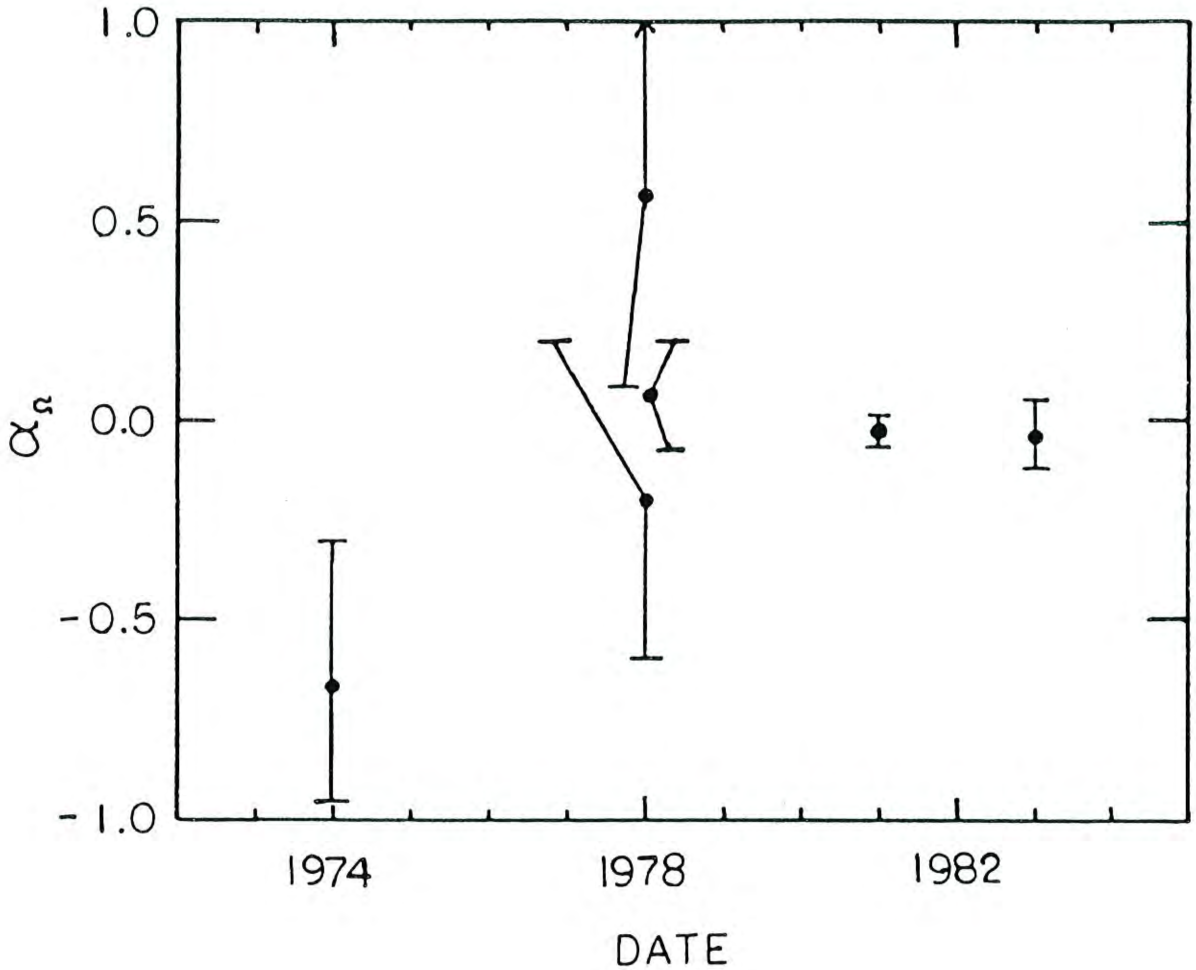

Figure 7.2 Measurements of the decay parameter, α_Ω, for the $\Omega^- \rightarrow \Lambda K^-$ decay mode (take from Reference 14). The last point is the result of this experiment.

Assuming that the observed polarization was significant and the spin component along the axis of quantization was $3\hbar/2$, the magnetic moment of the Ω^- was measured for the first time. The value obtained was -2.1 ± 1.0 which can be compared to the prediction of the broken SU(6) quark model. Since the magnetic moment of the strange quark is the same as the magnetic moment of the Λ which is -0.61 n.m. [14], the magnetic moment of the Ω^- should be -1.83 n.m. which is consistent with the measurement. Recently, based on a lattice QCD calculation in the quenched approximation (that is, neglecting the effects of the virtual quark pairs), C.Bernard et al. [42] found that the magnetic moment of the Ω^- to be -1.7 ± 0.6 n.m.. Again, this agrees with the experimental result.

REFERENCES

1. G.Bunce et al., Phys.Rev.Lett. 36 ,1113(1976).

2. K.Raychaudhuri et al., Phys.Lett. 90B , 319(1980).

3. K.Heller et al., Phys.Lett. 68B , 480(1977).

4. F.Lomanno et al., Phys.Rev.Lett. 43 , 1905(1979).

5. S.Erhan et al., Phys.Lett. 82B , 1325(1979).

6. K.Heller et al., Phys.Rev.Lett. 41 , 607(1978), Erratum, Phys.Rev.Lett. 45 , 1043(1980).

7. R.Grobel, Ph.D. thesis, University of Wisconsin (1980), unpublished.

8. G.Bunce et al., Phys.Lett. 86B , 386(1979).

9. P.T.Cox et al., Phys.Rev.Lett. 46 , 877(1981).

10. M.Corcoran et al., Phys.Rev. D22 , 2624(1980).

11. P.Yamin et al., Phys.Rev. D23 , 31(1981).

12. F.Lomanno et al., Phys.Lett. 96B , 223(1980).

13. L.Schachinger et al., Phys.Rev.Lett. 41 , 1348(1978).

14. Particle Data Group, Phys.Lett. 111B , April(1982).

15. There were 2 Ω^- decays observed in emulsion experiments : W.F.Fry, J.Schneps and M.S.Swami, Phys.Rev. 97 , 1189(1955); W.F.Fry, J.Schneps and M.S.Swami, Nuo.Cim. 2 , 346(1955).

16. Experiments with only a single Ω^- event are not cited here. See reference [14] for details.

17. R.B.Palmer et al., Phys.Lett. 26B , 323(1968).

18. P.F.Schultz et al., Phys.Rev. 168 , 1509(1968).

19. D.Scotter et al., Phys.Lett. 26B ,474(1968).

20. F.A.Dibianca and R.J.Endorf, Nucl.Phys. B98 , 137(1975).

21. M.Baubillier et al., Phys.Lett. 78B , 342(1978).

22. R.J.Hemingway et al., Nucl.Phys. B142 , 205(1978).

23. M.Gell-Mann, Phys.Lett. 8 , 214(1964).

24. G.Zweig, CERN reports No. Th. 401, 412(1964), unpublished.

25. M.Bourquin et al., Nucl.Phys. B153 , 13(1979).

26. M.Bourquin et al., Phys.Lett. 87B , 297(1979).

27. G.Sauvage, Proc. 19th Int. Conf. High En. Phys., Tokyo 1978, ed. by S.Homma et al.(Phys. Soc. of Japan, Tokyo, 1979), p.427.

28. M.Bourquin et al., Phys.Lett. 88B , 192(1979).

29. J.Finjord, Phys.Lett. 76B , 116(1978).

30. Result from the CERN charged hyperon group presented by R.Arnold in the 1981 EPS conf. on High Energy Phys., Lisbon(1981).

31. M.Suzuki, Prog. Theor. Phys. 32 , 138(1964).

32. Y.Hara, Phys.Rev. 150 , 1175(1966).

33. R.Rameika, Ph.D. thesis, Rutgers University (1981), unpublished.

34. L.Schachinger, Ph.D. thesis, Rutgers University (1978), unpublished.

35. P.Skubic et al., Phys.Rev. D18 , 3115(1978).

36. L.Deck, Ph.D. thesis, Rutgers University (1981), unpublished.

37. N.Byers and S.Fenster, Phys.Rev.Lett. 11 , 52(1963).

38. D.W.Merrill and J.Button-Shafer, Phys.Rev. 167, 1202 (1968).

39. G.Bunce, Nucl. Instru. Meth. 172, 553(1980).

40. V.Bargmann, L.Michel and V.L.Telegdi, Phys.Rev.Lett. 2, 433(1959).

41. J.F.Gunion, Phys.Lett. 88B, 150(1979).

42. C.Bernard et al., Phys.Rev.Lett. 49, 1076(1982).

APPENDIX

A Method For Determining the Polarization Vector of the Ω^- Hyperon

K. B. Luk

Department of Physics and Astronomy

Rutgers University,

Piscataway, N.J. 08854, U.S.A.

Abstract

An expression relating the vector polarization of the Ω^- to the polarization of the daughter particle is presented. Based on this relation, a spin test for the Ω^- is proposed. The equation can also be used to calculate the contribution of the polarization of the resonances to the polarization of the spin $\frac{1}{2}$ hyperons.

It is now a well-established fact that all spin $\frac{1}{2}$ hyperons produced in inclusive reactions with high energy protons are substantially polarized.[1] Although several models[2] have been proposed to explain this phenomenon, the underlying mechanism leading to the observed polarization is still unclear. Nevertheless, this discovery has provided an excellent way to measure the magnetic dipole moments of the hyperons[3] to high precision and this technique can be applied to the Ω^- if it is also produced polarized in a similiar fashion.

Since the quark model[4] predicts that the Ω^- is a spin $\frac{3}{2}$ particle, it can have vector polarization, alignment as well as other higher order tensor polarizations. If the Ω^- is produced with a non-zero production angle by strong interactions, its polarization vector must be normal to the production plane. Independent of the value of the spin, the precession of the polarization vector in a magnetic field is described by the BMT equation.[5] Therefore, knowing the vector polarization is sufficient to measure the magnetic dipole moment of the Ω^-.

The purpose of this paper is to present a relation that can be employed to determine the polarization vector of the Ω^-. Based on this relation, a spin test for the Ω^- is described. Furthermore, it is found that the relation also holds in strong decays. Thus, it can be used to estimate the contribution of the vector polarization of a resonance to the polarization of the decayed particles.

The three dominant decay modes of the Ω^- , namely, $\Omega^- \to \Lambda K^-$, $\Omega^- \to \Xi^0 \pi^-$ and $\Omega^- \to \Xi^- \pi^0$ typify the parity violating weak decay of the type $F_j \to F_{\frac{1}{2}} + B_0$, where the subscripts stand for the spins of the particles and j is a half integer. In terms of the two decay amplitudes $A_{j\pm\frac{1}{2}}$, three asymmetry parameters for the decay are customarily defined as

$$\alpha = 2\,\frac{Re(A^*_{j-\frac{1}{2}}\,A_{j+\frac{1}{2}})}{|A_{j-\frac{1}{2}}|^2 + |A_{j+\frac{1}{2}}|^2} \tag{1}$$

$$\beta = 2\,\frac{Im(A^*_{j-\frac{1}{2}}\,A_{j+\frac{1}{2}})}{|A_{j-\frac{1}{2}}|^2 + |A_{j+\frac{1}{2}}|^2} \tag{2}$$

$$\gamma = \frac{|A_{j-\frac{1}{2}}|^2 - |A_{j+\frac{1}{2}}|^2}{|A_{j-\frac{1}{2}}|^2 + |A_{j+\frac{1}{2}}|^2} \tag{3}$$

so that

$$\alpha^2 + \beta^2 + \gamma^2 = 1. \tag{4}$$

Following the treatment of Byers and Fenster,[6] the density matrix of F_j is expanded in terms of irreducible tensor operators T_{LM},

$$\rho = \frac{1}{2j+1} \sum_{L=0}^{2j} \sum_{M=-L}^{L} (2L+1)\, t^*_{LM}\, T_{LM} \tag{5}$$

where the quantities $t_{LM} = Tr(\rho T_{LM})$ are known as the multipole moments. In the representation with $|jm\rangle$ as basis, the tensor operators T_{LM} and the multipole moments t_{LM} are given by

$$T_{LM} = \sum_{m,m'} |jm\rangle\langle jm|jLm'M\rangle\langle jm'| \tag{6}$$

$$t^*_{LM} = \sum_{m,m'} \langle jm|jLm'M\rangle\, \rho_{mm'} \tag{7}$$

and they obey the relations

$$T_{L-M} = (-1)^M T^{\dagger}_{LM} \tag{8}$$

and $$t_{L-M} = (-1)^M t^*_{LM} \tag{9}$$

In addition, the normalization condition $Tr(\rho) = 1$ implies that $t_{00} = 1$. Fu:thermore, the multipole moments can also be expressed as the expectation values of the tensors formed from the components of j. In particular, the components of the polarization vector of F_j defined by

$$\vec{P} = \langle\vec{j}\rangle/j \tag{10}$$

are related to t_{1M}, $M = 0, \pm 1$ by

$$P_x = \left(\frac{j+1}{j}\right)^{\frac{1}{2}} \frac{(t_{1-1} - t_{11})}{\sqrt{2}} \tag{11}$$

$$P_Y = i\left(\frac{j+1}{j}\right)^{\frac{1}{2}} \frac{(t_{1-1} + t_{11})}{\sqrt{2}} \tag{12}$$

$$P_z = \left(\frac{j+1}{j}\right)^{\frac{1}{2}} t_{10}\,. \tag{13}$$

For the convenience of presenting the discussion, two coordinate systems $S = (\hat{X},\hat{Y},\hat{Z})$ and $S' = (\hat{x},\hat{y},\hat{F})$ are defined in the rest frame of F_j, where $\hat{Z}$ is the axis of quantization. S' is the helicity frame with the unit vector $\hat{F}$ along the flight direction of $F_{\frac{1}{2}}$ and

$$\hat{x} = \frac{\hat{F}\times(\hat{F}\times\hat{Z})}{|\hat{F}\times(\hat{F}\times\hat{Z})|} \tag{14}$$

$$\hat{y} = \frac{\hat{Z}\times\hat{F}}{|\hat{Z}\times\hat{F}|} \tag{15}$$

It can be shown that the angular distribution and the polarization components of $F_{\frac{1}{2}}$ are related to the multipole moments through the expressions

$$I(\theta,\varphi) = \Big(\sum_{\substack{L=0\\ \text{even}}}^{2j-1} + \alpha\sum_{\substack{L=1\\ \text{odd}}}^{2j}\Big)\sum_{M=-L}^{L} n^{j}_{L0}\, t_{LM} Y^{*}_{LM}(\theta,\varphi) \tag{16}$$

$$I\vec{P}'.\hat{F} = \Big(\alpha\sum_{\substack{L=0\\ \text{even}}}^{2j-1} + \sum_{\substack{L=1\\ \text{odd}}}^{2j}\Big)\sum_{M=-L}^{L} n^{j}_{L0}\, t_{LM} Y^{*}_{LM}(\theta,\varphi) \tag{17}$$

$$I\vec{P}'.(\hat{x}+i\hat{y}) = (-\gamma+i\beta)(2j+1)\sum_{\substack{L=1\\ \text{odd}}}^{2j-1}\sum_{M=-L}^{L} n^{j}_{L0}\left(\frac{2L+1}{4\pi}\right)^{\frac{1}{2}}\left[\frac{1}{L(L+1)}\right]^{\frac{1}{2}} \times t_{LM} D^{L}_{M1}(\varphi,\theta,0) \tag{18}$$

where $\vec{P}'$ is the polarization vector of $F_{\frac{1}{2}}$, θ and φ are the polar and azimuthal angles of $F_{\frac{1}{2}}$ in S and the quantities n^{j}_{L0} are given by

$$n^{j}_{L0} = (-1)^{j-\frac{1}{2}}\sqrt{\frac{2j+1}{4\pi}}\langle j\ j\ \tfrac{1}{2}\ {-\tfrac{1}{2}}|L\ 0\rangle \tag{19}$$

notice that

$$n^{j}_{10} = \sqrt{\frac{3j}{4\pi(j+1)}}\ \frac{1}{2j}\,. \tag{20}$$

In the case of the $\Lambda \rightarrow p\pi^-$ decay, equation (16), which gives the distribution of the proton in the Λ rest frame, is simplified to

$$I_p(\theta_p, \varphi_p) = \frac{1}{4\pi}(1 + \alpha_\Lambda \vec{P}_\Lambda . \hat{p}) \tag{21}$$

where $\hat{p}$ is the momentum unit vector of the proton and $\vec{P}_\Lambda$ is the Λ polarization.

We are now ready to derive the equation that can be used to determine the polarization vector of the Ω^-. Without loss of generality, consider the decay sequence

$$\begin{array}{l} \Omega^- \rightarrow \Lambda K^- \\ \qquad\quad \lfloor\!\!\rightarrow p\pi^- \end{array}$$

in which the joint distribution of the Λ and of the proton is given by

$$\begin{aligned} I(\theta_\Lambda, \varphi_\Lambda, \theta_p, \varphi_p) &= \frac{I(\theta_\Lambda, \varphi_\Lambda)}{4\pi}(1 + \alpha_\Lambda \vec{P}_\Lambda . \hat{p}) \\ &= \frac{1}{4\pi}\Big[I(\theta_\Lambda, \varphi_\Lambda) + \alpha_\Lambda I\ \vec{P}_\Lambda . \hat{\Lambda}\ \hat{\Lambda} . \hat{p} \\ &\quad + \alpha_\Lambda I\ \vec{P}_\Lambda . \hat{x}\ \hat{x} . \hat{p} + \alpha_\Lambda I\ \vec{P}_\Lambda . \hat{y}\ \hat{y} . \hat{p}\Big] \end{aligned} \tag{22}$$

where the distribution of Λ and the Λ polarization components $I\ \vec{P}_\Lambda . \hat{\Lambda}$, $I\ \vec{P}_\Lambda . \hat{x}$ and $I\ \vec{P}_\Lambda . \hat{y}$ are given by equations (16), (17) and (18).

With respect to the coordinate system S, the unit vectors $\hat{\Lambda}$, $\hat{x}$ and $\hat{y}$ are related to θ_Λ and φ_Λ by the expressions

$$\hat{\Lambda} = (\sin\theta_\Lambda \cos\varphi_\Lambda,\ \sin\theta_\Lambda \sin\varphi_\Lambda,\ \cos\theta_\Lambda) \tag{23}$$

$$\hat{x} = (\cos\theta_\Lambda \cos\varphi_\Lambda,\ \cos\theta_\Lambda \sin\varphi_\Lambda,\ -\sin\theta_\Lambda) \tag{24}$$

$$\hat{y} = (-\sin\varphi_\Lambda,\ \cos\varphi_\Lambda,\ 0) \tag{25}$$

or in terms of Y_{1M} and D^1_{M1} , m=-1,0,1,

$$\hat{\Lambda} = \left(\frac{1}{2}\sqrt{\frac{8\pi}{3}}(Y_{1-1}-Y_{11}),\ \frac{i}{2}\sqrt{\frac{8\pi}{3}}(Y_{1-1}+Y_{11}),\ \sqrt{\frac{4\pi}{3}}Y_{10}\right) \tag{26}$$

$$\hat{x} = \left(\frac{1}{2}(D^{1*}_{11} - D^{1*}_{-11} + D^1_{11} - D^1_{-11}),\ \frac{i}{2}(D^1_{11} - D^{1*}_{11} + D^1_{-11} - D^{1*}_{-11}),\ -\sqrt{2}D^1_{01}\right) \tag{27}$$

$$\hat{y} = \left(\frac{i}{2}(D^{1*}_{11} - D^1_{11} + D^1_{-11} - D^{1*}_{-11}),\ \frac{1}{2}(D^1_{11} + D^{1*}_{11} + D^1_{-11} + D^{1*}_{-11}),\ 0\right) \quad . \tag{28}$$

The distribution of the proton after integrating over the solid angle of the Λ in the Ω^- rest frame can be calculated from equation (22). The result is

$$\begin{aligned} I_p(\theta_p, \varphi_p) &= \int I(\theta_\Lambda, \varphi_\Lambda, \theta_p, \varphi_p)\, d\Omega_\Lambda \\ &= \frac{1}{4\pi}\left\{1 + \frac{\alpha_\Lambda}{2(j+1)}\left[1+(2j+1)\gamma_{\Lambda K}\right]\vec{P}_\Omega \cdot \hat{p}\right\} \end{aligned} \tag{29}$$

Comparing equation (29) with equation (21), the desired relation is found to be

$$\vec{P}_\Lambda = \frac{1}{2(j+1)}\left[1 + (2j+1)\gamma_{\Lambda K}\right]\vec{P}_\Omega \quad , \tag{30}$$

that is, the Λ polarization averaged over the direction of emission is only related to the polarization vector of the

Ω^-. Equation (30) is the generalization of the expression employed to measure the polarization of the Ξ^0 by G. Bunce et al.[7]

Several experiments have attempted to measure the spin of the Ω^-,[8] but failed to achieve a conclusive result. So far, only the spin $\frac{1}{2}$ assignment is ruled out. Based on equation (30), the spin of the Ω^- can be uniquely determined from the ratio of the polarization of the Λ and the Ξ^0 in the $\Omega^- \to \Lambda K^-$ and $\Omega^- \to \Xi^0\pi^-$ decays. The decay parameters $\alpha_{\Lambda K}$ and $\alpha_{\Xi^0\pi^-}$ have been determined to be -0.018 ± 0.039 and -0.013 ± 0.116 respectively.[9] Assuming that there is no final interactions and time reversal invariance holds (i.e. $\beta_{\Lambda K} = \beta_{\Xi^0\pi^-} = 0$), the magnitudes of $\gamma_{\Lambda K}$ and $\gamma_{\Xi^0\pi^-}$ are close to unity. Although some models predict[10] that the $\Omega^- \to \Lambda K^-$ and the $\Omega^- \to \Xi^0\pi^-$ decays are almost parity conserving, this assumption is not made in the following discussion. In this case, the polarization of the Λ is either given by

$$\vec{P}_\Lambda = \vec{P}_\Omega \qquad (\gamma_{\Lambda K} = 1) \tag{31}$$

or

$$\vec{P}_\Lambda = -\frac{J}{J+1}\vec{P}_\Omega \qquad (\gamma_{\Lambda K} = -1), \tag{32}$$

similarly for the $\vec{P}_{\Xi^0}$. If $\gamma_{\Lambda K} = \gamma_{\Xi^0\pi^-}$, then there is no spin test. If $\gamma_{\Lambda K} \neq \gamma_{\Xi^0\pi^-}$, let P1 (P2) be the polarization with the bigger (smaller) magnitude among $\vec{P}_\Lambda$ and $\vec{P}_{\Xi^0}$. Then, from equations (31) and (32), the ratio of P1 to P2 is given by

$$-1 \leqslant \frac{P_1}{P_2} = -\frac{j+1}{j} \leqslant -3 \quad . \tag{33}$$

Taking $P1 = 0.15$, then a sample of approximately 1,000 $\Omega^- \rightarrow \Lambda K^-$ and 1,000 $\Omega^- \rightarrow \Xi^\circ \pi^-$ decays should be good enough to distinguish $j = \frac{3}{2}$ from $j = \frac{5}{2}$ with a 3σ statistical significance.

Alternatively, equation (30) may provide a spin test if the decay parameter, γ , is -1. If the Z axis is taken to be the normal to the production plane, from equations (13) and (7), it can be shown that

$$|t_{10}| \leqslant \sqrt{\frac{j}{j+1}} \tag{34}$$

and thus

$$|P_z| = |t_{10}| \sqrt{\frac{j+1}{j}} \leqslant 1. \tag{35}$$

Therefore, from equation (30),

$$|P_z| \leqslant \frac{j}{j+1} \tag{36}$$

which provides a lower limit on the spin j. If it is found that $t_{L0} = 0$ for $L > 1$, then another tighter bound on t_{10} is obtained,

$$|t_{10}| \leqslant \frac{1}{3}\sqrt{\frac{j+1}{j}} \tag{37}$$

This leads to the inequality

$$|P_z| \leqslant \frac{1}{3} \tag{38}$$

which does not provide any spin test.

In the case of strong decays of the type $F_j \to F_{\frac{1}{2}} + B_0$, the parameters $\alpha = \beta = 0$ and γ can either be 1 or -1 depending on the decay being studied. Therefore, the derivation of equation (30) is still valid. It is known that a certain portion of the long-lived hyperons produced in inclusive interactions are the decay products of the resonances. For instance, the Λ can come from the decays of the $\Lambda(1670)$, $\Sigma(1385)$,[11] $\Xi(1820)$ and so on. This implies that part of the observed Λ polarization can be attributed to these resonances if they possess vector polarization. The amount of contribution from a resonance can be calculated from equation (30) if the relative yield of the resonance to the direct Λ in the production process is known.

As a final remark, there remains the question of how to produce a polarized Ω^- sample so that its spin and magnetic dipole moment can be determined. According to the contemporary picture of hadron production in the beam fragmentation region,[12] the produced hadron will contain as many valence quarks from the projectile as possible and a minimum number of sea quarks. Therefore, for the $\bar{\Lambda}$ or Ω^-

produced by a proton, all the quarks of the $\bar{\Lambda}$ and the Ω^- must come from the sea. Since the $\bar{\Lambda}$ is found to be unpolarized,[13] if we assume that the production mechanism for the $\bar{\Lambda}$ also works for the Ω^-, then the Ω^-'s produced by protons should not have any polarization. On the other hand, Ξ^-'s[14] and Λ's[15] produced by K^-'s are polarized but $\bar{\Lambda}$'s[15] are not. These results imply that the polarization is only related to the valence s-quark of the K^- and has nothing to do with the u-quark, disregarding how the other quarks are produced and recombine to form the hyperons. Thus, Ω^-'s produced in the K^- fragmentation region should be polarized.

The work was supported in part of the National Science Foundation.

References

1. G.Bunce et al., Phys.Rev.Lett. 36 , 1113(1976);

K.Heller et al., Phys.Lett. 68B , 480(1977);

S.Erhan et al., Phys.Lett. 82B , 301(1979);

F.Lomanno et al., Phys.Rev.Lett. 43 , 1905(1979);

K.Raychaudhuri et al., Phys.Lett. 90B , 319(1980);

C.Wilkinson et al., Phys.Rev.Lett. 46 , 803(1981);

Results from the Fermilab-Iowa-Iowa State-Yale Collaboration, presented by P.Cooper in the 5th Int. Symp. on High Energy Spin Phys., Upton, N.Y.(1982);

Results from the Michigan-Minnesota-Rutgers-Wisconsin Collaboration, presented by B.Lundberg in the 5th Int. Symp. on High Energy Spin Phys., Upton, N.Y.(1982).

2. See, for example, K.Heller, University of Michigan preprint UM-HE-77-38, 1977, unpublished;

T.DeGrand and H.I.Miettinen, Phys.Rev. D24 , 2419(1981);

B.Andersson, G.Gustafson and G.Ingelman, Phys.Lett. 85B , 417 (1979);

J.Szwed, Phys.Lett. 105B , 403(1981).

3. L.Schachinger et al., Phys.Rev.Lett. 41 , 1348(1978);

P.T.Cox et al., Phys.Rev.Lett. 46 , 877(1981);

R.Rameika, Ph.D. thesis, Rutgers University (1981), unpublished;

L.Deck, Ph.D. thesis, Rutgers University (1981),unpublished;

Results from the Fermilab-Iowa-Iowa State-Yale Collaboration, presented by J.Marriner in the 5th

Int. Symp. on High Energy Spin Phys., Upton, N.Y.(1982).

4. M.Gell-Mann, Phys.Lett. 8 , 214(1964);

G.Zweig, CERN reports No. Th. 401, 412(1964).

5. V.Bargmann, L.Michel and V.L.Telegdi, Phys.Rev.Lett. 2 , 433(1959).

6. N.Byers and S.Fenster, Phys.Rev.Lett. 11 , 52(1963);

D.W.Merrill and J.Button-Shafer, Phys.Rev. 167 , 1202(1968).

7. G.Bunce et al., Phys.Lett. 86B , 386(1979).

8. M.Deutschmann et al., Phys.Lett. 73B , 96(1978);

R.J.Hemingway et al., Nucl.Phys. B142 , 205(1978);

M.Baubiller et al., Phys.Lett. 78B , 342(1978).

9. Preliminary results from the CERN charged hyperon group presented by R.Arnold in the 1981 EPS conf. on High Energy Phys., Lisbon(1981).

10. Y.Hara, Phys.Rev. 150 , 1175(1966);

M.Suzuki, Prog.Theor.Phys. 32 , 138(1964);

J.Finjord, Phys.Lett. 76B , 116(1978).

11. H.Kichini et al., Phys.Rev. D20 , 37(1979);

G.J.Bobbink et al., CERN preprint CERN-EP/82-181, 1982.

12. See, for example, R.Hwa, Phys. Rev. D22 , 1593(1980).

13. K.Heller et al., Phys.Rev.Lett. 41 , 607(1978);

F.Lomanno et al., Phys.Lett. 96B , 223(1980).

14. S.N.Ganguli et al., Nucl.Phys. B128 , 408(1977);

M.Baubillier et al., Nucl.Phys. B129 , 1(1981).

15. S.U.Chang et al., Phys.Rev. D11 , 1010(1975);

H.Abramowicz et al., Nucl.Phys. <u>B105</u> , 222(1976);

S.N.Ganguli et al., Nucl.Phys. <u>B128</u> , 408(1978);

H.Grassler et al., Nucl.Phys. <u>B136</u> , 386(1978);

M.L.Faccini-Turluer et al., Z.Phys. <u>C1</u> , 19(1979).

CURRICULUM VITAE

Kam-Biu Luk

1953	Born March 6 in Kowloon, Hong Kong.
1973	Graduated from Ying Wa College, Kowloon, Hong Kong.
1973-1976	Physics major, University of Hong Kong, Hong Kong.
1975-1976	Undergraduate thesis -- 'The Thermodynamic Model of Hadron Collisions and Lepton Production'.
1976	B.Sc.(Honour), University of Hong Kong.
1976-1977	Graduate Master of Heep Yunn School, Kowloon, Hong Kong. Taught General Science, Physics and Mathematics.
1976	'Resource Letter on Cosmic Ray experiments in the Undergraduate Laboratory', Proc. of Asian Symp. on Secondary Cosmic Rays, Hong Kong (1976).
1977-1979	Teaching Assistant for undergraduate Physics Laboratories.
1979-1983	Graduate Assistant in High Energy Physics. Worked with the Fermilab Neutral Hyperon Group. Active participation in E495, E361, E620, E555 and E619.
1981-1983	Thesis experiment -- completed data taking and analysis of the properties of the .

'Polarization of Σ^+ Hyperons Produced by 400 GeV Protons', Phys. Rev. Lett. 46 , 803(1981).

'Precise Measurement of the Ξ^0 Magnetic Moment', Phys. Rev. Lett. 46 , 877(1981).

'Precise Measurement of the Asymmetry Parameter in the Decay $\Xi^0 \to \Lambda\pi^0$ ', Phys. Rev. D25 , 639(1982).